

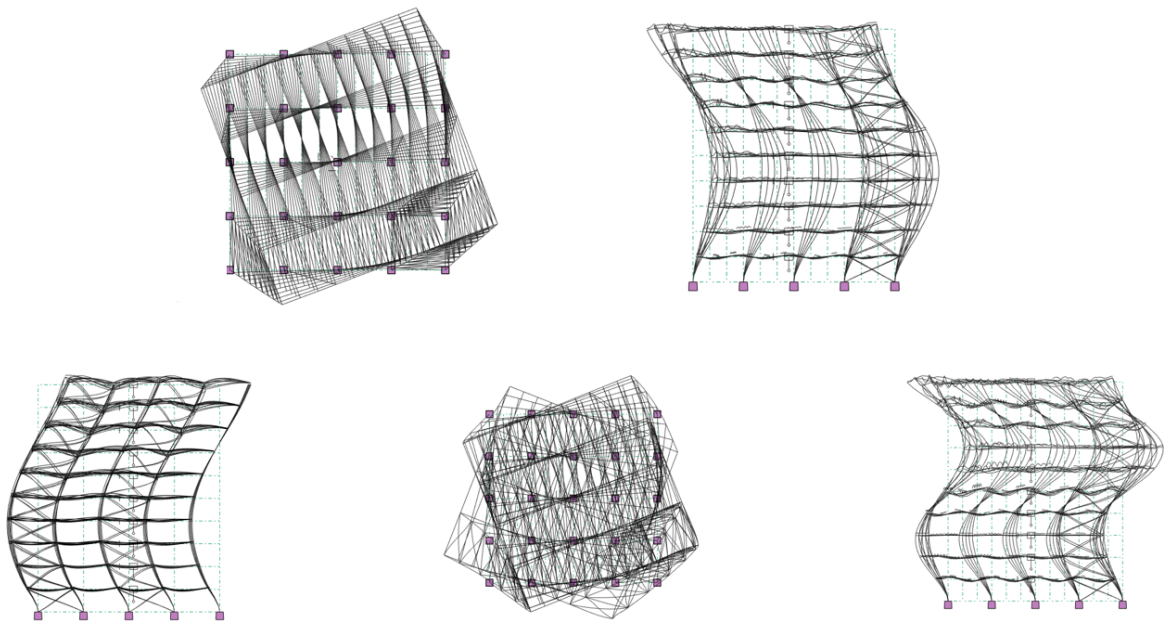
Earthquake Design

Response assessment of steel structure under earthquake effect

10th June, 2020

Group:
Filippos Filippou
Theodoros Kazakopoulos

Supervisor:
Lars Damkilde





AALBORG UNIVERSITET
STUDENTERRAPPORT

The Faculty of Engineering and Science
Structural & Civil Engineering
Thomas Manns Vej 23
9220 Aalborg SØ
<http://www.civil.aau.dk>

Title:

Earthquake Design - Response assessment of steel structure under earthquake effect

Project:

4th Semester - M.Sc. Structural and Civil Engineering

Project period:

February 3rd - June 10th 2020

Project group:

Filippos Filippou - Theodoros Kazakopoulos

Authors:

Filippos Filippou
Theodoros Kazakopoulos

Supervisor:

Lars Damkilde

Pages: 88

Appendix: 41

Finished 10-06-2020

Summary:

The aim of this project is to design and investigate the behaviour of a steel structure under earthquake effect. For this purpose, four different methods according to EC8 are used. First, the design of the structure is implemented. The structure is simulated by use of the commercial finite element software *Robot* and a modal analysis is applied. Moreover the structural regularity criteria are investigated. Then, two linear elastic analysis are performed: Modal response spectrum analysis and Equivalent static method of analysis. The two methods indicate a large difference to their outputs. Modal response spectrum is considered to be more accurate. Therefore, the design of the structure is implemented according to this method. Second, the response assessment of the building is implemented by means of nonlinear analysis. The finite element software *Seismostruct* is used for both static and dynamic time history analysis. The static nonlinear analysis determines the capacity curves of the structure for both principal horizontal directions. Additionally, the dynamic nonlinear analysis is implemented by use of three different accelerograms. Accordingly, the structural responses are evaluated by means of structural displacements and plastic deformations. Finally, the base isolation concept is investigated. Elastomeric bearings are added to the model and dynamic nonlinear analysis is implemented. A comparison between base isolated and fixed base structure's results is performed.

Preface

This report has been written by F.Filippou and T.Kazakopoulos in the 4th semester of Structural and Civil Engineering (Master) at Aalborg University. The project started on the 3rd of February and was finished on the 10th of June 2020.

The authors would like to address an expression of gratitude to our supervisor, Lars Damkilde, professor at the Department of Civil Engineering at Aalborg University, for help and guidance throughout our studies.

Reading guide

The whole report consists of the main report and an appendix where extra documentations are located. The chapters for the appendix are named by the letters of the alphabet, written as A.1, A.2, B.1, B.2... when making the reference to the appendix within the report.

The report uses the harvard-method for literature references, where sources that are used refer to the author's last name and the year of the publication in brackets - [Surname, Year]. Alternatively the citation is incorporated directly into the sentence and it refers the last name outside and the year inside parenthesis - ...Surname (Year).

Tables and figures produced by the project group do not have sources. In case of a figure or table taken from a source, but which has been modified by the project group, a reference to the source is written with the same reference format as mentioned above.

Tables, figures and equations are numbered by chapter, number and location in the chapter.

Filippos Filippou

Theodoros Kazakopoulos

Table of Contents

I Main Report	1
Chapter 1 Introduction	1
1.1 Background	1
1.2 Structural analysis	2
1.3 Problem formulation	4
1.4 Report structure	5
Chapter 2 Earthquakes	6
2.1 Introduction	6
2.2 Types of earthquakes	7
2.3 Earthquake magnitude and Intensity	7
2.4 Earthquake depth	8
2.5 Earthquake Effects	9
2.6 Earthquake characteristics	9
2.7 Forces and Structure Resistance	12
2.8 Ductility	12
2.9 Torsional Forces	13
Chapter 3 Principles of earthquake design	14
3.1 Regularity in plan	14
3.2 Regularity in elevation	16
3.3 Capacity design concept	17
3.4 Ductility classes for cross sections	21
3.5 Seismic mass and load combinations	22
Chapter 4 Earthquake design of steel building.	23
4.1 3D model configuration	23
4.2 Modal analysis of 3D model	26
4.3 Fundamental period calculation using Rayleigh's method	28
4.4 Regularity criteria	29
4.5 Modal response spectrum analysis	32
4.6 Equivalent static method of analysis	37
4.7 Criterion of the second order effects	39
4.8 Steel members validation	41
4.9 Capacity design	43
Chapter 5 Response assessment by means of nonlinear analysis	46
5.1 Aspects of nonlinear analysis	46
5.2 Modeling of bracing system	48
5.3 Models' verification	49
5.4 Nonlinear Static analysis	50
5.5 Nonlinear time history analysis	61

Chapter 6 Base isolation	75
6.1 Modeling of elastomeric bearings	77
6.2 Preliminary study of elastomeric bearings	78
6.3 3D model with elastomeric bearings	82
6.4 Perspectives of base isolation design	86
Chapter 7 Conclusion	87
Bibliography	89
II Appendix	92
Appendix A Analysis Methods	93
A.1 Elastic response spectrum	93
A.2 Ductility and design spectrum	94
A.3 Modal response spectrum analysis	97
A.4 Equivalent static analysis	99
A.5 Nonlinear static analysis	100
A.6 Non-linear time history analysis	103
Appendix B EC8 table	104
Appendix C Modal response spectrum analysis results	106
C.1 Second load combination	106
C.2 Third load combination	108
C.3 Fourth load combination	110
Appendix D Equivalent static method of analysis results	114
D.1 Second load combination	114
D.2 Third load combination	115
D.3 Fourth load combination	115
Appendix E Calculation note	117
Appendix F Verification example of tension only elements	118
Appendix G Pushover analysis results: Model 2	121
G.1 X direction	121
G.2 Y direction	123
Appendix H Nonlinear time history results	126
H.1 Northridge's original accelerogram, X direction	126
H.2 Northridge's original accelerogram, Y direction	127
H.3 Artificially generated accelerogram, X direction	129
H.4 Artificially generated accelerogram, Y direction	131

Part I

Main Report

The aim of this project is to examine the behaviour of a steel structure under earthquake forces. For this reason a ten storey building is designed and is subjected to several different seismic analysis in order to provide a clear overview of the structural behaviour.

1.1 Background

As an earthquake can be characterized any sudden shaking of the ground which is caused by the passage of seismic waves through Earth's surface. Earthquake is a dangerous phenomenon of great importance. Over the past centuries, earthquakes are responsible for millions of deaths and also damage of properties and infrastructures. According to their intensity, they can tip over buildings and bridges, rupture gas pipelines and any other infrastructure.



Figure 1.1: Damage to apartment buildings caused by soil liquefaction during the June 16, 1964, Niigata (Japan) earthquake[Seth Stein, 2005]



Figure 1.2: Parking structure that collapsed during the 1994 Northridge earthquake, California State University, Northridge Campus[Erdey, 2007]

Earthquakes are mainly manifested along fault lines. These regions are characterized as areas of high seismic activity. As it can be seen in Figure 1.3, faults are described as boundaries between tectonic plates and they can be hundreds of miles long and more than 100 miles deep. Most of the world's earthquakes occur within the Ring of Fire, a long horseshoe-shaped belt of earthquake epicentres, volcanoes, and tectonic plate boundaries fringing the Pacific basin. However, it is straight forward from Figure 1.3, that humankind has to deal with earthquake phenomenon all over the world. Furthermore, many earthquakes occur away from the plate boundary and are related to strains developed within the broader zone of deformation caused by major irregularities in the fault trace.

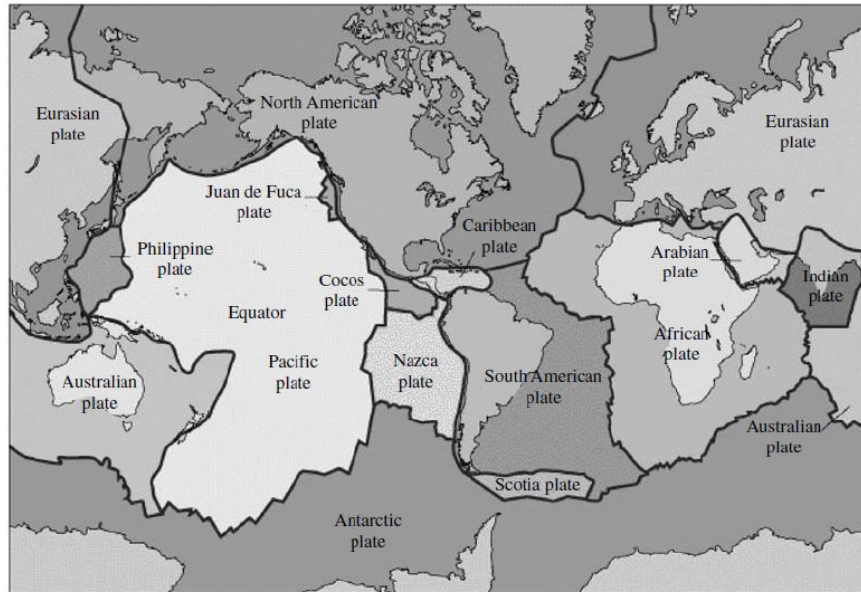


Figure 1.3: Global tectonic plates, [W.F. Chen, 2005]

In order to prevent human deaths and costly disasters, two sciences, engineering seismology and earthquake engineering, are linked together. Their joint goal is firstly to understand the earthquake ground motions that can damage buildings and other critical structures, and secondly to design structures that at least can ensure the safety of the inhabitants.

Earthquake engineering is a field of engineering which designs and analyses structures, such as buildings and bridges, so that they can resist earthquakes. Earthquake engineering is a multi-phased process that ranges from the description of earthquake sources, to characterization of site effects and structural response, and also to description of measures of seismic protection. It includes geophysical modeling, ground-motion modeling, stochastic and nonlinear dynamic analysis, design and experimentation. The prediction of strong ground motion is one of the most important areas in earthquake engineering. Several geophysical models are being considered for simulating strong ground motion, and the recorded motions from recent earthquakes are being studied for their characteristics and damage potential. The past earthquakes have shown that science has not yet succeeded in defining ground-motion parameters that correlate well with observed damage. It is crucial to develop damage models for structural response, improve the seismic risk analysis and also characterize ground motions based on damage potential. As the demand for construction of high rises has increased the last years, Structural engineers have been giving more importance to Earthquake induced loads for designing a building along with taking into consideration the Dead, Live and Wind loads. But not only the high rise building can cause great damage and loss of life during an earthquake, also structures like dams and bridges are equally susceptible to the earthquake and if they are not able to withstand the earthquake forces they will also cause loss of life.

1.2 Structural analysis

There are several different methods which structural engineers use in order to analyse the response of a structure which is subjected to seismic actions. At this point, it has to be noticed that earthquake design and in general dynamic analysis of buildings would have been impossible without the use of **Finite element method**.

Structural engineering has traditionally been based on simplified regulations. Typically, a building was designed to resist a seismic lateral load (static analysis) with magnitude determined by factors that account for the type of building, the natural period(s) of the structure, the foundation type, etc. However, a seismic action is a sequence of accelerations (or displacements) over the time which is acting on the foundation of the structure. Hence, it is straight forward that this phenomenon can not be fully described by lateral loads acting on the superstructure. Moreover, under strong ground motion the actual structural behaviour can be transformed from linear elastic to nonlinear inelastic, as the induced energy need to be dissipated through large displacements and material yielding. Therefore, an advanced structural analysis need to take into account the **geometric and material nonlinearities**.

In recent years structural design is rapidly moving towards the use of sophisticated computational methods (Finite element method) in engineering practice. This development is motivated by improved capabilities to numerically simulate nonlinear structural behavior during strong ground motion. However, in practice the simplified methods are still the most common methods of analysis. The proposed by EN1998-1 [2004] methods of analysis are the followings:

- The most common method used in design is the **Modal response** using a design spectrum. It is a linear method where the inelastic behaviour is considered in the design spectrum by use of a behaviour factor.
- The **Lateral force** method, which is a simplified version of the modal response method. It is actually a static analysis, which can be used only for regular structures which respond essentially in one single mode of vibration.
- The **Pushover analysis** is a a non-linear static analysis which is implemented under constant gravity loads and monotonically increasing horizontal loads. It can be used ideally in order to estimate the expected plastic mechanisms and the distribution of damage and also assess the structural performance of existing or retrofitted buildings.
- The **Non-linear time-history analysis** is a dynamic analysis which is obtained through direct numerical integration of the differential equations of motion. The earthquake action is simulated via accelerograms. The accelerations are applied to the restrain nodes of foundation. This method is strongly used for research and code background studies.

The structures should be designed so that they can resist the lateral loading while they maintain their bearing capacity (Dead and Live loads). For this reason, o proper structural configuration should be chosen. Moreover, according to the chosen structural system the failure mechanism of the structure is defined. Structural failure can be categorized as overall failure or component failure. The overall failure involves the collapse of the entire structure and it is crucial to be avoided. On the other hand, the component failure refers to the formation of plastic zones to the structural elements (beams, columns etc.). As for the steel structures two major lateral force -resisting systems exist:

- Moment resisting frames
- Braced frames

In general, experience has shown that steel structures are good at resisting earthquakes and this can be explained due to the importance of ductility, flexibility and low weight. There are two main ways by which the earthquake may be resisted:

- Structures which are made of sufficiently large sections and they are expected to have a linear elastic response.

- Structures made of smaller sections, designed to form numerous plastic zones (Ductile structures).

A structure which is designed by large sections will be expensive and may not provide a safety margin to cover earthquake actions that are higher than expected, as element failure is not ductile. In case of designing a structure with ductile behaviour (plastic zones), the structure can dissipate a significant amount of energy through plastic deformations. Ductile structures, which have extended deformation capacity, are generally better to resist earthquakes because they lead to more economically efficient solutions and they are able to resist earthquakes of higher magnitude than the expected ones. Steel structures are in general more flexible than other types of structure and lower in weight, and this is why forces in the structure and its foundations are therefore lower, as it is explained later in this report. Hence, this reduction of forces leads to a reduction of cost for the superstructure and also the foundation of the construction.

1.3 Problem formulation

The earthquake phenomenon as it is mentioned above has several different effects on the infrastructures. Therefore, a more detailed design and investigation of the structural response under seismic loading is required. The design for the earthquake resistance should be balanced between the seismic capacity of the structure and the feasible dimensions of it. The main goal for the design structure is to withstand the seismic effects while sustaining an acceptable level of damage. Consequently, apart from the dynamic response, the importance of the nonlinear behaviour of the structure should be taken into account. The damage development (nonlinear behaviour) and the motion of the structure are the main mechanisms of energy dissipation. Furthermore, the use of external damping or seismic isolation devices can beneficially contribute to this purpose. In this report the following aspects are investigated:

- What is an earthquake
- Earthquake design principles
- Earthquake design of steel structure
- Response assessment of steel structure under earthquake effect
- Base isolation

1.3.1 Project limitations

Comparing this report with an applied earthquake-resistance design project, the following limitations exist:

- the soil behaviour as well as the soil structure interaction are not examined
- foundation's design is not considered. The structure is assumed to be fixed at the ground level
- steel joints' design is not implemented. The connections between steel elements are assumed either rigid or pinned
- The serviceability limit state is not investigated. The structure is only designed against ultimate limit state actions
- Wind and snow loading are not included
- It is assumed that the infills of the buildings do not influence the structural response

1.4 Report structure

Firstly some general information about earthquakes are given and also the main characteristics of an earthquake are introduced and explained.

Secondly the earthquake design principles are described. The definition of regularity for a structure is explained and analysed for both in plan and elevation. Moreover, the frame configurations which are used to resist earthquake actions and the capacity design concepts are discussed.

In the next chapter the design of a ten-storey steel building is implemented, according to EN1993-1-1 [2005] and EN1998-1 [2004]. For this purpose the commercial finite element software Robot by Autodesk is used. A modal response spectrum analysis and a lateral force method of analysis are implemented. Furthermore, the cross sectional dimensions of steel members are validated and the capacity design requirements are investigated.

In the following part, response assessment analyzes for the ten-storey steel building are performed. The aspects of nonlinear analysis are introduced and the simulation procedure is described in detail. A static nonlinear (pushover) analysis and also dynamic nonlinear time history analysis is conducted by use of the finite element software Seismostruct.

Finally, the seismic base isolation concept is investigated. The two base isolation techniques are described. Moreover, a framed structure which is based on different kind of elastomeric bearings is simulated. Then, linear dynamic analyzes, for all the cases, are implemented and the structural responses are compared. In the end, a nonlinear dynamic analysis for the ten-storey building which is based on elastomeric bearings is implemented and the results are compared with the corresponding fixed based structure's response.

Earthquakes 2

2.1 Introduction

An earthquake can be explained as the the passage of vibrations (seismic wave) that spread out in all directions from the source of the disturbance when rocks are suddenly disturbed. It is caused by the sudden slip on a fault and in order to describe it, epicenter, focus, focal depth, after shock, fore shock, magnitude of earthquake are used. The stresses in earth's outer layer push the sides of the fault together. As a result of the generation of stress the rocks suddenly slips, releasing energy in waves that travel through the earth's crust and cause the shaking that is felt during an earthquake. With more simple words, earthquake is the violent release of energy due to rapid displacement on a fault plane. Other possible causes of an earthquake could also be the human activity such as injection of fluids into deep wells for waste disposal and also the use of nuclear detonations. The continual slow movement of the tectonic plate, the outermost part of the earth is the plate tectonics. Earthquakes are caused by this movement. Fault is a fracture or zone of fracture among two rocks, Figure2.1. A fault can range in length between a few meters up to thousands of kilometers T.A. Adagunodo [2015]. Over an earthquake the one side of the fault quickly slips with respect to the other. A fault can be either horizontal or vertical. There is a clear relation between earthquakes and faults.

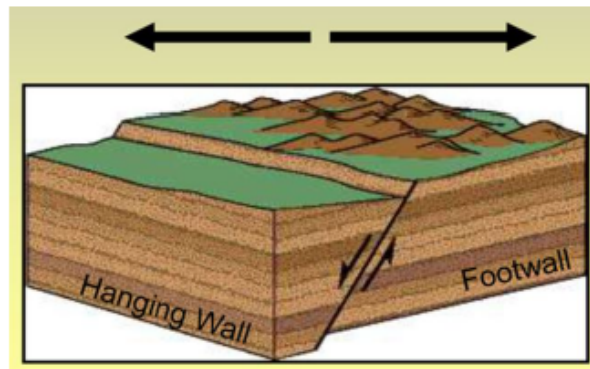


Figure 2.1: Relative movement of two blocks indicating a normal fault, [T.A. Adagunodo, 2015]

As it is up mentioned there can be several different causes that generates an earthquake. According to Erdey [2007] the main sources of an earthquake are :

- Orogenic movements such as mountain building
- Subduction and plate convection followed by geothermal and mechanical disturbances
- Volcanic activity
- Land erosion

2.2 Types of earthquakes

A brief explanation of the different types of earthquakes is given below:

- **Tectonic Earthquakes:** Tectonic earthquake are the most usual type of earthquake among the others. These type is created by several global forces, which cause the abruptly braking of a rock. Due to the fact that they pose huge hazard, tectonic earthquakes are significant important to study.
- **Volcanic Earthquake:** The second well known type of earthquake is the one which appears collectively with volcanic eruptions. This type of earthquake is the one which is related with volcano activity and it is believed that both eruption and earthquake are result from tectonic forces in the rocks.
- **Collapse Earthquakes:** Those are earthquakes which occurs in regions with mines and underground caverns. As a result of the ground shaking the roof of the mine or cavern collapse. A common observed variation of this phenomenon is called "mine burst". According to this phenomenon, the induced stresses around the mine working place cause large masses of rock to fly off the mine face explosively and produce seismic waves.
- **Explosion earthquakes:** By using nuclear devices or chemicals the explosion earthquakes are generated. When a nuclear device is exploded underground in a borehole, huge amounts of nuclear energy are produced. In a few milliseconds the pressure increases thousands of time the atmospheric Earth pressure and as a result the temperature increases by million degrees.

2.3 Earthquake magnitude and Intensity

The earthquake magnitude is the measurement of the "size" or the amplitude of the seismic waves which are produced from an earthquake and are reported by the seismographs. Due to the fact that there is a big variation in size among the earthquakes it is mandatory for comparison reasons to compress and scale the range of waves amplitudes measured on seismographs by means of a mathematical device. For this reason the seismologist named Charles Richter developed a scale, which mathematically adjusts the readings for the distance of the instrument from the epicenter. The Richter scale is logarithmic. By making use of a standard horizontal Wood–Anderson seismograph, the magnitude

$$M = \log_{10} A \quad (2.1)$$

where A denotes the trace amplitude in micrometers for an epicentral distance of 100 km. If the distance from the epicentral is more than 100m, then

$$M = M_{\Delta} - \frac{1.73 \log_{10} 100}{\Delta} \quad (2.2)$$

where where M_{Δ} is the magnitude at a distance Δ calculated from the basic Richter formula Erdey [2007].The smallest quake that a human being can feel is of magnitude 3. The largest earthquakes that have ever been recorded under this scale system are 9.25 in 1969 which occurred in Alaska while 9.5 in 1960 occurred in Chile. A current form of the Richter scale is shown in the table following table:

Table 2.1: Richter scale of earthquake magnitude,[Seth Stein, 2005]

magnitude level	Description	Average annually
8.0 and higher	great	fewer than 3
7.0–7.9	major	3–20
6.0–6.9	strong	20–200
5.0–5.9	moderate	200–2,000
4.0–4.9	light	2,000–12,000
3.0–3.9	minor	12,000–100,000
less than 1.0 to 2.9	micro	more than 100,000

Intensity means the severity of earthquake shaking which is assessed by using a descriptive scale, the modified Mercalli scale(by Harry O. Wood and Frank Neumann in 1931). The current form of this scale is represented in the 2.2 table:

Table 2.2: Modified Mercalli scale of earthquake intensity

Category	Definition
1: Imperceptible	Barely sensed only by a very few people
2: Scarcely felt	Felt only by a few people at rest in houses or on upper floors.
3:Weak	Felt indoors as a light vibration. Hanging objects may swing slightly.
4: Largely observed	Generally noticed indoors, but not outside, as a moderate vibration or jolt.
5: Strong	Generally felt outside and by almost everyone indoors. Most sleepers are awakened.
6: Slightly damaging	Felt by all, many are frightened and run outdoors. Persons walk unsteadily.
7: Damaging	General alarm. People experience difficulty standing.
8: Heavily damaging	Alarm may approach panic. Some buildings are damaged and less are destroyed.
9: Destructive	Some buildings are damaged and many weak buildings are destroyed
10:Very destructive	Many buildings are damaged and most weak buildings are destroyed.
11: Devastating	Most buildings are damaged and many buildings are destroyed.
12: Completely devastating	All buildings are damaged and most buildings are destroyed.

2.4 Earthquake depth

The earthquake depth is an important factor for shaping the characteristics of the waves and their produced damage. The focal depth can be categorized in the next following categories:

Table 2.3: Earthquake depth categories

A/a	Kilometers beyond the ground
deep	300-700
intermediate	60-300
shallow	less than 60 km

In case of deep focus earthquakes, due to the fact that the wave amplitude is greatly weakened by the time it reaches the surface, those earthquakes are less catastrophic. The shallow focus earthquakes are more usual and are extremely dangerous because of their close nearness to the surface.

2.5 Earthquake Effects

Earthquakes have several effects, including changes in geologic features, damage to man-made structures, and impact on human and animal life. The primary hazards associated with earthquakes are fault displacement and ground shaking, while the secondary includes ground failure, liquefaction, landslides and avalanches, and tsunamis.

- **Fault displacement and ground shaking:** Fault displacement can cause severe damage in foundations of buildings on or near the fault area or even displace the land, resulting troughs and ridges. The damage that is caused, depends on the size of the earthquake, the earthquake depth, the buffering power of the location's rocks and soils, and the type of buildings being shaken, T.A. Adagunodo [2015]. The secondary shaking of the ground is called aftershock and may cause further damage. There is a possibility that those tremors will last for weeks or even years after the initial quake.
- **Ground failure:** Seismic vibrations are possible to cause settlement beneath buildings while soils consolidate or compact. Specific soil types like alluvial or sandy are more likely to fail in an earthquake.
- **Liquefaction:** A certain type of ground failure is liquefaction, where the saturated soil loses its strength and collapses (liquefies). Buildings can sink, otherwise undamaged, during the few seconds of peak ground shaking, and end up permanently stuck when the shaking stops and the soil resolidifies. A dramatic example of the liquefaction phenomenon took place in Jamaica in 1692, where much of the town of Port Royal, built upon sand, sank about 4m beneath the ocean, Seth Stein [2005]
- **Landslides and Avalanches:** The slope instability is possible to cause landslides and snow avalanches during an earthquake. There are factors like steepness, weak soils and presence of water which probably contribute to susceptibility from landslides, Seth Stein [2005]
- **Tsunamis:** The definition tsunami came from a Japanese word which means "harbor wave". Usually they are referred as tidal waves, although the attractions of the Moon and Sun play no role in their formation. The most common cause of a tsunami is the sudden displacement in a seabed which is responsible for the sudden raising or lowering of a large body of water. An earthquake is probably the culprit for this deformation, or it may be a submarine landslide arising from an earthquake, Seth Stein [2005]

2.6 Earthquake characteristics

2.6.1 Acceleration and inertia Forces

An Inertial force is generated inside a body, when an outside force tries to change its position. When a building is facing an earthquake, it is subjected to inertial forces and obeys the second Newton's law of motion:

$$F = ma \tag{2.3}$$

where m is the mass of the building and a is the acceleration. By taking into consideration that the mass is equal with the height of the building, easily can be explained, why a light structure tend to resist better than heavier in an earthquake.

Accelerations are primarily responsible for building destruction. It is measured in terms of acceleration due to gravity. During an earthquake the acceleration is measured by devices which are called accelerometers. A poorly designed building starts to suffer damage approximately at 10 percent g ($0.1g$). During a moderate earthquake, the vibration waves may last for a few seconds and the acceleration may be close to $0.2g$, T.A. Adagunodo [2015]. The most significant measure in order to determine the forces acting on a building, is the combination of acceleration with duration. The term "bracket duration" describes the duration of a quake over a threshold value (usually $0.05g$) and is defined as the time between the first and last peaks of motion that exceeds this threshold value.

2.6.2 Velocity and displacement

The displacement is measured by the distance where the points of the ground are moved due to the seismic waves. Usually those distances are small and are measured in centimeters. The velocity of the ground caused by the seismic waves is in general slow and varies between 2cm/s and 60cm/s . In most earthquakes, there is a relation between ground acceleration, velocity, and displacement with frequency of the wave motion. High-frequency waves (over 10 hertz) tend to have high amplitudes of acceleration, but small amplitudes of displacement, compared to low-frequency waves, which have small accelerations and relatively large velocities and displacements, Arnold [2015].

2.6.3 Ground amplification, Period and Resonance

As the shaking propagates to the surface, there is a possibility to be amplified, depending on the intensity of shaking, the nature of the rock and, above all, the surface soil type and depth. At long periods the amplification is more intense while at short periods, it isn't so significant. For all the above reasons, the earthquake damage is larger in areas with soft grounds.

Natural period can be described by using an object and applying a horizontal force. The rate at which it will go back and forth is the definition of natural period. In the same way, when a building is subjected under an earthquake it will tend to move back and forth at its natural period. A four-story building will sway at about a 0.5 second period while a taller one between 10-20 stories building will sway about 1 to 2 sec visualised in Fig2.2.

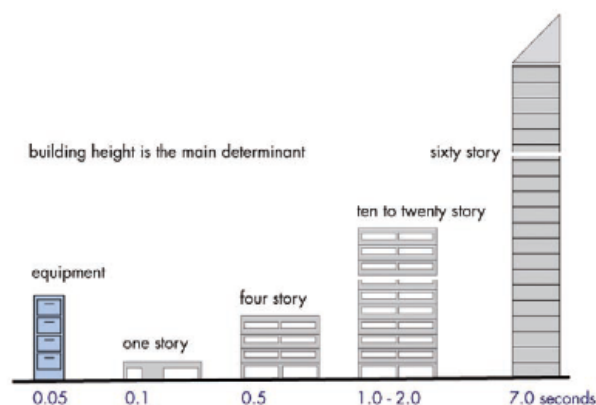


Figure 2.2: Comparative building periods, determined by height, [Arnold, 2015]

Resonance is describing the phenomenon where at vibrating object is given addition pushes that are the same at its natural period, which will result a serious increase in vibration and also the

acceleration will increase up to four or five times. The ground's natural period varies from about 0.4 seconds to 2 seconds depending on the nature of the ground. Due to the fact that this range is well within the range of common buildings' period, it is possible to occur resonance in some cases. For these reasons it should be ensured that the building period should not coincide with the ground period.

2.6.4 Response Spectrum

By taking into consideration all the above, it can be seen that buildings with different frequencies will give a variation of responses to the same earthquake. Moreover every building will react in a different way to different quakes. For this reason and for design purposes it is crucial to represent this building variation response to ground motion. This representation is called response spectrum. In a response spectrum graph the values of acceleration, velocity and displacement are plotted against period. The seismic codes have provided us with a standardized response spectrum that is illustrated in Fig 2.3

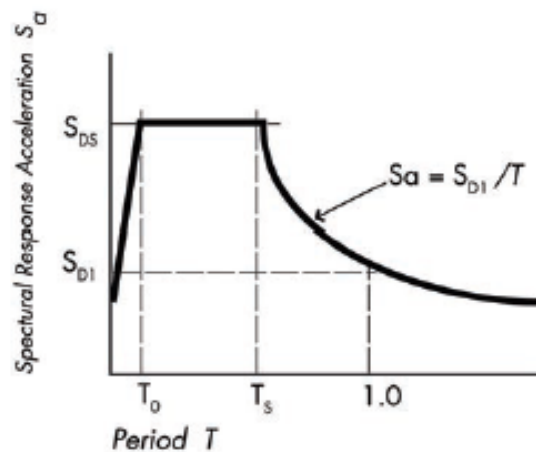


Figure 2.3: Simple response spectrum, for use in seismic codes, [Arnold, 2015]

For larger buildings the geotechnical engineer has to cooperate with the structural engineer in order to end up with a response spectrum.

2.6.5 Damping

As it is expected, in a vibrating structure after a while the amplitude of vibration will decrease and finally the structure will remain stable. The measurement of this decay of the amplitude is damping. Every structure has different damping, which depends on the nature of the structure. It is obvious that a heavy structure will provide more damping than a lighter structure. In order to have a reference point of damping, the term critical damping is used and denotes a theoretical damping level. Critical damping is the least amount of damping that is needed in order to allow a vibrating structure to return to its initial position without any further vibration. In general the damping ratio of a structure varies between 3 percent and 10 percent of the critical damping, Arnold [2015]. The main significance of damping is that accelerations created by ground motion increase rapidly as the damping value decreases.

2.7 Forces and Structure Resistance

No matter if a building is well damped and its unlikely to resonate, there is a possibility to be subjected in its lifetime under much higher forces than it was designed. The reason for not design every building with an extreme safety factor is the cost that would demand. A structure with massive structural members and structural walls with very limited openings would have been really expensive and unrealistic. A characteristic that can provide a safety margin in the event of encounging forces during an earthquake is ductility.

2.8 Ductility

The solution in the gap that is created between the capacity and the possible actual forces acting on a structure is given by a material property called ductility. This is the material property, according to which material fails only after considerable inelastic deformation has taken place. As a result this deformation dissipates a big amount of energy of an earthquake. Some materials are more ductile than others(Figure2.4: For example steel is more ductile than plastic).

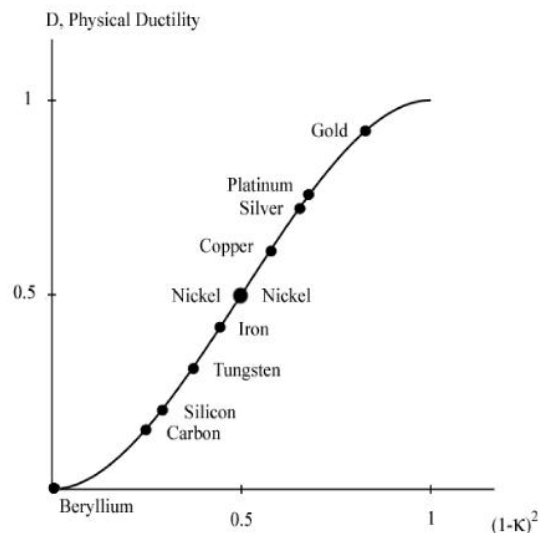


Figure 2.4: Physical Ductility of elements [Christensen, 2019]

Unreinforced buildings fail suddenly with minimum prior distortion. For this reason steel bars are used in reinforced concrete and give to the structure the willing ductility. There is close relation between ductility and reverse capacity. Reverse capacity is called the ability of a structure to resist overload and is related with ductility of every member of the structure. In general buildings are designed in a way that even of higher forces than the designed are applied, the materials will distort without braking.

2.8.1 Definition of Stress and Stiffness

Strength and stiffness are two of the most important characteristics of every structure. Sufficient strength for a structure means that it can support the induced load without exceeding certain stress values. Stress refers to the internal forces within a member that are created as a result from the applied load.

Stiffness is measured in terms of deflection, which actually means the extent to which a structural member bends when it is subjected to a load. As it concerns, in seismic design deflection of structural members such as beams and columns is termed as "drift". Limitations on drift might impose more strict requirements than those which are referring to strength. As a story drift is denoted the difference of the deflections between the top and bottom of the story. Usually it is expressed as a ratio between the deflection and the story, or floor-to-floor height as it is illustrated in Figure 2.5.

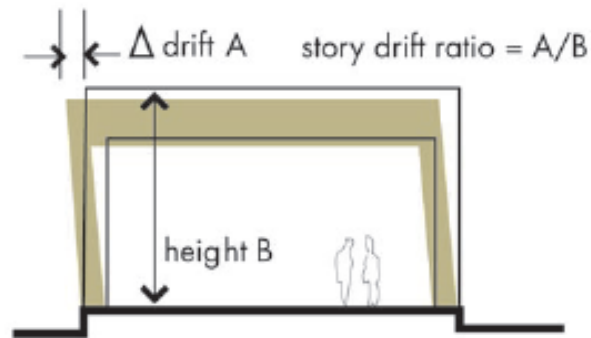


Figure 2.5: Story drift ratio [Arnold, 2015]

2.9 Torsional Forces

The center of mass or center of gravity for every object is defined as the point where the object is balanced without any rotation. As for a building, the most of the lateral force is contributed by the weight of the floors, walls and roofs. This force is applied through the center of mass which is usually the geometric center of the floor (in plan). When a lack of balance is observed between the resisting elements and the arrangement of the mass in a building, torsional forces are generated. This is known as eccentricity between the center of mass and the center of resistance, and makes the building which is subjected to ground motion to rotate around its center of resistance.

Principles of earthquake design 3

In this chapter the principles of earthquake design are introduced. The concepts of regularity in plan and elevation as well as capacity design concept are described.

3.1 Regularity in plan

According to EN1998-1 [2004], there are specific criteria for assessing structural regularity in plan. A "non-regular" in plan building requires a 3D simulation and the seismic actions should be combined in two principal horizontal directions of the building. Moreover the behaviour factor q , see Section A.2, should be treated with caution and its value should be reduced. Finally, when a non-linear static analysis (Pushover) of an irregular 3D model is performed, there is difficulty in capturing the lateral-torsional modes of response, Elghazouli [2017]. In addition, in building irregular in plan, significant torsional behavior may arise under earthquake effects, Figure 3.1.

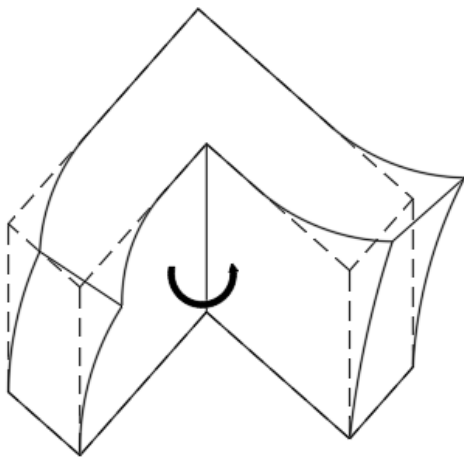


Figure 3.1: Torsional effect due to asymmetrical shape

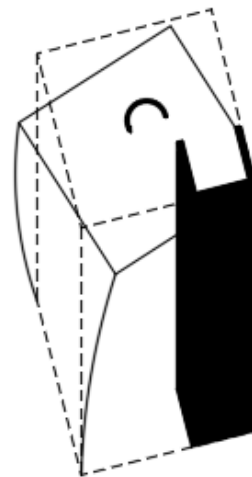


Figure 3.2: Torsional effect due to lateral stiffness concentration

The classification as regular in plan is done according to the following criteria:

- The distribution in plan of the lateral stiffness and the mass is approximately symmetrical with respect to two orthogonal horizontal axes. Normally, the horizontal components of the seismic action are applied along these two axes. It is up to the designer to judge whether this

condition is met or not. This condition is strongly validated when shear walls, concrete cores or braced frames are distributed asymmetrically in the plan of the building.

- The outline of the structure in plan should have a compact configuration, described by a convex polygonal line. This line is defined in plan by the vertical elements of the structure, and not the floor (including balconies and any other cantilevering parts) Any single re-entrant corner or edge recess of the outline of the structure in plan should not leave an area between it and the convex polygonal line enveloping it which is more than 5% of the area inside the outline.

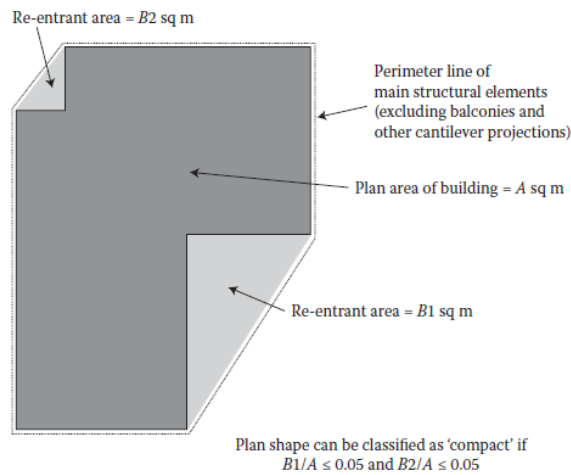


Figure 3.3: Definition of compact shape, [Elghazouli, 2017]

- The floors are considered as rigid diaphragms, in the sense that their in-plane stiffness is sufficiently large, so that the floor's in-plan deformation due to the seismic action is minor compared with the inter-storey drifts and has an insignificant effect on the distribution of seismic loading among the vertical structural elements. Moreover, a diaphragm to be considered rigid, it has to be free of large openings, especially in the vicinity of the main vertical structural elements. However, it is a common approach in the designing process that concrete slab may be considered as a rigid diaphragm, if its thickness and reinforcement are sufficient.
- The ratio of the floor plan, L_{max}/L_{min} , where L_{max} and L_{min} are respectively the larger and smaller in-plan dimensions of the floor measured in any the two principal horizontal directions, should not be larger than 4.
- In each of the two principle horizontal directions, x and y, the 'static' eccentricity, e, between the floor centre of mass and the storey centre center of stiffness is not greater than 30% of the corresponding storey torsional radius, r. Where the center of stiffness and the torsional radius are approximated with the following equations:

$$x_{cs} \approx \sum \frac{(xEI_y)}{EI_y} \quad y_{cs} \approx \sum \frac{(yEI_x)}{EI_x} \quad (3.1)$$

$$r_x \approx \sqrt{\sum \frac{(x^2EI_y + y^2EI_x)}{\sum (EI_y)}} \quad r_y \approx \sqrt{\sum \frac{(x^2EI_y + y^2EI_x)}{\sum (EI_x)}} \quad (3.2)$$

These equations are not exact definitions of center of stiffness and torsional radius. According to Elghazouli [2017], the exact solution might be obtained by of finite element analysis. More detailed, these values are obtained from the deflections and rotations at each floor level found from the application of unit forces and torsional moments. These process is not straightforward, therefore many different combination should be applied.

- the torsional radius must exceed the radius of gyration l_s , otherwise the building is classified as ‘torsionally flexible’, and the behaviour factor must be greatly reduced. The radius of gyration is the square root of the ratio of the polar moment of inertia to the mass. The the polar moment of inertia being calculated about the centre of mass.

3.2 Regularity in elevation

Uniformity over the elevation of the building is critical for the response of the structure under earthquake effects. It avoids the development of sensitive zones where concentrations of stresses and large ductility demands might provoke a collapse mechanism. Moreover, regularity in elevation apart with a the capacity design secure the structure against the occurrence of “*soft floor*”, see Section 3.3. Finally, the equal distribution of structural elements increases the capacity of the structure to redistribute the developed actions and widespread the dissipation of energy across the entire structure. Therefore when earthquake design is implemented, it is critical to ensure the regularity in elevation. However when this is not possible, different structural systems such as bracing or shear walls might be beneficial. Two examples of irregularity in elevation are illustrated in Figures 3.4 and 3.5.

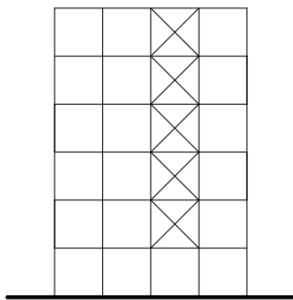


Figure 3.4: Irregularity due to abrupt change of the lateral stiffness

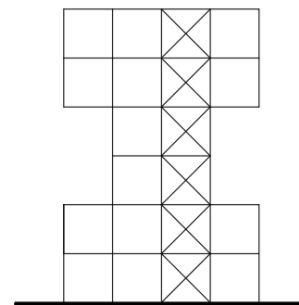


Figure 3.5: Irregularity due to discontinuity of vertical load resisting elements

According to EN1998-1 [2004], buildings can be characterized as regular in elevation by fulfilling the following requirements:

- The vertical-load-resisting elements should be undisturbed from the foundation level until the top of the building, or if setbacks exists, until the top of the setback.
- The mass and stiffness should be unchanged with height or reduce only gradually without sudden changes. The recommendation from EN1998-1 [2004] is that buildings where the mass or stiffness of any storey is less than 70% of that of the storey above or less than 80% of the average of the three storeys above should be classified as irregular in elevation.
- For the buildings with moment resisting frames, the lateral resistance of each storey shouldn't vary improperly between storeys. In general there are no quantified limits by EN1998-1 [2004], despite the fact that special rules are given where the variation in lateral resistance is caused

by the masonry infill within the frames. According to EN1998-1 [2004] manual, the buildings where the strength of any store is less than 80% from the one which is above should be classified as irregular in elevation.

- Buildings with setbacks are in general irregular but there is a chance to be characterized as regular if less than limits defined in the code. In presence of setback the following additional conditions are recommended by EN1998-1 [2004]:
 - a for gradual setbacks preserving axial symmetry, the setback at any floor shall be not greater than 20 % of the previous plan dimension in the direction of the setback (see Figure 3.6 and Figure 3.7).
 - b for a single setback within the lower 15 % of the total height of the main structural system, the setback shall be not greater than 50 % of the previous plan dimension (see Figure 3.8 . In this specific case the structure of the base zone within the vertically projected perimeter of the upper storeys should be designed to resist at least 75% of the horizontal shear forces that would develop in that zone in a similar building without the base expansion.
 - c for the case where the setbacks do not maintain any symmetry, in each face the sum of the setbacks at all storeys shall be not greater than 30% of the plan dimension at the ground floor above the foundation or above the top of a rigid basement. Moreover the individual setbacks must not be greater than 10 % of the previous plan dimension (see Figure 3.9).

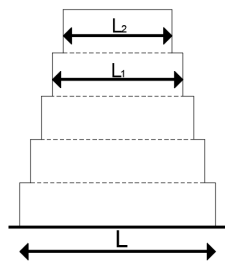


Figure 3.6: Criterion (a) for regularity of buildings, [EN1998-1, 2004]

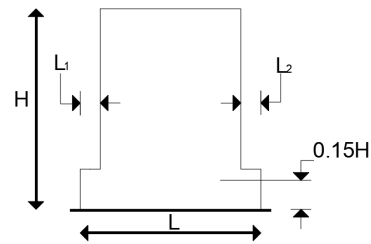


Figure 3.7: Criterion (b) for regularity of buildings, [EN1998-1, 2004]

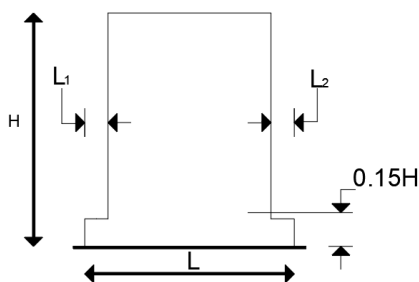


Figure 3.8: Criterion (c) for regularity of buildings, [EN1998-1, 2004]

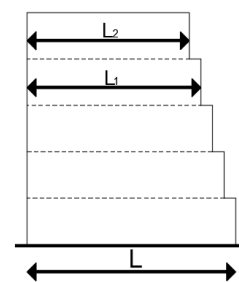


Figure 3.9: Criterion (d) for regularity of buildings, [EN1998-1, 2004]

3.3 Capacity design concept

According to EN1998-1 [2004], earthquake design contains some specific design methods. These methods ensure an overall dissipative and ductile behaviour of the structure and prevent formation

of unstable failure mechanism. This specific designing procedure is called capacity design and it is used to obtain the hierarchy of failure mechanism of the structure, so that a desired plastic response, instead of brittle failure, will be obtained. A suitable example is given in M. J. N. Priestly [1992], which compares the principle of capacity design with a "*ductile chain*". This concept illustrates that one ductile link may be sufficient to achieve ductility for the entire chain if, the strength of the brittle links is in excess of the ductile weak link.

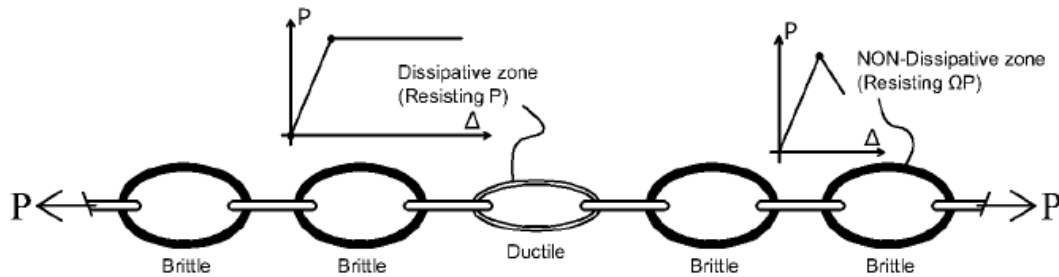


Figure 3.10: Principle of capacity design, [Muhammad Tayyab Naqash, 2014]

Steel structures, according to EN1998-1 [2004], are designed either as dissipative or non-dissipative. The last, expected to response mainly in the elastic range. Designing non-dissipative structures in regions of high seismicity will turn out in unfeasible dimensions and significant increase of the cost. Therefore, design by employing dissipative response, in which inelastic deformations are expected, is implemented. When the case is a simple regular structure, the inelastic response is taken into account by applying the behaviour factor, see Section A.2. However when a more complicated structural system is analysed, the use of non-linear analysis methods might be employed.

There are three main structural steel frame configurations, which are used to resist earthquake actions:

- Moment resisting frames
- Centrically braced frames
- Eccentrically braced frames

However different combination of moment resisting frames and shear walls or concrete cores might be used.

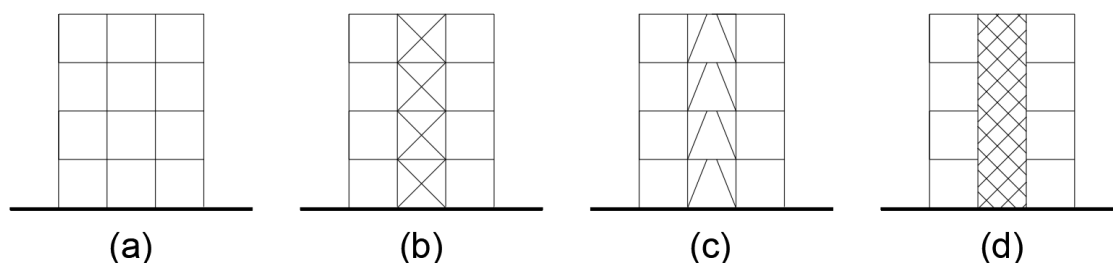


Figure 3.11: Structural systems: (a) Moments resisting frame, (b) Centrically braced frame, (c) Eccentrically braced frame, (d) Combination of moment resisting frame with concrete shear wall

3.3.1 Moment resisting frames

Moment resisting frames are designed so that plastic hinges are formed initially in beams rather than columns. This method demands weak beams and strong columns design. The contrary concept,

strong beams, weak columns, provides significant deformations apart with second order effects, might cause a fatal failure mechanism. Exception of this requirement is the bottom part of the first floor columns, where plastic hinges might be formed, see Figure 3.12.

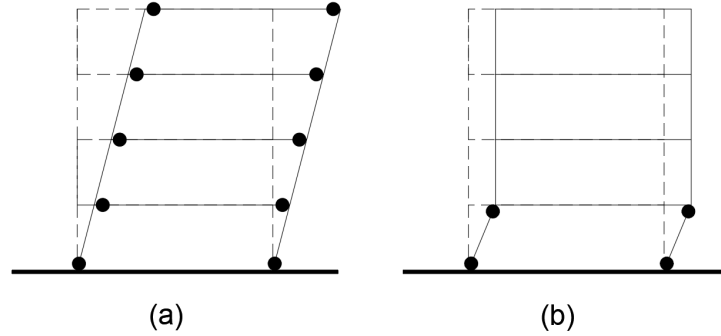


Figure 3.12: Weak-beam/strong-column and weak-column/strong-beam behaviour in moment-resisting frames. (a) Beam mechanism. (b) Storey column mechanism

According to EN1998-1 [2004], a general requirement of capacity design is that the sum of the design values of the moments of resistance of the columns framing the joint should be 1.3 times larger than the values of the sum of the moments of resistance of the beams framing the same joint:

$$\sum M_{Rc} \geq 1,3 \sum M_{Rb} \quad (3.3)$$

Beams

The desired failure mechanism is obtained by checks implementation so that the full plastic resistance development is ensured. Therefore, the following criteria should be fulfilled at all the critical cross sections of beams:

$$\begin{aligned} M_{Ed}/M_{pl,Rd} &\leq 1.0 \\ N_{Ed}/N_{pl,Rd} &\leq 0.15 \\ V_{Ed}/V_{pl,Rd} &\leq 0.50 \end{aligned} \quad (3.4)$$

Where M_{Ed} , N_{Ed} , V_{Ed} are the applied design bending moment, axial and shear force respectively and $M_{pl,Rd}$, $N_{pl,Rd}$ and $V_{pl,Rd}$ are the corresponding plastic capacities of the cross sections calculated according to EN1993-1-1 [2005].

Columns

Moreover, according to Section 6.6.3 of EN1998-1 [2004]. columns should satisfy for the most unfavourable combination of bending moments and axial forces the following equations:

$$\begin{aligned} M_{Ed} &= M_{Ed,G} + 1.1\gamma_{ov}\Omega M_{Ed,E} \\ N_{Ed} &= N_{Ed,G} + 1.1\gamma_{ov}\Omega N_{Ed,E} \\ V_{Ed} &= V_{Ed,G} + 1.1\gamma_{ov}\Omega V_{Ed,E} \end{aligned} \quad (3.5)$$

where Ω is the minimum over-strength factor in the connected beams, $\Omega_i = M_{pl,Rd}/M_{Ed,i}$, $M_{Ed,G}$ and $M_{Ed,E}$ are the bending moments of the earthquake design situation due to gravity loads and lateral earthquake actions respectively, see Figure 3.13. Additionally the most unfavourable shear force V_{Ed} coming out of the structural analysis must be less than 50% of the ultimate shear plastic resistance.

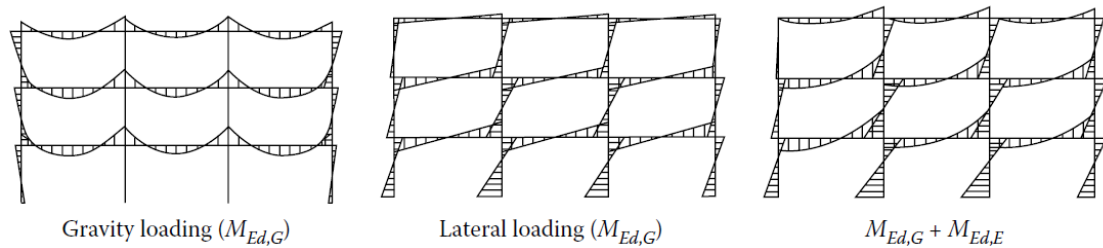


Figure 3.13: Moments due to gravity and lateral loading components in the seismic situation, [Elghazouli, 2017]

Stability and drift consideration

Due to the flexibility of moment resisting frames, EN1998-1 [2004] recommends deformation related criteria which often govern the design. The ultimate limit state is associated with the "second order effects". This requirement is specified through an inter storey drift sensitivity coefficient (θ) given as:

$$\theta = \frac{P_{tot}d_r}{V_{tot}h} \quad (3.6)$$

where P_{tot} and V_{tot} are the total gravitational axial force and seismic shear force, respectively, at the storey under consideration and h is the storey height. d_r is the design inter-storey drift which is product of the behaviour factor, q and the elastic inter-storey drift, output of the elastic structural analysis. Instability is assumed when θ is higher than 0.3. If $\theta \leq 0.1$, second order effects are considered as insignificant.

3.3.2 Concentrically braced frames

Because of their geometry, concentrically braced frames provide a truss behaviour, with members subjected to large axial forces. It is a common approach to design the diagonal members so that they develop only axial forces. According to EN1998-1 [2004] recommendations, it is considered that the horizontal seismic actions are mainly resisted by the axially loaded members. Moreover, yielding of diagonals members should take place before yielding or buckling of the beams or columns and before failure of the connections.

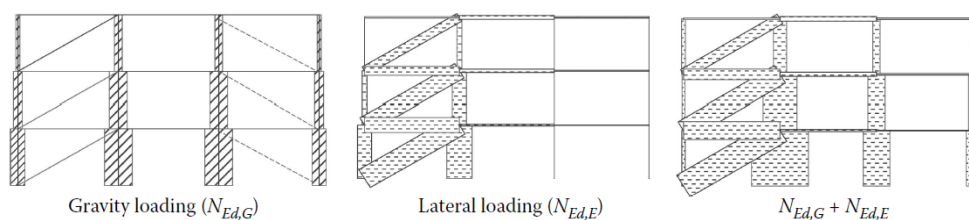


Figure 3.14: Axial forces due to gravity and lateral loading in the seismic design situation, [Elghazouli, 2017]

According to Elghazouli [2017], in diagonal bracing systems, the horizontal forces can be assumed to be resisted by the corresponding tension members only, with the contribution of the compression parts to be neglected. Ignoring the compression brace can have favourable or detrimental effects on the actual response, depending on the frame configuration and design situation Elghazouli [2003]. However, by taking into account both braces, non-linear static or time history should be used.

As it is mentioned before, it has to be ensured that the bracing system yields before the associated beams or columns fail. Therefore, the last should be capacity designed for seismic combination actions and should satisfy the following criterion:

$$N_{Ed}(M_{Ed}) \geq N_{Ed,G} + 1.1\gamma_{ov}\Omega N_{Ed,E} \quad (3.7)$$

where $N_{Ed}(M_{Ed})$ is the axial design resistance of beam or column by taking into account the interaction with the bending moment, $N_{Ed,G}$ and $N_{Ed,E}$ are the axial load due to gravity and lateral actions, respectively, in the seismic design situation, as illustrated in Figure 3.14. Furthermore, Ω is the minimum value of axial brace over-strength of all the diagonals of the frame and γ_{ov} is the material over-strength. It has to be noticed that Ω of each diagonal should not differ from the minimum value more than 25%, so that a reasonable distribution of ductility is ensured. However in real cases, the 25% limit might be difficult to be fulfilled.

3.4 Ductility classes for cross sections

For elements in compression or bending, under seismic loading scenario, EN1998-1 [2004] requires the restriction of the width over thickness ratio (b/t) so that local buckling effects are avoided. However an increase of this ratio results in lower element plasticity and therefore the reduction of energy dissipation capacity of the element. The classification of the cross section is done according to EN1993-1-1 [2005], see Figure 3.15 and it influences the value of the behaviour factor, see Table 3.1

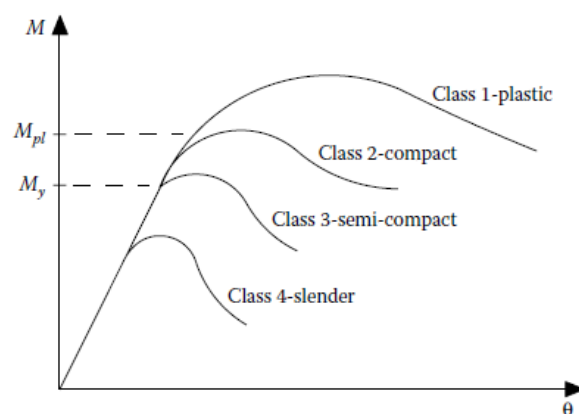


Figure 3.15: Moment–rotation characteristics for different cross-section classes, [Elghazouli, 2017]

Table 3.1: Cross section classes and the corresponding behaviour factor ranges

Cross-section class	q factor's ranges
Class 1, 2 or 3	$1.5 < q < 2$
Class 1 or 2	$2.0 < q < 4.0$
Class 1	$q > 4$

3.5 Seismic mass and load combinations

The mass of the structure under earthquake effects is calculated as the sum of the full permanent loads (G_{ki}) plus the variable loads (Q_{ki}) multiplied by a reduction factor ψ_{Ei} . This factor is calculated as the product of the reduction factor ψ_{2i} , see EN1990 [2002], and a further reduction factor ϕ which allows for the incomplete coupling between the structure and its variable load.

$$M_d = \sum G_{ki} + \sum \Psi_{Ei} Q_{ki} \quad \text{where} \quad \psi_{Ei} = \psi_{2i} \phi \quad (3.8)$$

Basic load combinations are given according to EN1990 [2002]. The seismic load combination is implemented conforming to the following equation:

$$E_d = \sum G_{ki} + A_{Ed} + \sum \Psi_{2i} Q_{ki} \quad (3.9)$$

where, E_d is the design action effects, $\sum G_{ki}$ is the permanent actions, A_{Ed} are the earthquake actions and $\sum \Psi_{2i} Q_{ki}$ is the reduced variable actions. Furthermore, earthquake analysis is done in respect of the two principal horizontal directions. Exceptions are some cases in which the vertical component of the seismic action is taken into account. Therefore, the final results of the structural analysis are calculated by the most unfavourable of the following combinations:

$$\begin{aligned} A_{Ed} &= \pm E_{Edx} \pm 0, 3E_{Edy} \pm 0, 3E_{Edz} \\ A_{Ed} &= \pm 0, 3E_{Edx} \pm E_{Edy} \pm 0, 3E_{Edz} \\ A_{Ed} &= \pm 0, 3E_{Edx} \pm 0, 3E_{Edy} \pm E_{Edz} \end{aligned} \quad (3.10)$$

Earthquake design of steel building. 4

In this chapter the design of a multi-storey steel building is implemented. The regularity in plan and elevation are investigated. Then, the modal response spectrum and the lateral force method of analysis are applied according to EN1998-1 [2004] and the elements' dimensions are verified according to EN1993-1-1 [2005]. Finally, the specific requirements of capacity design are investigated.

4.1 3D model configuration

A 3D model is developed by use of commercial finite element software *Robot* by *Autodesk*. *Robot* is able to perform both linear and non-linear analysis and it is a proficient tool for steel member design, according to *EC3*. The structure under investigation is a fictional ten-storey office building with an elevation shaft. The beam and the columns of the structure are made out of structural steel (*S355*), while the slabs are constructed from reinforced concrete (*C20/25*). The total height of the building is 40 meters, while its length in two principal horizontal directions is 32 meters. For a better understanding of structural configuration the 3D model is illustrated in Figure 4.1.

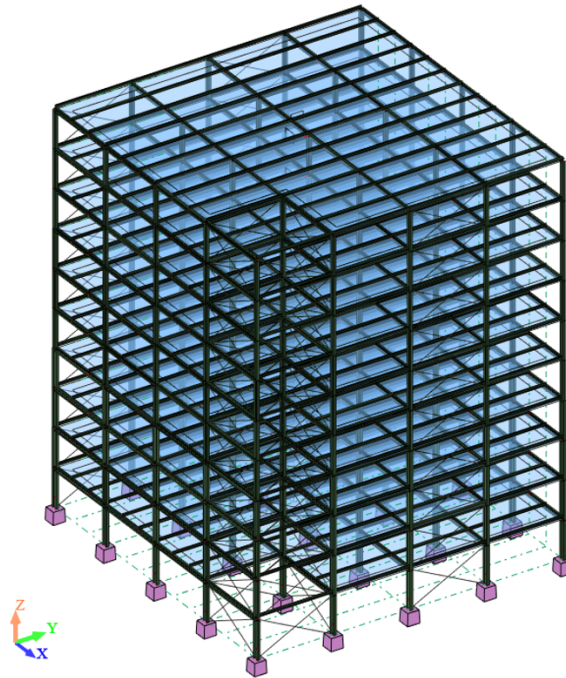


Figure 4.1: 3D model of the building

The building is consisted of five moment resisting frames which are expanded in the $X - axis$ and

they are repeated, along the $Y - axis$, every 8.00 meters. They are connected between them with gravity beams which are repeated every 2.66 meters. These beams are supported by shear tab connections at the two ends while the beams and the columns of the moment resisting frames are connected with rigid (moment) connections. It is assumed that the moment resisting frames are able to resist the horizontal actions in the $X - axis$. However this is not the case for the $Y - axis$ due to the fact that the beams and columns are connected with shear tab connections. Therefore, two concentrically braced frames are designed in the perimeter of the building, so that the structural stiffness of $Y - axis$ is increased.

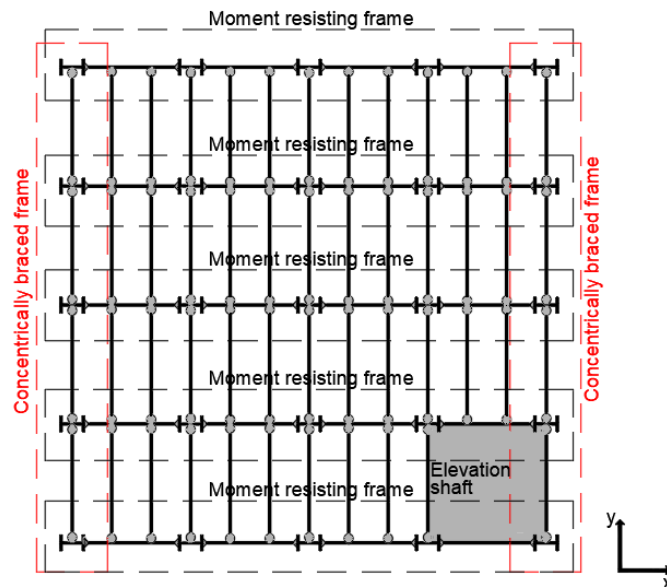


Figure 4.2: Plan of the building

The structural system of the moment resisting and the concentrically braced frames can be seen in Figure 4.3. The bracing bars are supported by *pinned – pinned* connections at the two ends and therefore they are able to develop only axial forces. Under earthquakes the bracing system provide a truss behaviour which results to large axial forces. Thereafter, the configuration of the elevation shaft can be seen in Figure 4.3 which consist of four concentrically braced frames.

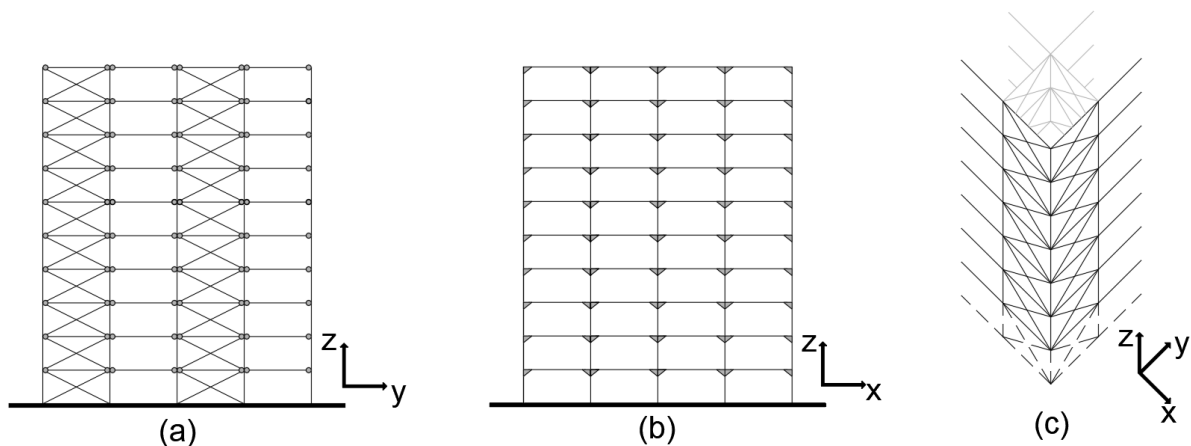


Figure 4.3: (a) concentrically braced frame, (b) moment resisting frame, (c) elevation shaft configuration

In addition, the floor system consisted of reinforced concrete slabs of 15cm which are engaged in full composite action with the supporting gravity beams. The slabs provide the adequate stiffness in the $XY - plane$ so that they are considered as rigid diaphragm, according to EN1998-1 [2004].

Finally, general information about modeling procedure is given below:

- All steel elements are modelled as beam elements, see R.D.Cook [2002].
- Nor material neither geometrical nonlinearities are taken into account. Therefore, all analysis methods are linear elastic.
- Consistent mass matrix is used.
- All elements are considered fully fixed in the ground level (foundation).
- Frames are connected together by means of rigid diaphragms (in horizontal plane XY) at each floor. Slabs loads are transferred to beams by simplified trapezoidal or triangular method.
- Infills are not taken into account.

4.1.1 Modeling of bracing system

As it is mentioned in Section 3.3, the bracing system should be designed so that it resists the horizontal actions only by the corresponding tension members. The contribution of the compression parts should be neglected due to the assumption that compressed elements which reach their buckling resistance, they are not able to carry any additional axial force.

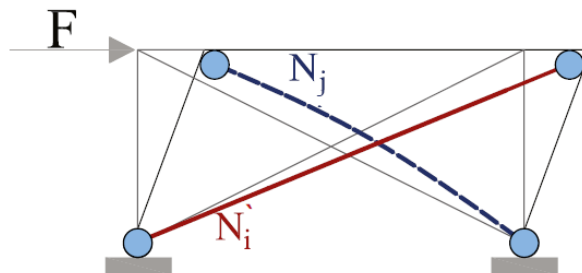


Figure 4.4: Couple of braces' behaviour, [Alessia Di Cuiaa, 2017]

When a modal response spectrum analysis is carried out it, the identification of the compressed member is difficult to be done due to the loss of sign. In *Robot* there is the option to use tension-only members. However this option will turn the analysis to a non-linear analysis, which is not compatible with modal response spectrum method. Therefore the following method is implemented so that non-linear problem is linearized. According to Martinelli [1996] a 3D model with both braces is simulated. However the bracing bars are modeled with reduced axial stiffness. In this project the axial stiffness is reduced by 50%. Later, the actual response of structure, hence the actual response of the bracing system, is evaluated by static and dynamic nonlinear analysis.

4.1.2 Member dimensions

As shown in Table 4.1, the gravity beams in all floors are *IPE270* while the primary beams are *HEA400* for the four lower floors and *HEA340* for the rest. Accordingly, the columns of the four lower floors are chosen to be *HEB550*, for the next three floors *HEB400* and for the three higher floors *HEB340*. The bracing bars in every floor are chosen to be *UPE240*.

Table 4.1: Member cross section in every floor

Storey	Columns	Primary beams	Gravity beams	Bracing bars
1st to 4th	HEB 550	HEA 400	IPE 270	UPE 240
5th to 7th	HEB 400	HEA 340	IPE 270	UPE 240
8th to 10th	HEB 340	HEA 340	IPE 270	UPE 240

4.1.3 Dead and live static loads

The dead load includes loads that are relatively constant over time, including the weight of the structure itself (beam, columns, slabs) and immovable fixtures such as walls, plasterboard or carpet. As live are characterized loads that do, or can, change over time, such as people walking around a building (occupancy) or movable objects such as furniture. The self weight of the material and the value of the live loads are calculated according to EN1991-1-1 [2002]:

- self weight of reinforced concrete ($C20/25$): $25kN/m^3$
- self weight of structural steel ($S355$): $77kN/m^3$
- non-structural dead load: $1kN/m^2$
- live load for office building: $2kN/m^2$

The design of the structure for the ULS , accounting for dead and live loads, is implemented according to the following combination: $1.35G + 1.5Q$. The resultant bending moments are illustrated in Figures 4.5 and 4.6. The maximum developed bending moment is $283.08kNm$ while the minimum value is $-373.26kNm$. From these figures it is obvious that the beams and the columns of moment resisting frames ($XZ - plane$) are connected with rigid supports and they are able to develop large bending moments, while the gravity beams are single supported ($YZ - plane$).

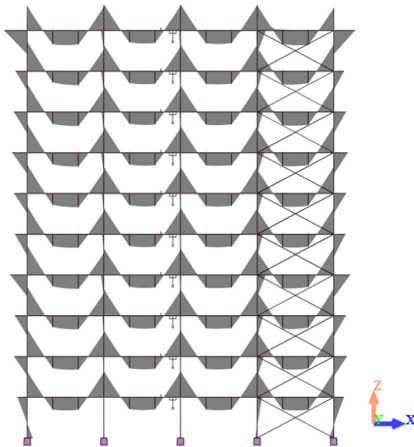


Figure 4.5: Bending moment out of static analysis ($XZ - plane$)

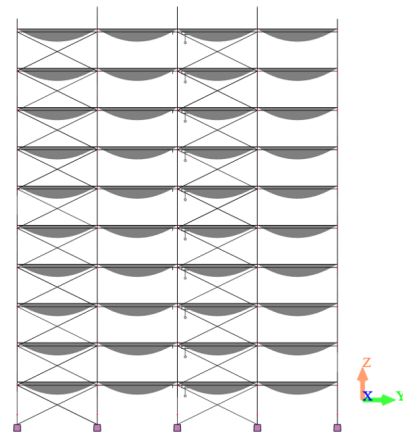


Figure 4.6: Bending moment out of static analysis ($YZ - plane$)

4.2 Modal analysis of 3D model

A modal analysis is performed, so that the eigenmodes and the eigenfrequencies to be calculated. A structure's response to ground motion can be analysed through a sufficient amount of vibration shapes. The eigenperiod has a dominant role depending on mass and stiffness of the system,

and provides the time required for one cycle of harmonic motion in one of the eigenmodes. In other words, the eigenmodes illustrate the deformed shaped of the structure if it was subjected to harmonic loading with frequency equal to its eigenfrequency. The equation of modal analysis is stated as following:

$$[M]\{\ddot{D}\} + [K]\{D\} = 0 \quad (4.1)$$

Moreover, modal analysis is essential to be conducted, so that the the boundary conditions and in general the finite element model is validated. A detailed description of the two critical eigenmodes of the structure can be seen in Figure 4.7. According to the first eigenmode the structure is displaced mainly in the $X - axis$. However there is a small part of motion which takes place in the $Y - axis$. In line with the second eigenmode the structure is shifted in the $Y - axis$ while there is a small contribution in the $X - axis$. The torsional deformation are predominant in the third eigenmode.

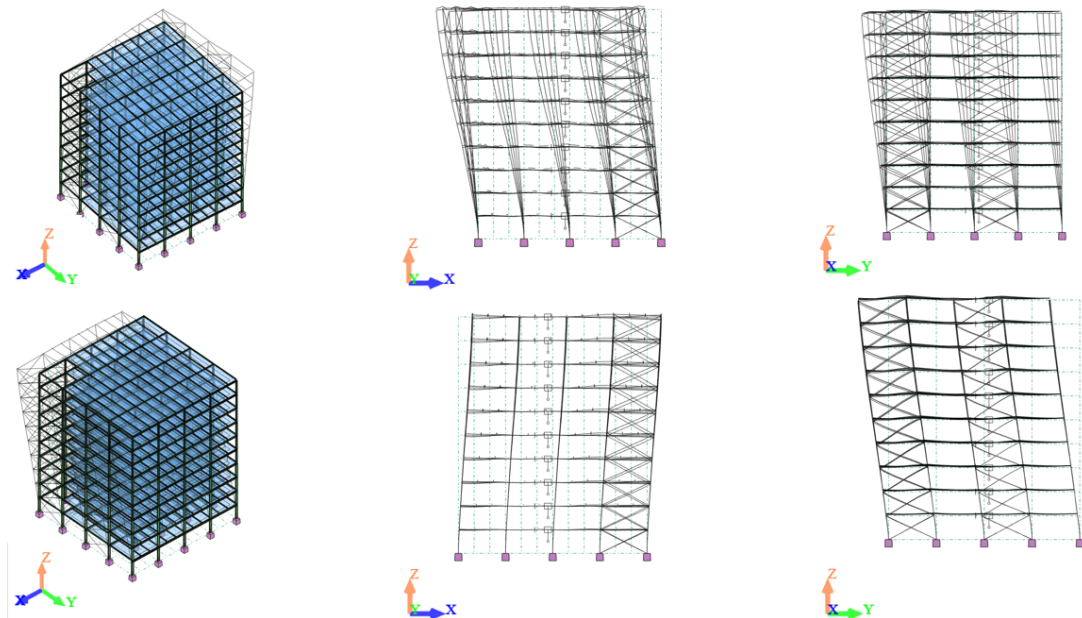


Figure 4.7: Detailed description of two critical eigenmodes.

Modal mass, a constant which represents the part of the structures total mass which is activated from the particular mode. It gives an indication of the importance of each mode. As it is described in Appendix A.3, EN1998-1 [2004] allows neglecting contribution from modes with modal mass less than 5%. Moreover the number of essential modes is increased until the limit of 90% mass participation in two principal horizontal directions of the structure is reached.

For this building the crucial number of modes is seven. In Table 4.2, the mass participation for each mode can be seen. It is obvious that the first and the second eigenmodes are the most crucial for the structure, due to their large mass participation factors ($UX = 55.47\%$ and $UY = 63.09\%$ respectively). Furthermore, it can be seen that there is an important torsional effect for the third eigenmode ($RZ = 52.68\%$). Finally the rest of the mode-shapes can be seen in Figure 4.8.

Table 4.2: Modal analysis results

Eigenmode	Frequency (Hz)	Period (sec)	Mass UX (%)	Mass UY (%)	Mass RZ (%)
1st	0.50	2.00	55.47	12.80	5.03
2nd	0.54	1.87	13.39	63.09	0.01
3rd	0.84	1.19	5.55	1.03	52.68
4th	1.50	0.67	11.99	0.90	0.74
5th	1.68	0.60	1.01	14.14	0.03
6th	2.59	0.39	0.66	0.24	9.27
7th	2.69	0.37	4.12	0.15	0.02

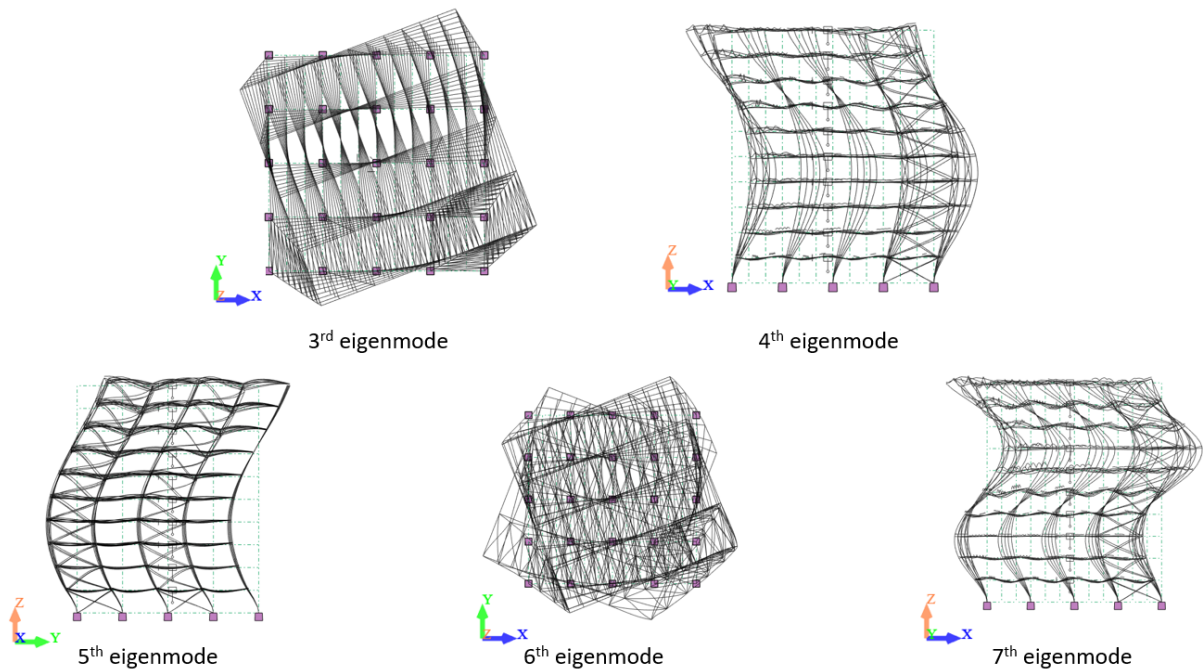


Figure 4.8: 3rd to 8th mode-shapes

4.3 Fundamental period calculation using Rayleigh's method

The fundamental eigenperiod for each horizontal directions can be calculated according to Rayleigh method, *which is very effective in establishing simple estimates of the eigenfrequencies in more complicated FEM models*, L.Damkilde [2018]. According to this procedure, two load combinations are applied, one in X-direction and one in Y-direction. Horizontal, forces are applied to the center of mass in every storey level, and the corresponding displacements are calculated in the two principal directions. It is assumed that the horizontal forces are triangular distributed, see Figures 4.9 and 4.10.

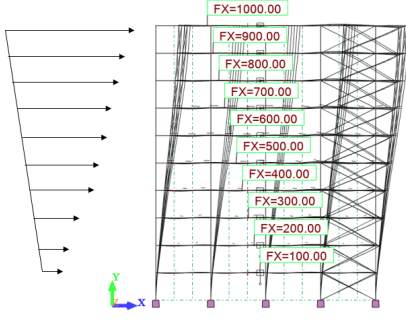


Figure 4.9: Horizontal forces distribution in X-direction

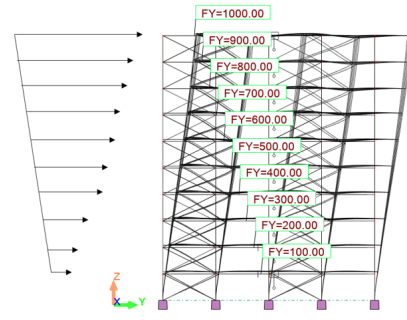


Figure 4.10: Horizontal forces distribution in Y-direction

Hereafter, the fundamental periods are calculated according to the following equation:

$$T = 2\pi \sqrt{\frac{\sum_{i=1}^n (M_i \cdot U_i^2)}{\sum_{i=1}^n (F_i \cdot U_i)}} \quad (4.2)$$

where where $n = 10$ is the number of storey levels, M_i are storey masses, F_i are horizontal forces acting on storey i in centres of storey masses and U_i are displacements of masses caused by horizontal forces F_i .

Table 4.3: Quantities needed for the determination of the fundamental period using Rayleigh method

Storeys	$F_{iX} = F_{iY}$ (kN)	U_{iX} (m)	U_{iY} (m)	M_i (ton.)
1st	100	1.10E-2	1.50E-2	4.75E+2
2nd	200	3.00E-2	3.40E-2	4.75E+2
3rd	300	5.20E-2	5.40E-2	4.75E+2
4th	400	7.30E-2	7.50E-2	4.75E+2
5th	500	9.80E-2	9.70E-2	4.68E+2
6th	600	1.23E-1	1.18E-1	4.68E+2
7th	700	1.46E-1	1.38E-1	4.68E+2
8th	800	1.67E-1	1.57E-1	4.65E+2
9th	900	1.84E-1	1.74E-1	4.65E+2
10th	1000	1.96E-1	1.89E-1	4.65E+2

The fundamental periods T_X , T_Y are calculated 1.94sec. and 1.89sec. respectively. It can be noticed that there is a considerable agreement with modal analysis output, see Table 4.2. The error is calculated as 3% for X, 0.6% for Y direction and the reason is that the estimated mode shapes are a little different from the exact solution, see Figure 4.7. However, there is a better agreement between the second eigenmode and the estimated mode shape in Y direction.

4.4 Regularity criteria

It is obvious that the building meets the elevation regularity criteria as, they are described in Section 3.2. Therefore, no further investigation is need in order to characterize the building as regular in

elevation. However this is not the case for the plan regularity, owing to the fact that the elevation shaft provides concentrated stiffness. Consequently, the distribution in plan of the lateral stiffness and the mass is not symmetrical with respect to the principal horizontal axes. Therefore a further investigation is needed.

4.4.1 Static eccentricity

Initially the "static" eccentricity between the center of mass and center of rigidity at each floor has to be calculated. The center of mass is taken directly from *Robot*. However, the coordinates of the center of rigidity which are based on Equations 3.2, are not adopted due to the fact that the bracing system is not taken into account, according to *Robot*'s manual. The recommended procedure in line with P. Bisch [2012] is used:

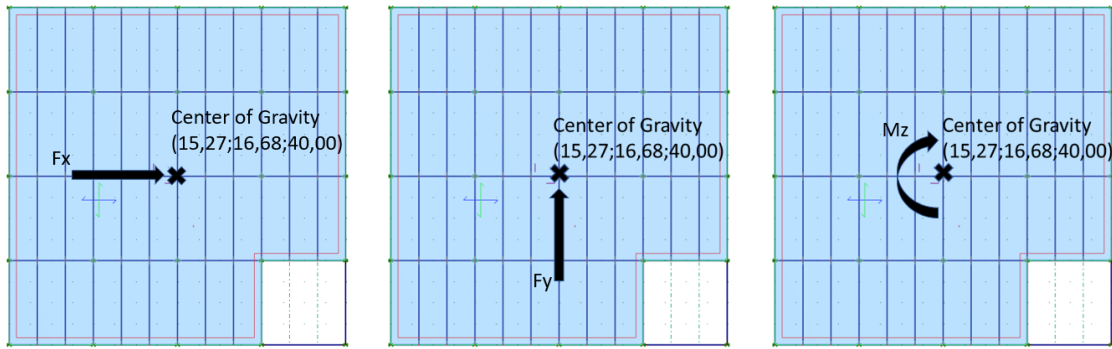


Figure 4.11: Calculation of center of rigidity

For each floor three load cases are defined, according to Figure 4.11. Thereafter the center of rigidity is calculated through the following process which has to be repeated in every floor.

- step 1 applies load, $F_x = 10^6 kN$, to the center of mass, such that the node is rotated $R_z(F_x)$.
- step 2 applies load, $F_y = 10^6 kN$, at the same point, causing rotation $R_z(F_y)$
- step 3 applies moment, $M_z = 10^6 kNm$ about z - axis, causing rotation $R_z(M_z)$.
- step 4 calculates the eccentricities, in respect of the center of mass as $e_x = -R_z(F_y)/R_z(M_z)$ and $e_y = R_z(F_x)/R_z(M_z)$.

The results of the aforementioned analysis can be seen in the following table:

Table 4.4: Calculation of eccentricities

Storey	$R_z(F_x)$ (Rad)	$R_z(F_y)$ (Rad)	$R_z(M_z)$ (Rad)	e_x (m)	e_y (m)
1st	-9.00E-3	-5.00E-3	5.00E-3	1.00	-1.82
2nd	-4.60E-2	-1.80E-2	1.40E-2	1.29	-3.29
3rd	-9.40E-2	-3.30E-2	2.40E-2	1.38	-3.91
4th	-1.46E-1	-5.00E-2	3.50E-2	1.43	-4.17
5th	-2.12E-1	-6.90E-2	4.90E-2	1.41	-4.33
6th	-2.88E-1	-9.10E-2	6.30E-2	1.44	-4.57
7th	-3.70E-1	-1.17E-1	8.10E-2	1.44	-4.57
8th	-4.62E-1	-1.46E-1	1.02E-1	1.43	-4.53
9th	-5.57E-1	-1.80E-1	1.25E-1	1.44	-4.46
10th	-6.58E-1	-2.17E-1	1.52E-1	1.43	-4.33

4.4.2 Torsional radius

Furthermore, the torsional radius need to be determined. For this purpose a similar procedure is followed, in agreement with P. Bisch [2012]. The torsional radius (r_x, r_y) is defined as the square root of the ratio of the torsional stiffness ($K_t(M_z)$) to the lateral stiffness in one direction ($K_x(F_x)$, $K_y(F_y)$).

$$r_x = \sqrt{\frac{K_t(M_z)}{K_y(F_y)}} \quad \text{and} \quad r_y = \sqrt{\frac{K_t(M_z)}{K_x(F_x)}} \quad (4.3)$$

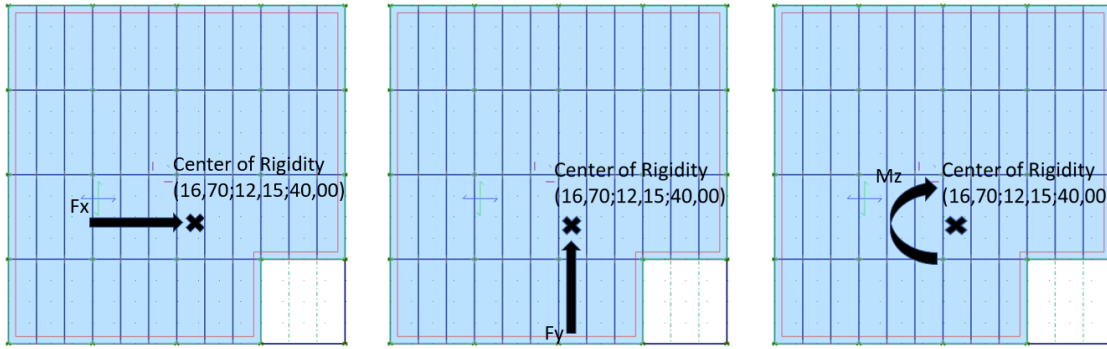


Figure 4.12: Calculation of torsional radius

The procedure for the determination of the torsional and lateral stiffness is similar to that for the determination of structural eccentricity. Three static load cases are defined for each storey level, and loads are represented by F_x , F_y and M_z , respectively. The forces and moment are applied in the centre of rigidity. The torsional and lateral stiffness for both directions are calculated as follows:

$$K_t(M_z) = \frac{1}{R_z(M_z)}, \quad K_x(F_x) = \frac{1}{U_x(F_x)}, \quad K_y(F_y) = \frac{1}{U_y(F_y)} \quad (4.4)$$

where $R_z(M_z)$ is the rotation of each storey about the vertical axis due to applied moment, $U_x(F_x)$ is the displacement of each storey in direction X and $U_y(F_y)$ is the displacement in direction Y. The applied loads are: $F_x = 10^6 kN$, $F_y = 10^6 kN$ and $M_z = 10^6 kNm$.

Table 4.5: Calculation of torsional radius

Storey	$U_x(F_x)$ (m)	$U_y(F_y)$ (m)	$R_z(M_z)$ (Rad)	r_x (m)	r_y (m)
1st	1.14	2.36	5.00E-3	21.72	15.10
2nd	4.04	5.42	1.40E-2	19.65	16.97
3rd	7.51	8.62	2.40E-2	18.94	17.68
4th	11.39	12.28	3.50E-2	18.74	18.04
5th	16.20	18.53	4.90E-2	19.44	18.18
6th	21.83	22.53	6.30E-2	18.92	19.23
7th	28.18	27.48	8.10E-2	18.38	18.61
8th	35.61	34.56	1.02E-1	18.41	18.67
9th	43.82	42.98	1.25E-1	18.57	18.73
10th	53.00	53.07	1.52E-1	18.15	18.15

From Tables 4.4 and 4.5, it is obvious that $e_x \leq 0.30r_x$ and $e_y \leq 0.30r_y$ in any case. Hence, this criterion is fulfilled. Finally, for meeting the criteria for regularity in plan, the radius of gyration of the floor mass (l_s) is also needed. The radius of gyration is determined as the square root of mass moment of inertia over mass in every storey level. These two quantities are given as output from *Robot*. Looking at Table 4.6 it is clear that $r_x, r_y > l_s$ in every case. Therefore the structure is characterized as **regular in plan**, according to EN1998-1 [2004].

Table 4.6: Radius of gyration

<i>Storey</i>	<i>Mass (Kg)</i>	<i>I_z (Kgm²)</i>	<i>l_s (m)</i>
1st to 4th	4.75E+5	1.55E+8	13.20
5th to 7th	4.68E+5	1.51E+8	13.15
8th to 10th	4.65E+5	1.49E+8	13.11

4.5 Modal response spectrum analysis

Since the critical eigenmodes and eigenperiods and the corresponding mass participation factors have been determined, the next step is the implementation of the modal response spectrum analysis. For this reason it is essential the elastic response spectrum to be determined and consequently the design response spectrum, see Section A.2.

- Soil type A: values of T_B , T_C , T_D and S can be found in Table B.1.
- The reference peak ground acceleration is decided to be $a_{gR} = 0.35g$.
- The building is classified as importance class II and the corresponding importance factor amounts to $\gamma_i = 1.0$
- Therefore the peak ground acceleration is equal to the reference peak ground acceleration $a_g = \gamma_i a_{gR} = 0.35g$
- The elastic response spectrum was defined for damping 5%

For the design response spectrum the behaviour factor q , which depends on the type of the structural system, regularity in elevation and plan, and ductility class should be determined. As it is turned out in Section 4.4 the structure meets the regularity criteria. Moreover the structure will be designed with a medium ductility class. Finally, the structural system is different in direction X and direction Y and due to the presence of the elevation shaft is difficult to be categorized in one structural system. Therefore a conservative estimation of the behaviour factor has been done, $q = 3.0$.

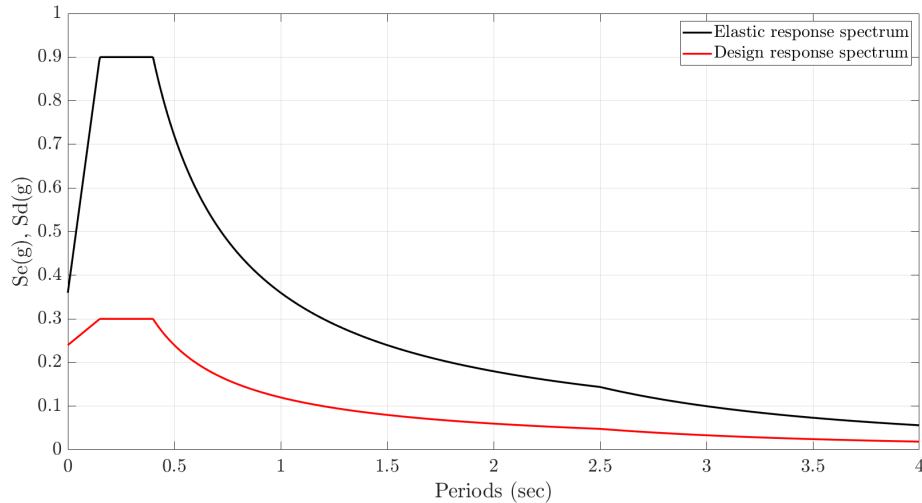


Figure 4.13: Elastic and design response spectrum

Modal response spectrum analysis is performed independently for the ground excitation in principal horizontal directions, hence the design spectrum is used accordingly in X and Y direction. The two critical eigenperiods, as they are determined in Section 4.2, are $T_1 = 2.00\text{sec}$ and $T_2 = 1.87\text{sec}$ for the Y and X direction respectively. It is straight-forward, by looking at Figure 4.13, that relatively small values of spectral accelerations are applied for those two critical eigenperiods. The combination of different mode shapes is implemented by use of *CQC* rule, see Appendix A.3. Moreover the torsional effects are taken into account by applying accidental eccentricities equal to 5% of the floor dimensions, according to EN1998-1 [2004].

The resultant base shear forces out of modal response spectrum analysis can be seen in Figures 4.14 and 4.15. As it was expected, slightly higher base shear force is applied in the Y-direction, due to the fact that the fundamental period in the this direction, T_2 is slightly lower than the fundamental period in the X-direction, T_1 . Therefore, it results to higher spectral accelerations in correlation with the fundamental eigenmodes ($S_d(T_1) = 0.06g$, $S_d(T_2) = 0.064g$). However the difference of the base shear between two directions is insignificant.

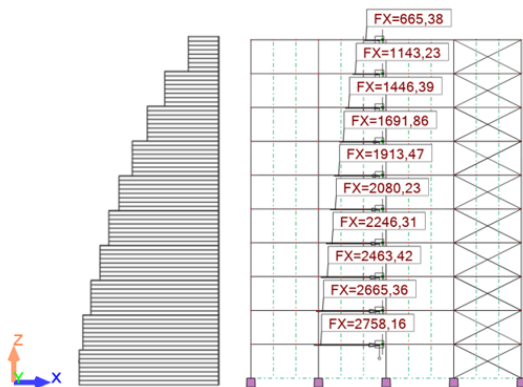


Figure 4.14: Storey shear forces along the elevation for X-direction

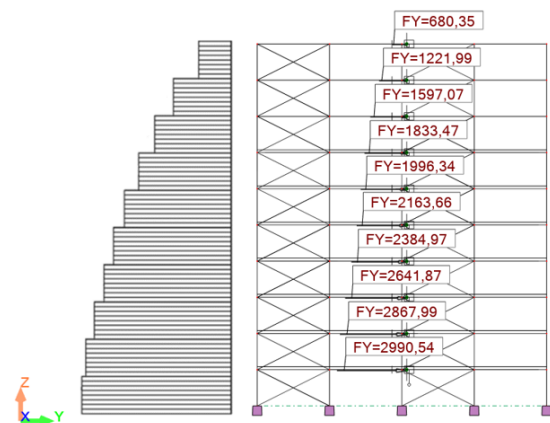


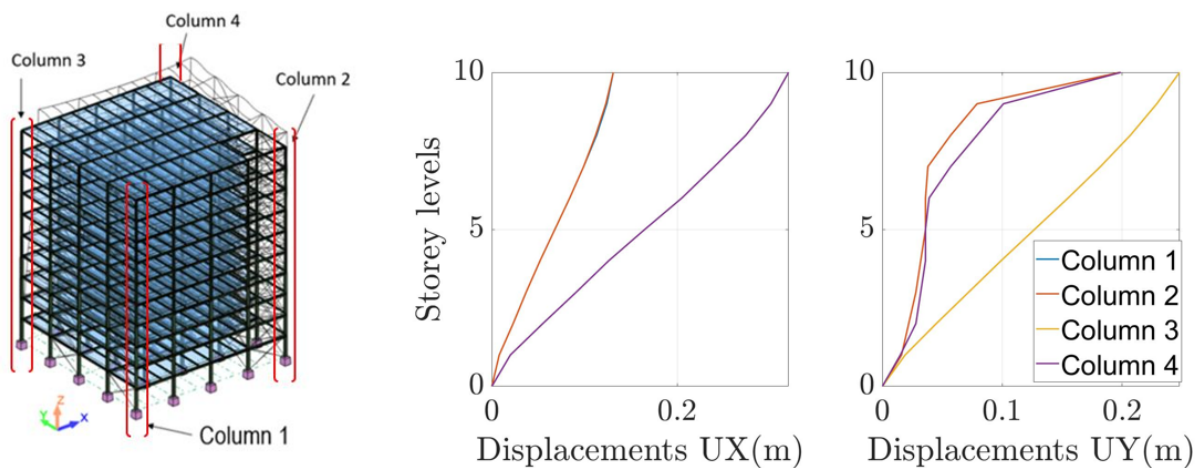
Figure 4.15: Storey shear forces along the elevation for Y-direction

According to P. Bisch [2012], a quick validation of the calculated base shear can be done by comparing it with the upper and lower bound values of base shear. Upper bound value can be calculated by multiplying the total mass of the structure with the design spectral acceleration at the fundamental period in the relevant direction. Considering $M_{total} = 4.70E + 6Kg.$ and $Sd(T = 2.00s) = 0.061g$ in direction X and $Sd(T = 0.066s) = 0.064g$ in direction Y, the upper bound values for base shear, shown in Table 4.7 are obtained. The lower bound values can be obtained in a similar way, but considering the effective mass for the relevant fundamental mode 55.47% and 63.09%, see Table 4.2, of the total mass. As it can be seen, the calculated base shear is close to the upper bound.

Table 4.7: Base shear forces

Base shear	Lower bound (kN)	Upper bound (kN)	Calculated value (kN)
Direction X	1560	2813	2758
Direction Y	1920	3043	2990

In Figure 4.16, the corner columns' displacements out of the first load combination ($1.00G + 0.3Q + E_{Edx} + 0.3E_{Edy}$) are illustrated, see Section 3.5. The columns are displaced equally in pairs, in X direction. The displacements of the first and second columns are the same in X-direction, as well as the third column is displaced the same amount as the fourth column. In contrast, in Y-direction, the first and third columns are displaced equally. However, there is a small difference between column two and four. The maximum displacement is observed in the X direction on the top node of column four (three) and it amounts to $0.32m$. Accordingly the maximum displacement in Y-direction amounts to $0.25m$ and it is observed on the top node of column one (three).

Figure 4.16: Corner columns' displacements for the first combination ($1.00G + 0.3Q + E_{Edx} + 0.3E_{Edy}$)

A better view of deformed shape is given in Figure 4.17. The displacements of the two corner columns in each direction are illustrated. Moreover a better view of the columns' relative displacements as well as storey levels' relative displacements is given. It is clear that torsional effects are developed in both directions due to the increased stiffness in the location of elevation shaft.

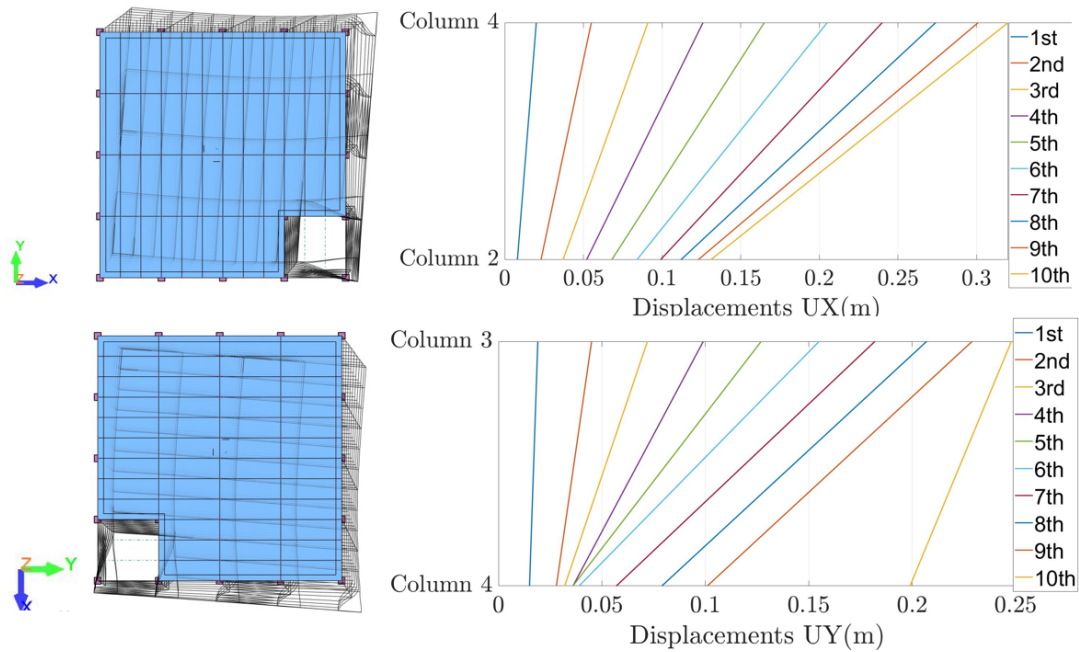


Figure 4.17: Corer columns' displacements in plan, for the first combination $(1.00G + 0.3Q + E_{Edx} + 0.3E_{Edy})$

Furthermore, the developed internal forces for the first load combination $(1.00G + 0.3Q + E_{Edx} + 0.3E_{Edy})$ can be seen in the following figures. It is clear that the induced base shear in X-direction is mainly resisted by the moment frames. As a result large bending moments and shear forces are developed in this direction. On the other hand, the applied base shear in Y-direction is mainly resisted by axial forces. Therefore the developed bending moments and shear forces are insignificant in this direction. As a comparison, the maximum and the minimum bending moment in X-direction is $207.02kN$ and $-394.67kN$ respectively while in Y-direction they are $9.72kN$ and -33.53 . Hence, the shear forces are distributed accordingly, see Figures 4.20 and 4.21.

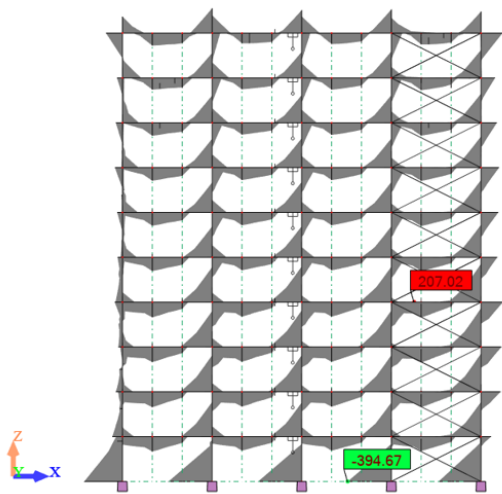


Figure 4.18: Bending moments in X-direction out of the load combination $1.00G + 0.3Q + E_{Edx} + 0.3E_{Edy}$

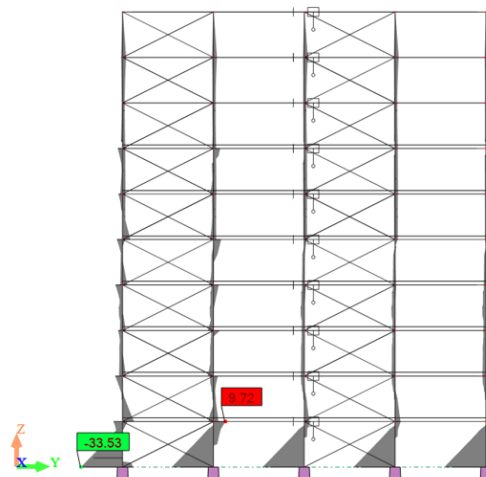


Figure 4.19: Bending moments in Y-direction out of the load combination $1.00G + 0.3Q + E_{Edx} + 0.3E_{Edy}$

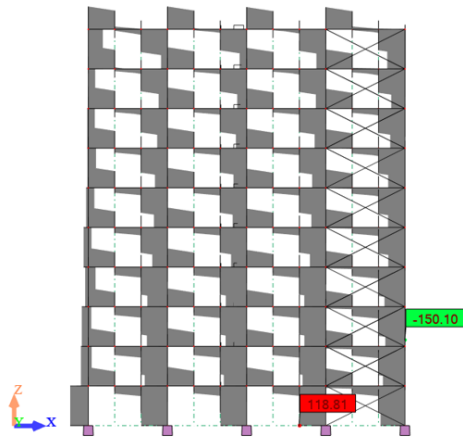


Figure 4.20: Shear forces in X-direction out of the load combination $1.00G + 0.3Q + E_{Edx} + 0.3E_{Edy}$

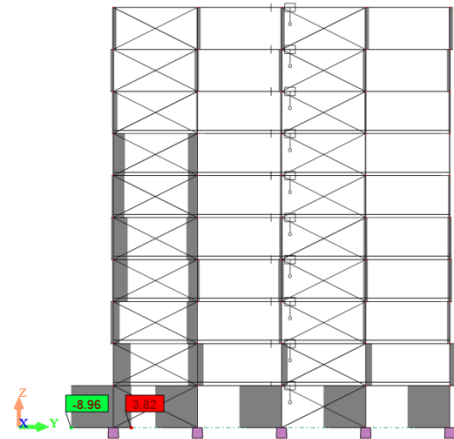


Figure 4.21: Shear forces in Y-direction out of the load combination $1.00G + 0.3Q + E_{Edx} + 0.3E_{Edy}$

In Figure 4.22 a better view of the concentrically braced frame's truss behaviour is given. It can be seen that bracing bars develop axial forces. Moreover one associated column, out of two braced columns, is under compression while the second one is under tension. The maximum axial force amounts to $3014.07kN$ and the minimum $-693.91kN$. Therefore, the developed axial force due to the induced base shear, for the column which is under tension, not only neutralizes the gravitational axial force but it is higher. As a result the column is subjected to tension. On the other, the associated braced column is subjected to compression not only due to gravitational forces but also due to the induced base shear. This is evidence of truss behaviour of concentrically braced frames.

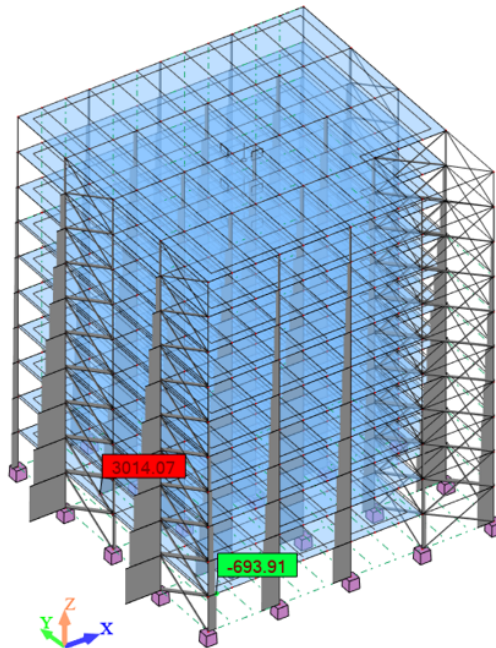


Figure 4.22: Axial forces out of load combination $1.00G + 0.3Q + E_{Edx} + 0.3E_{Edy}$

4.6 Equivalent static method of analysis

In the case of the investigated structure, the equivalent static method is allowed, because both requirements in EN1998-1 [2004] are satisfied. The structure is categorized as being regular in elevation and in plan, see Section 4.4, and the fundamental mode periods in both directions ($T_x = 2.00sec$ and $T_y = 0.87sec$) are equal or smaller than $2sec$. Even though, the reference structure in this report was analysed by modal response spectrum analysis (Section 4.5), the output of the equivalent static method is presented in this section. According to EN1998-1 [2004] the reference method is the modal response spectrum and it is considered as more accurate than the lateral force method.

The fundamental period, in this case, is calculated by the approximate formula recommended in EN1998-1 [2004].

$$T_1 = C_t H^{0.75} \quad (4.5)$$

where H is the total height of the building. The coefficient C_t is decided to be equal to 0.0085 in X-direction considering that the building in this case is consisted of moment resisting frames. In Y-direction the building is structured by concentrically braced frames, hence the coefficient C_t amounts to 0.0075. The fundamental periods in X and Y directions are calculated $1.35sec$ and $1.19sec$

It has to be noticed that there is a significant difference with the fundamental period calculated out of modal analysis, $T_1 = 2.00sec$ and $T_2 = 1.87sec$. The reason why is that the empirical formula is based on structure's characteristic, such as dimensions and material, with the tendency of underestimating the period in order to conservatively estimate the base shear, see Chopra A. K. & Goel R. K. [2000]

Next step is the calculation of the base shear force. The seismic base shear force F_b for each horizontal direction is determined by the following expression:

$$F_b = \lambda M_{total} S_d(T) \quad (4.6)$$

where λ is a constant which amounts to 1.00, since for both horizontal principal direction the calculated fundamental periods are higher than $2T_C$. The total mass of the structure is represented by the constant M_{total} and it is equal to $4.70E + 6Kg$. The spectral accelerations, $S_d(t)$, are determined for the corresponding fundamental periods from the design spectrum in Figure 4.13. Therefore they are defined as $S_d(T_x = 1.35) = 0.088g$ and $S_d(T_y = 1.19) = 0.1g$.

By comparison of the calculated base shear of equivalent static method and the base shear out of modal response spectrum analysis (see Table 4.7) a huge difference is observed. This is mainly caused by the crude approximation of the fundamental eigenperiods. Hence, this is one of the reasons that the modal response spectrum analysis is considered as a more accurate method. An other reason is that the equivalent static method takes into consideration only the two principal eigenmodes and it neglects the higher eigenmodes. In this analysis this is obvious since the modal response spectrum takes into consideration seven eigenmodes, see Section 4.5.

Table 4.8: Base shear force of equivalent static method

Direction	Base shear (kN)
X	4060
Y	4601

Thereafter the horizontal forces are distributed in every floor according to the following equation. In this case, the fundamental mode shape is approximated by horizontal displacements increasing linearly along the height.

$$F_k = F_b \frac{z_k m_k}{\sum_{j=1}^k z_j m_j} \quad (4.7)$$

where m_k (m_j) are the storey masses and z_k (z_j) are the heights of the masses above the ground level, see Appendix A.

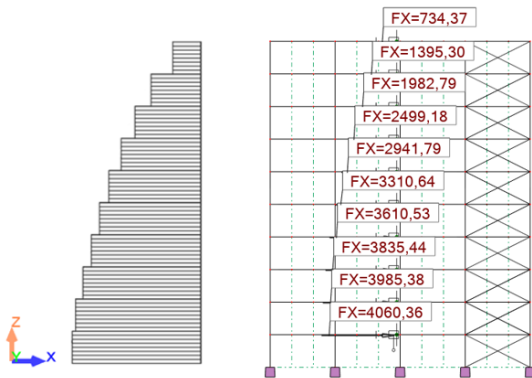


Figure 4.23: Storey shear forces along the elevation for X-direction

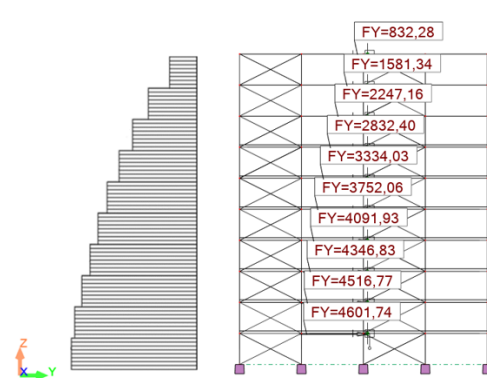


Figure 4.24: Storey shear forces along the elevation for Y-direction

To be in consistence with the modal response spectrum analysis, the corner columns' displacements, out of the first load combination, $1.00G + 03Q + 1.00E_{Edx} + 0.3E_{Edy}$, can be seen in Figure 4.25. Again, the columns are displaced equally in pairs. However in this case, as it is expected due to the overestimated base shear, the displacements are higher. The maximum displacement in X-direction is $0.55m$ while the maximum displacement out of modal response spectrum analysis is $0.32m$. In Y-direction, the maximum displacements are $0.26m$ out of equivalent static method and $0.25m$ out of modal response spectrum analysis.

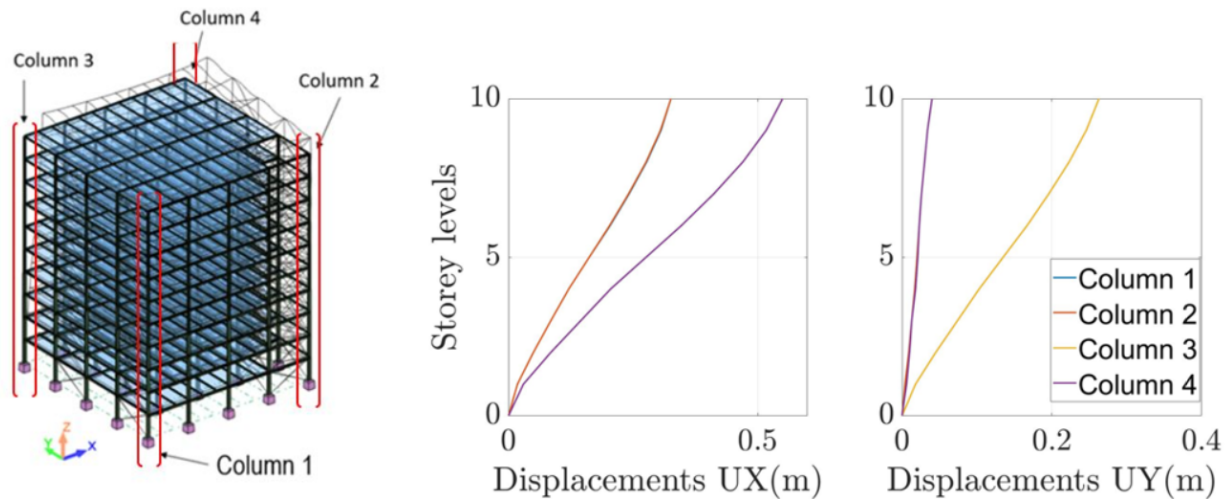


Figure 4.25: Corner columns' displacements for the first combination ($1.00G + 0.3Q + E_{Edx} + 0.3E_{Edy}$)

The displacements in plan can be seen in Figure 4.26. It is obvious that torsional effect is developed due to concentrated stiffness in the area of elevation shaft. Moreover, the storey drift can be seen through the distance between lines. It is clear that the drift is more significant in the lower levels since there is larger distance between the lines.

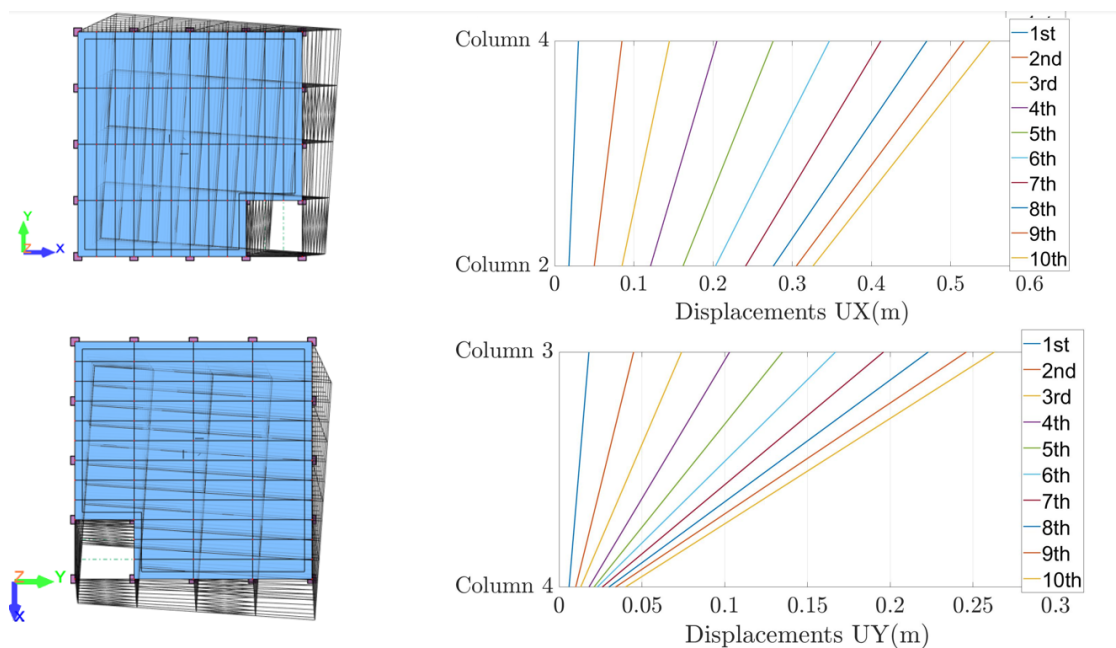


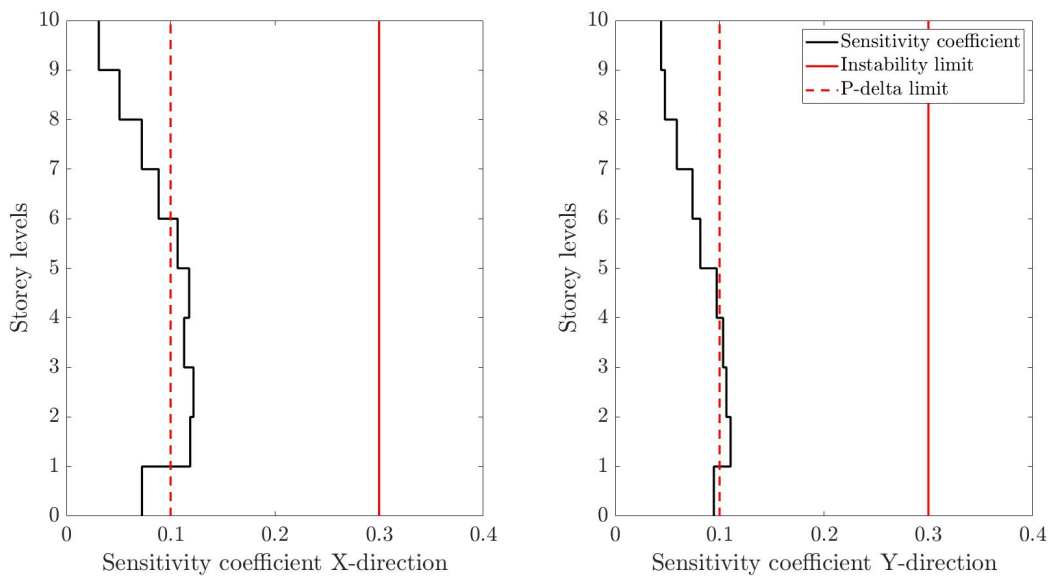
Figure 4.26: Corner columns' displacements in plan, for the first combination ($1.00G + 0.3Q + E_{Edx} + 0.3E_{Edy}$)

4.7 Criterion of the second order effects

The criterion for taking into account the second order effect is based on the inter-storey drift sensitivity coefficient, θ , as it is described in Section 3.3.1. The sensitivity coefficients along the elevation for both directions are determined in Table 4.9. The inter-storey drift has been chosen for the most unfavourable load combination.

Table 4.9: Determination the inter-storey drift sensitivity coefficient θ

Storey	P_{tot} (kN)	$V_{tot,X}$ (kN)	$V_{tot,Y}$ (kN)	$d_{r,X}$ (m)	$d_{r,Y}$ (m)	θ_X	θ_Y
1st	4.71E+4	2.76E+3	2.99E+3	1.70E-2	2.40E-2	7.25E-2	9.45E-2
2nd	4.23E+4	2.67E+3	2.87E+3	3.00E-2	3.00E-2	1.18E-1	1.11E-1
3rd	3.75E+4	2.46E+3	2.64E+3	3.20E-2	3.00E-2	1.12E-1	1.06E-1
4th	3.28E+4	2.25E+3	2.38E+3	3.10E-2	3.00E-2	1.13E-1	1.03E-1
5th	2.80E+4	2.08E+3	2.16E+3	3.50E-2	3.00E-2	1.18E-1	9.72E-2
6th	2.33E+4	1.91E+3	2.00E+3	3.50E-2	2.80E-2	1.07E-1	8.15E-2
7th	1.87E+4	1.69E+3	1.83E+3	3.20E-2	2.90E-2	8.85E-2	7.40E-2
8th	1.40E+4	1.45E+3	1.60E+3	3.00E-2	2.70E-2	7.24E-2	5.90E-2
9th	0.93E+4	1.14E+3	1.22E+3	2.50E-2	2.50E-2	5.10E-2	4.76E-2
10th	0.46E+4	6.65E+2	6.80E+2	1.80E-2	2.60E-2	3.11E-2	4.40E-2

Figure 4.27: Sensitivity coefficient θ for both directions

In the case of the investigated building the second order effects do not cause any instability as it can be seen in Figure 4.27. However they have to be taken into account in the design process due to the fact that the sensitivity coefficient is higher than the limit of 0.1. According to EN1998-1 [2004], second order effects may be approximately accounted for in seismic action effects through the multiplier $1/(1 - \theta)$. Therefore, this multiplier increases the resultant bending moments, shear and axial forces of the earthquake effect. The multiplier is determined according to the maximum sensitivity coefficient, $\theta = 0.1850$. In this way, the **geometric nonlinearities** are taken into consideration while a linear elastic analysis is implemented.

4.8 Steel members validation

A critical step of designing procedure is the code checks of steel members. The elements are analysed for the load combinations, $1.00G + 0.3Q \pm E_{Edx} \pm 0.3E_{Edy}$ and $1.35G + 1.5Q$, according to EN1993-1-1 [2005]. For this project, only the relative with *Ultimate limit state* provisions are taken into account. Furthermore, for every element a critical load combination is determined. According to this, it is decided whether the dimensions of the cross section are sufficient or not. Moreover, some basic assumptions are made and they are presented below:

- The columns are considered as pinned at both ends so that the buckling length is conservatively estimated.
- The moment diagram of columns is considered that varies linearly in both directions.
- For main beams, the buckling length around Z-axis (local coordinate system, see Figure 4.28) is taken as $2.66m$ due to the fact that they are braced from the gravity beams. The same approach is adopted for the lateral buckling length of upper flange.
- The moment diagram of main beams is considered as uniform-loaded-fixed-beam shape in Z-axis (local coordinate system) and as varying-linearly shape in Y-axis (local coordinate system).
- The gravity beams are considered as totally engaged with the reinforced slab. Therefore nor torsional, flexural-torsional buckling neither lateral buckling checks are implemented.
- The bracing bars are assumed to resist only axial tensile actions without developing bending moments. Therefore no buckling checks are implemented.
- Due to the slabs rigid diaphragm behaviour, the main as well as the gravity beams do not develop any axial force.
- the code checks are applied in ten points along element's length.

Hereafter, the implemented code checks for the fifth column are presented. The position of the column can be seen in Figure 4.28 and the critical load combination is: $1.00G + 0.3Q + E_{Edx} - 0.3E_{Edy}$. It has to be noticed that a local coordinate system is used for element's cross sections. The X-axis coincides with the longitudinal dimension of the element, the Z-axis and Y-axes concur with the strong and the weak axis of the cross section, respectively, see Figure 4.28. Finally, in the same figure, the design internal forces are illustrated. The strong axis of this element is aligned with X-axis of the global coordinate system, hence this column resist the seismic actions in X-direction, as part of the moments resisting frame. Therefore, the design bending moment around Y-axis (local coordinate system) (M_y), the shear force in Z-axis (V_z) and the axial force (N) are the critical internal forces for this element. On the other hand, in Y-axis of the global coordinate system, this column belongs to the concentrically braced frame, hence the horizontal actions in this direction are resisted mainly by the bracing system along with the associated columns. Therefore, the bending moment M_z and the shear force V_y are insignificant.

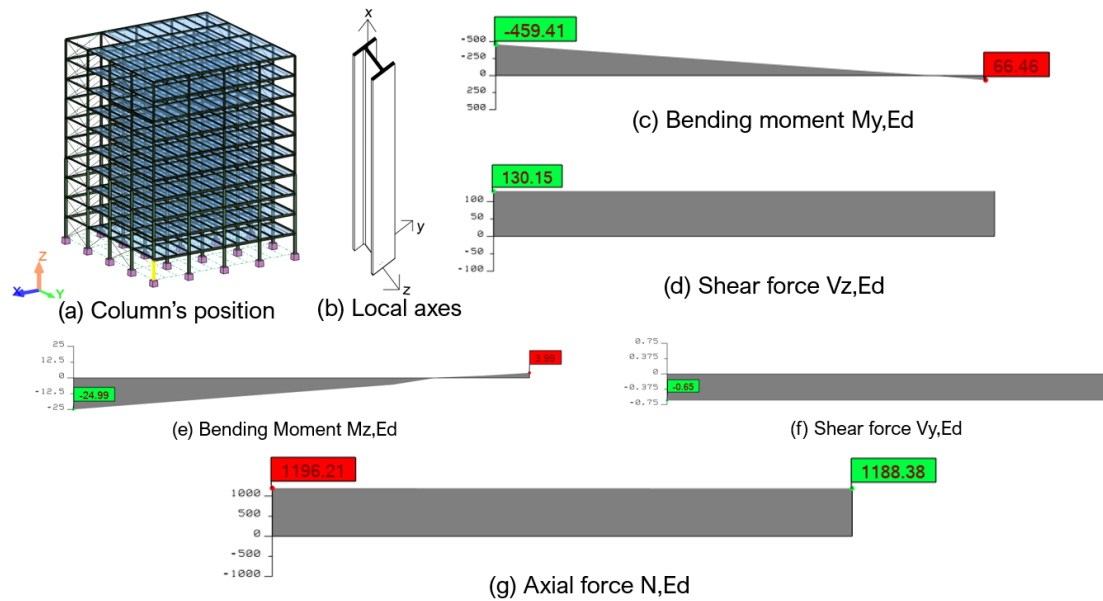


Figure 4.28: Internal forces of column 5 out of load combination $1.00G + 0.3Q + E_{Edx} + 0.3E_{Edy}$

According to internal forces diagrams the critical cross sections are located at the bottom of the column. Initially the classification of the cross section is **Class 1**. It has to be mentioned that all the structural elements of the building are designed so that they are classified as class 1 or class 2. Consequently the ductility criterion, see Table 3.1, is fulfilled.

Initially, the cross section strength check are applied, according to EN1993-1-1 [2005]. The design resistance for uniform compression, bending moment and shear force about principal axes is validated. Moreover, combinations of the aforementioned actions are considered. It has to be mentioned that torsional actions are taken into account, even though their effects are of minor importance.

Table 4.10: Cross section strength check

Code check	Result	limit
$N_{Ed}/N_{c,Rd}$	0.13	1.00
$M_{y,Ed}/MN_{y,Rd}$	0.23	1.00
$M_{z,Ed}/MN_{z,Rd}$	0.01	1.00
$[M_{y,Ed}/MN_{y,Rd}]^a + [M_{z,Ed}/MN_{z,Rd}]^b$	0.06	1.00
$V_{y,Ed}/V_{y,Rd}$	0.01	1.00
$V_{z,Ed}/V_{z,Rd}$	0.01	1.00

Then, the global stability check of member is examined. Instability may occur in members where compression stresses exist. Compression stresses are caused due to bending moments, or due to compressing axial force. Therefore the most susceptible members are the columns, since they combine both high axial forces and bending moments. According to EN1998-1 [2004], the members are validated against flexural-torsional buckling and lateral-torsional buckling.

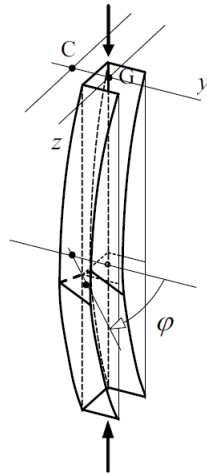


Figure 4.29: Flexural-torsional buckling, [Luis S. da Silva, 2010]

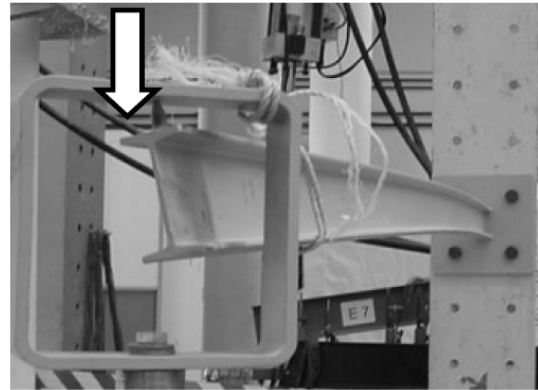


Figure 4.30: Lateral-torsional buckling, [Luis S. da Silva, 2010]

According to Luis S. da Silva [2010], *flexural torsional buckling consists of the simultaneous occurrence of torsional and bending deformations along the axis of the member and lateral-torsional buckling is characterized by lateral deformation of the compressed part of the cross-section.* The results of the above-mentioned code checks are illustrated on Tables 4.11 and 4.12. More information about steel member design procedure can be found in EN1993-1-1 [2005]. Moreover the calculation note of column 5, see Figure 4.28, can be found in Appendix E.

Table 4.11: Flexural-torsional buckling check

Flexural-torsional buckling
$N_{Ed}/\min(N_{b,Rd}, N_{b,T,Rd}, N_{b,TF,Rd}) = 0.17 < 1.00$
$M_{y,Ed,max}/M_{b,Rd} = 0.23 < 1.00$

Table 4.12: Lateral-torsional buckling check

Lateral-torsional buckling
$N_{Ed}/(\chi_y N_{Rk}/\gamma_{M1}) + k_{yy} M_{y,Ed}/(\chi_{LT} M_{y,Rk}/\gamma_{M1}) + k_{yz} M_{z,Ed}/(M_{z,Rk}/\gamma_{M1}) = 0.31 < 1.00$
$N_{Ed}/(\chi_z N_{Rk}/\gamma_{M1}) + k_{zy} M_{y,Ed}/(\chi_{LT} M_{y,Rk}/\gamma_{M1}) + k_{zz} M_{z,Ed}/(M_{z,Rk}/\gamma_{M1}) = 0.27 < 1.00$

4.9 Capacity design

For each structural type, modern seismic codes define structural members that should dissipate energy during the ground motion by means of their hysteretic behaviour (dissipative members) and members that should remain elastic, M. Bosco [2014]. The ten-storey building under consideration contains two different structural types, moment resisting frames and concentrically braced frames. As it is stated in Section 3.3 some specific requirements need to be satisfied so that the structure is considered as capacity designed.

The moment resisting frames resist the seismic actions in X-direction. Initially the general requirement of capacity design, as it is stated in Section 3.3 (Equation 3.3), need to be fulfilled.

According to this requirement the dissipative elements of moment resisting frames are the beams, while the columns is expected to remain elastic. Therefore the minimum plastic moment resistance of columns is compared with the maximum moment resistance of associated beams in every joint. It has to be mentioned that only the beams in X-direction are taken into account, due to the fact that the beams in Y-direction are considered as pinned. Hence it is not expected to develop any bending moment. The code checks are implemented for the most unfavourable joints.

Table 4.13: Member cross section in every floor

Storey	Columns	Primary beams	$\sum M_{Rc} / \sum M_{Rb}$
1st	2 HEB550	2 HEA400	1.09 < 1.3
2nd	2 HEB550	2 HEA400	1.26 < 1.3
3rd	2 HEB550	2 HEA400	1.06 < 1.3
4th	1 HEB550 1 HEB400	2 HEA400	1.55 > 1.3
5th	2 HEB400	2 HEA340	1.41 > 1.3
6th	2 HEB400	2 HEA340	1.52 > 1.3
7th	1 HEB400 1 HEB340	2 HEA340	1.29 < 1.3
8th	2 HEB340	2 HEA340	1.15 < 1.3
9th	2 HEB340	2 HEA340	1.20 < 1.3
10th	1 HEB340	2 HEA340	0.61 < 1.3

It can be seen that the capacity design of *strong columns-weak beams* ($\sum M_{Rc} \geq 1, 3 \sum M_{Rb}$) is not satisfied. The structure need to be re-designed with smaller dimensions of beams. However, in this project the structure's cross sections remain the same and the overall behaviour of the structure is evaluated by means of nonlinear analysis.

4.9.1 Over-strength parameter

Next step is to calculate the minimum over-strength parameter Ω , see Section 3.3. For the structure under examination, which contains both moment resisting and concentrically braced frames, two parameters are defined. Then the maximum between them is chosen.

Initially, a parameter Ω_1 is calculated out of primary beams. It is calculated separately for *HEA400* and *HEA340*. For each cross section the higher bending moment out of earthquake design situation, $M_{Ed,E}$, is chosen so that, the minimum over-strength parameter is obtained, $\Omega_1 = M_{pl,Rd}/M_{Ed}$. Therefore Ω_1 amounts to 2.31, which is the minimum value between the two of them.

Table 4.14: Over-strength parameter Ω_1

Cross section	$M_{pl,Rd}$ (kNm)	$max M_{Ed}$ (kNm)	Ω_1
HEA400	909.22	392.05	2.31
HEA340	656.57	280.30	2.34

Secondly, an over-strength parameter, Ω_2 is calculated for the concentrically braced frames. Now, the definition of this parameter is different, since it is defined as the minimum value of axial brace over-strength of all diagonals. Therefore the maximum value of diagonals' axial force is chosen so that the minimum over-strength parameter is obtained, $\Omega_2 = N_{pl,Rd}/N_{Ed}$. It has to be noticed that

the obtain values out of modal response spectrum analysis, for the bracing elements, are multiplied by the factor 2, because a reduced axial stiffness is adopted, see Section 4.1.1.

Table 4.15: Over-strength parameter Ω_2

Cross section	$N_{pl,Rd}$ (kN)	$maxN_{Ed}$ (kN)	Ω_2
UPE270	1366.76	809.38	1.68

Therefore, Ω is equal to 2.34. Next step is two validated the steel elements against seismic action as it is described in Section 4.8. However, in this case the seismic action has to multiplied by Ω and a safety factor, $\gamma_{ov} = 1.25$, according to EN1998-1 [2004]. Therefore, the load combinations are now modified as Equation 4.8. The above-mentioned modification is implemented so that the requirements, which are described in Section 3.3 (Equations 3.4, 3.5 and 3.7) to be validated.

$$E_d = 1.00G + 0.3Q \pm 1.1\gamma_{ov}\Omega(A_x \pm 0.3A_y) \quad (4.8)$$

Response assessment by means of nonlinear analysis

5

In this chapter, the response assessment of ten-storey steel building is implemented by means of nonlinear analysis. Initially, the aspects of nonlinear analysis and the simulation procedure are described. Thereafter, static and dynamic nonlinear analysis are conducted, by use of the commercial finite element software, Seismostruct.

5.1 Aspects of nonlinear analysis

According to R.D.Cook [2002] the nonlinear behaviour admits a wide variety of phenomena, possibly interacting one with each another and it might be difficult to formulate. In structural mechanics, material might yield, local buckling phenomena may arise and gaps might open. Therefore the types of nonlinearity include the following:

- **Material nonlinearity**, in which material properties depend on stress or strain.
- **Contact nonlinearity**, in which a gap between to parts may open or close
- **Geometric nonlinearity**, in which deformation is large enough that equilibrium equations must be written with respect to the deformed structural geometry.

Problems included in these categories are characterized as nonlinear due to the fact that stiffness and perhaps loads as well, become functions of displacements. Therefore, the solution of equations is no more straightforward as it is in linear problems.

In the framework of this project only the two out of three aforementioned categories are investigated. These are the material and geometric nonlinearities. The first one is taken into account by definition of a adequate constitutive model to the structural elements. In this case, the elements are made out of structural steel, S355. Therefore a bilinear kinematic hardening model is used. The uniaxial bilinear stress-strain model is illustrated in Figure 5.1. More information about constitutive model can be found in Krabbenhøft [2002].

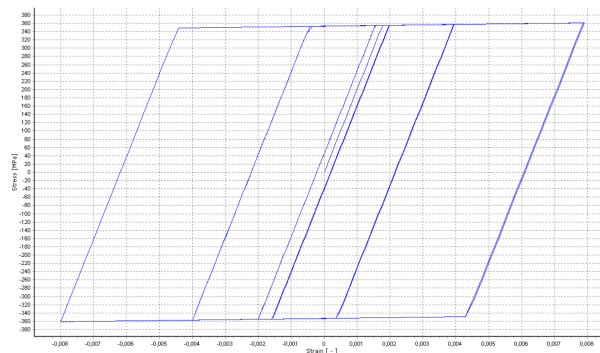


Figure 5.1: Bi-linear kinematic hardening model of steel S355.

The simulation is implemented by use of inelastic force-based frame element type, *infrmFB*. According to Seismosoft [2020], this element type is capable of modelling members of space frames with geometric and material nonlinearities. The sectional stress-strain state of frame elements is obtained through the integration of the nonlinear uniaxial material response of the individual fibres in which the section has been subdivided, see Figure 5.3, fully accounting for the distribution of plasticity along member's length and across the section depth. In line with Seismosoft [2020], single-material sections is usually adequately represented by 100 fibres. In this project, after a brief sensitivity study the number of 150 fibres is assigned.

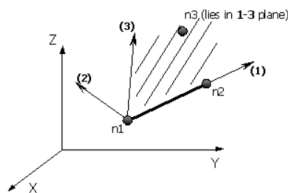


Figure 5.2: Local axes, [Seismosoft, 2020]

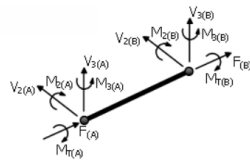
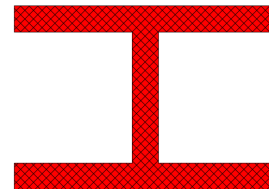


Figure 5.3: Individual section's fibres



Thereafter, the geometric nonlinearity is taken into consideration by assembly of geometric stiffness matrix. In terms of structural elements which are subjected to axial loading, the lateral stiffness can be decreased. As it is illustrated in Figure 5.4 a horizontal rod with axial loading is subjected to lateral displacements. Thus, additional forces F_1 and F_2 must be developed to maintain the equilibrium of the element, see R.D.Cook [2002]. Moreover, a specific category of geometric nonlinearity is the so called $P - \Delta$ effects, see Figure 5.5. They might be of significant importance, especially in high rise buildings.

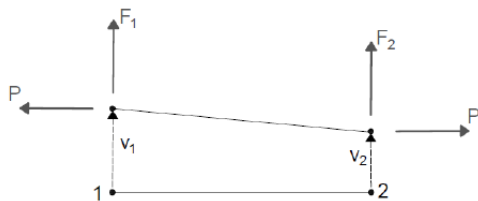
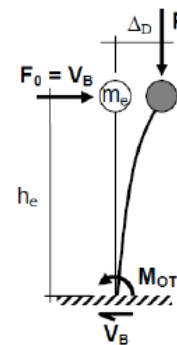


Figure 5.4: Forces acting on a rod element, [R.D.Cook, 2002]

Figure 5.5: Effect of $P - \Delta$ on a cantilever single degree of freedom system [Pettinga and Priestley, 2008]

Finally, since the aforementioned nonlinearities are taken into consideration, the static and dynamic finite element configuration is modified as follows:

- **Static nonlinear analysis:** $[K(D)]\{D\} = [R]$
- **Nonlinear time history analysis:** $[M]\{\ddot{D}\} + [C]\{\dot{D}\} + [K(D)]\{D\} = [R(t)]$

As it can be seen the stiffness matrix is a function of displacements. The solution of these equations

demands an iterative process. In this project the *Newton – Raphson* scheme is used, see R.D.Cook [2002].

5.2 Modeling of bracing system

As it is mentioned in Section 4.1.1, only the bracing bar which subjected to tensile axial forces resists the horizontal actions and the contribution of the compression part should be neglected. For the linear elastic analysis, Chapter 4, this assumption is simulated by considering reduced axial stiffness of the bracing elements. The reduction factor is decided to be 0.5 and both tensile and compressive contribution is taken into account. However, in case of nonlinear analysis a second model is applied and the response of both models is evaluated.

5.2.1 Tension only elements

The tension only bracing system is modelled in *Seismostruct* by use of link elements. A verification example, of a simple concentrically braced frame can be found in Appendix F. The 3D link elements are characterized by uncoupled axial, shear and moment actions. The link elements connect two initially coincident structural nodes and require the definition of an independent force-displacement (or moment-rotation) response curve for each of its local six degrees of freedom, see Figure 5.6. Therefore, they connect the two coincident nodes ($n1$ and $n2$) and the last one is connected with the bracing bar. The other end of the bracing bar is connected to the structural node of beam column joint.

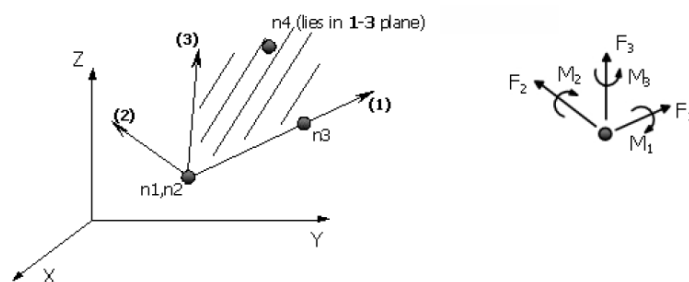


Figure 5.6: Link elements.

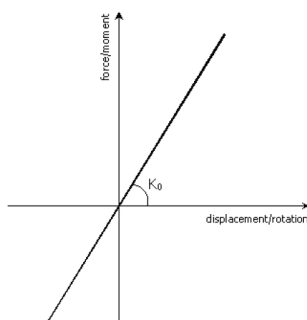


Figure 5.7: Linear symmetric response curve, [Seismosoft, 2020]

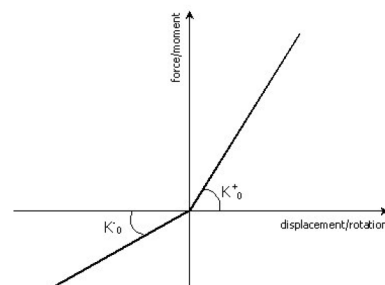


Figure 5.8: Linear asymmetric response curve, [Seismosoft, 2020]

Thereafter, the force-displacement and moment-rotation response curve of the link element should be defined. The response curve of all degrees of freedom, apart of the axial one, are described

by symmetric linear curve, see Figure 5.7, with large stiffness value, due to the fact that they are considered as rigidly linked. The stiffness of the response curve is defined 250 times higher than the expected developed internal forces, according to Seismosoft [2020]. In this point, it has to be mentioned that the bracing bars are allowed to develop only axial forces.

In case of the axial degree of freedom, the adopted response curve is an asymmetric linear curve, see Figure 5.8. For the tensile (positive) stiffness is assigned a value 250 times higher than the expected axial forces, Seismosoft [2020]. Therefore, in this direction the bracing bar is rigidly linked with the associated beam-column joint. For the compressive (negative) zero stiffness should be applied. However, this might cause convergence difficulties, according to Seismosoft [2020], hence a small value, 0.001 is adopted.

5.3 Models' verification

As it is described in Section 4.2, a modal analysis is implemented, so that the boundary conditions and the general response of the finite element model are evaluated. The first 7 eigenmodes are calculated and the results are compared with the output of Section 4.2. Moreover, the results of Rayleigh's method, see Section 4.3, are also taken into consideration. In this case the modal analysis is applied for two models:

- **Model 1:** The concentrically bracing system is simulated by use of link elements. Therefore, tension only bars are considered.
- **Model 2:** The concentrically bracing system is simulated with 50% reduced axial stiffness. Consequently both tensile and compressive bars are considered.

In Figure 5.9, the first two eigenmodes for each model are illustrated. As it can be seen the responses of the two models are identical. The same behaviour is also observed for higher modes.

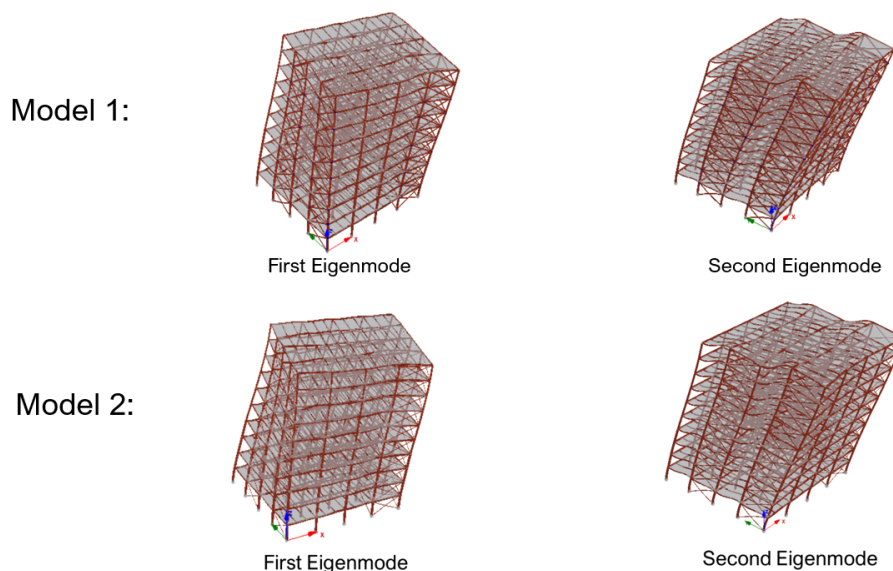


Figure 5.9: First and second mode shape for **Model 1** and **Model 2**

Furthermore, the eigenperiods of the first seven eigenmodes are illustrated in Table 5.1. It has to be noticed that, the output of **Model 2** is identical with the model simulated in *Robot*, Chapter 4. However, there is small deviation for **Model 1**.

Table 5.1: Modal analysis results

Eigenmode	Model 1	Model 2	Error (%)
1st	1.90	2.00	5
2nd	1.60	1.76	9
3rd	1.11	1.22	7
4th	0.61	0.66	9
5th	0.46	0.54	14
6th	0.34	0.39	12
7th	0.32	0.36	11

The error between the calculated eigenperiods can be seen in Table 5.1. As it can be seen, the error between the first three eigenperiods is less than 10%. However, it is slightly increased for higher eigenmodes.

As long as the Rayleigh method concerns, the fundamental eigenperiods are calculated as $1.94sec$ and $1.89sec$ for X and Y direction respectively, see Section 4.3. The agreement between Rayleigh method and **Model 1** is sufficient in X direction. However there is a higher deviation in Y direction.

To sum it up, the error between the two models might be caused due to the defined stiffness of link elements. It is likely, that a lower values for link element's stiffness would be more accurate. It would result in higher values of eigenperiods for **Model 1** due to the reduction of global stiffness and therefore the error between the two models would be lower. In the framework of this project, the response of the models is considered identical due to the fact that the error remains small. However, a further investigation in this topic might be required. Furthermore in this project, the responses of **Model 1**, with tension only bracing bars, and **Model 2**, with reduced axial stiffness of bracing bars, are investigated by means of nonlinear static analysis.

5.4 Nonlinear Static analysis

In this section a static non-linear analysis (Pushover) under permanent vertical loads and gradually increasing lateral loads is implemented. According to EN1998-1 [2004], the vertical loads for a seismic situation are calculated as $1.00G + 0.3Q$, where G represents the dead loads and Q represents the live loads. The earthquake effect is simulated by incremental lateral static nodal loads, distributed over the high of the structure. Lateral load may represent the range of base shear induced by earthquake loading, and its configuration may be proportional to the distribution of mass along building height, mode shapes, or another practical means. Therefore, the building is subjected to a monotonic displacement-controlled lateral load pattern which continuously increases through elastic and inelastic behavior until failure (numerical instability) is reached. The numerical configuration of this problem can be seen below:

$$[K(D)]\{D\} = [R] \quad (5.1)$$

5.4.1 Lateral load distribution

A nominal load value is assigned in every node. It has to be noticed that only the relative value of the load is important, and not the absolute value, due to the fact that the loads are monotonically increased by a load factor λ . As it is mentioned above, load distribution might be done in several ways. In this project the distribution is implemented according to the critical mode shapes.

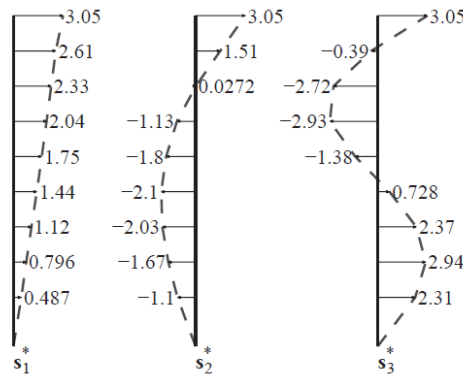


Figure 5.10: Lateral force distributions for the first three modes, [Chopra, 2012]

In case of the structure under investigation, the first eigenmode is the critical one in X-direction and the second eigenmode in Y-direction. Therefore, the load distribution in X-direction is applied proportional to modal displacements UX as they are calculated from the first eigenmode. The loads are applied to nodes where beam and columns are engaged, see Figure 5.11. The same procedure is carried out in Y-direction.

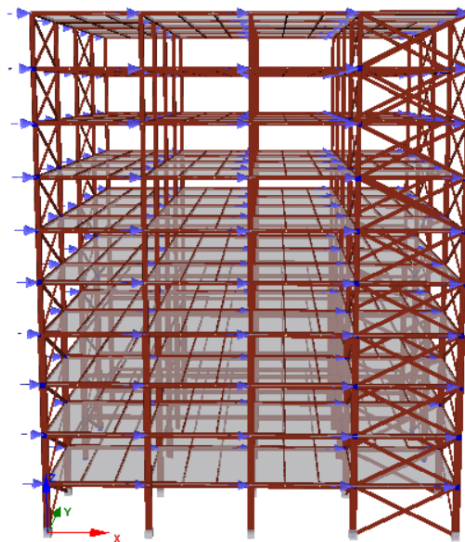


Figure 5.11: Lateral force distributions in a part of the structure (X-direction)

5.4.2 Capacity curve and target displacement

The above-mentioned procedure leads to the capacity curve. The capacity of structure is represented by this curve, which is a load deformation relation and represents the induced base shear and the displacements of a control node. According to EN1998-1 [2004], the control node may be taken at the centre of mass of the top of the building. This procedure is followed in this report. Therefore,

it can be determined whether the building is safe or not by comparing this curve with the target displacement, see Appendix A.5. The target displacement is determined for every limit state.

According to EN1998-1 [2004], three limit states are defined. The response spectrum is modified according to the estimated return period of each limit state, see Figure 5.12. The modification factor is calculated as $(T_{LR}/T_L)^{(-1/\kappa)}$, where T_{LR} is the reference seismic action with return period 475 years and T_L is the return period corresponding to each limit state. The factor κ depending on the seismicity but generally amounts to the order of 3. More information can be found in EN1998-1 [2004].

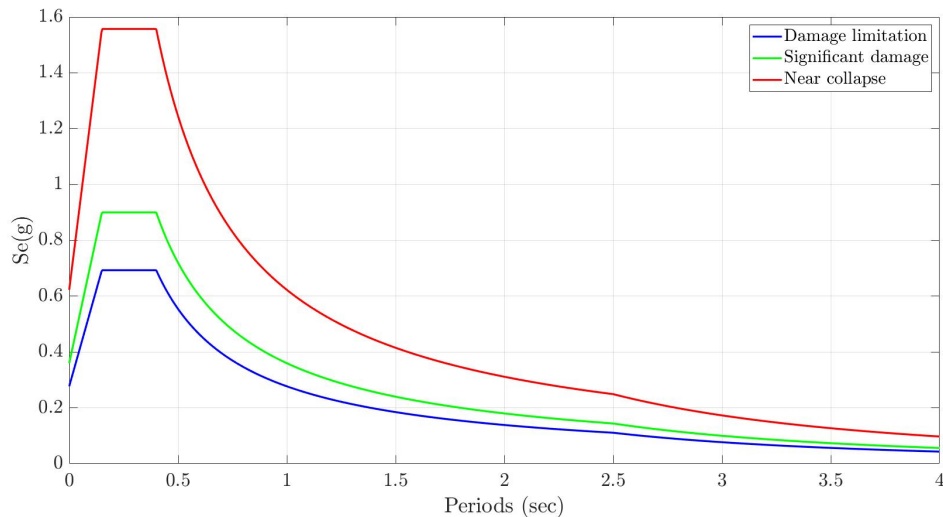


Figure 5.12: Lateral force distributions in a part of the structure (X-direction)

- **Damage limitation:** the structure is only lightly damaged with structural elements retaining their strength and stiffness. Permanent drifts are negligible. Return period of 225 years.
- **Significant damage:** The structure is significantly damaged with some residual strength and stiffness. Moderate permanent drifts are present. Return period of 475 years.
- **Near Collapse:** The structure is heavily damaged with low residual lateral stiffness. Large permanent drifts are present. Return period of 2475 years.

5.4.3 Pushover analysis results

X-direction

In this Section, the results out of nonlinear static analysis for **Model 1** with tension only bracing system are presented. The results for the second model, **Model 2**, can be found in Appendix G. As it has been mentioned before:

- **Model 1:** The concentrically bracing system is simulated by use of link elements. Therefore, tension only bars are considered.
- **Model 2:** The concentrically bracing system is simulated with 50% reduced axial stiffness. Consequently both tensile and compressive bars are considered.

The capacity curve of the ten-storey steel building, in X-direction, can be seen in Figure 5.13. It is obvious that the structure reaches the target displacements for the most unfavourable limit state., while there is still some residual lateral stiffness. This indicates that the structural behaviour is sufficient, and the structure can resist even the higher expected seismic actions in its life time.

The maximum base shear that the structure can resist is $12650kN$ and the maximum distance that top floor's center of mass can be displaced is $1.5m$. After this point the solution becomes unstable even with very small load increments. From the idealized capacity curve is obvious that the load required to cause formation of a collapse mechanism amounts to $12650kN$ and the corresponding displacement is $0.612m$

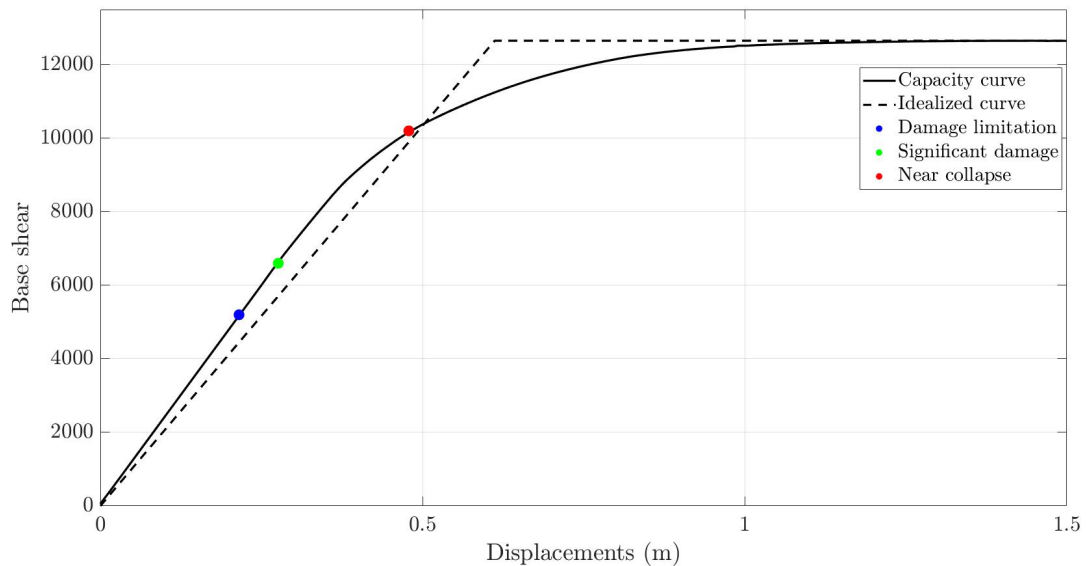


Figure 5.13: Capacity curve in X-direction

Furthermore, the deformed shape of the structure for the three limit states is illustrated in Figure 5.14. In the same figure, the developed damages are represented by black points. As damaged are defined the cross sections in which strains larger than 0.002 are obtained. This is the yielding point of uniaxial stress-strain curve of steel *S355*. As it has been mentioned before, the cross sectional stress-strain state of frame elements is obtained through integration of the nonlinear uniaxial response of the individual fibres in which the cross section has been subdivided.

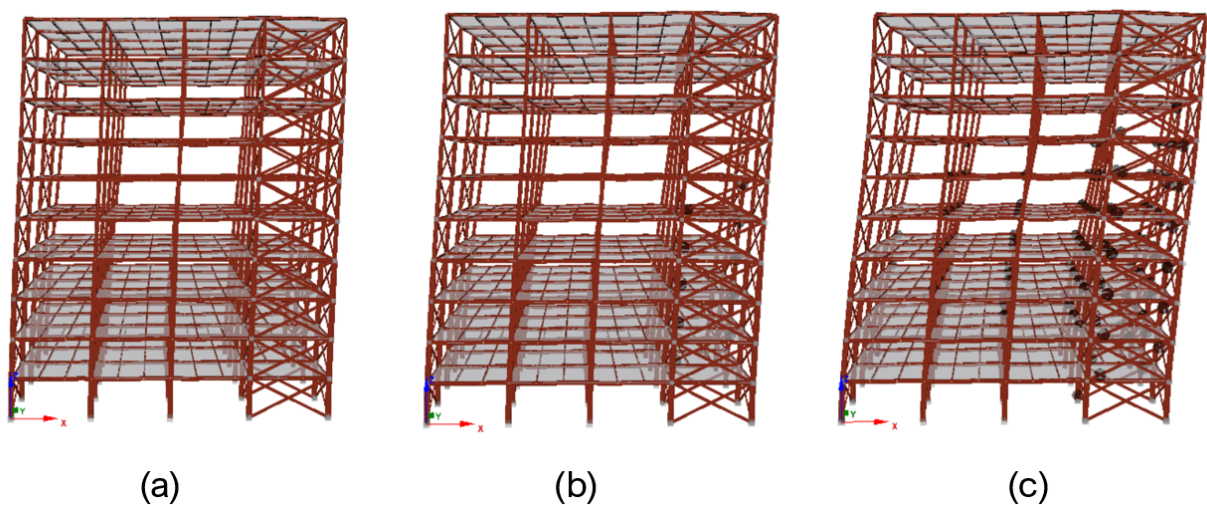


Figure 5.14: Deform shape in limit states:(a) Damage limitation, (b) Significant damage, (c) Near Collapse

It is clear that for the **damage limitation** state there are not damages in the structural elements and no significant drifts between the storey levels are observed. Even for the next limit state (**significant damage**), in which significant damages are expected, the structure can resist the induced base shear without developing extensive damages. Only four bracing elements yield due to axial loading. Moreover, in the last limit state (**near collapse**) the structure experiences some significant damages in the bracing bars and in the primary beams. However the structure is still able to resist gravitational and later loading. Therefore, the structure is actually far from the near collapse state.

The structure is pushed furthermore until it reaches the failure. In this case the failure occurs at top displacement of $1.50m$. The deformed shape of the structure is illustrated in Figure 5.15. At this state the structure develops several damages in beams columns and bracing bars. It can be seen that only the tension bars have failed due to the fact that bracing bars under compression are inactive. Furthermore, the higher inter-storey drifts occurs in lower levels, while smaller drifts are observed at the top higher storeys. Hence it can be explained why there are not damages at the higher levels.

In general the sequence of failure is bracing bars, then primary beams and then columns. Hence the structural response can be characterized as acceptable.

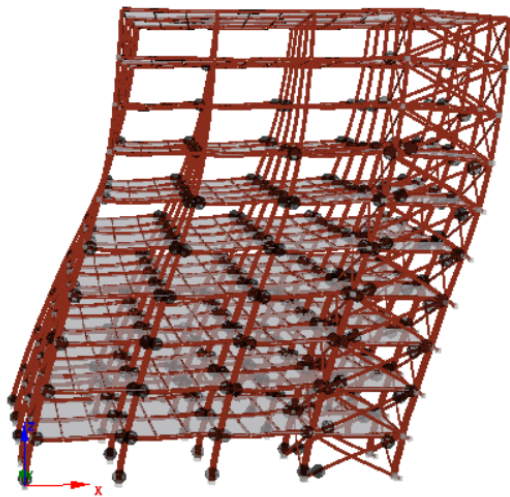


Figure 5.15: Deformed shape of the structure at failure state

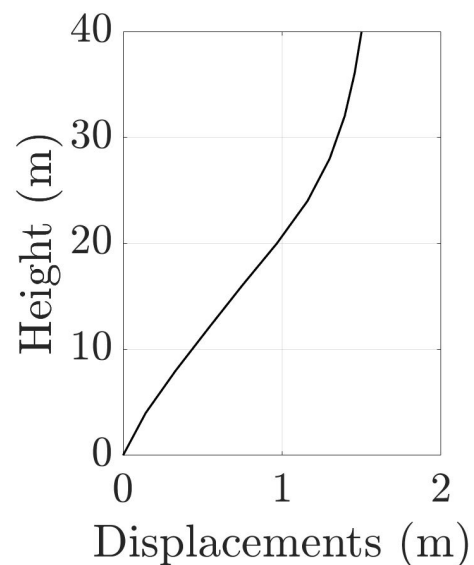


Figure 5.16: Displacements at the center of mass in every level

Furthermore, in Figure 5.17, the deformed shape of the building in plan is depicted. In Figure 5.18, the displacements in X-axis of the two corner columns are illustrated. In this figure a better illustration of inter-storey drifts is given. As it can be seen the relative displacements of the lower storeys are higher (longer distances between lines). Moreover the torsional deformation of the structure is illustrated. The torsional effects are more significant at the higher levels of the building. This can be explained by taking into consideration that the bracing bars of those levels are not yielding at all. Hence, they provide a concentrated lateral stiffness which causes the torsion. In addition, it has to be taken into account that the load distribution is done according to the first eigenmode. Consequently, this is another reason that enforces torsional effects.

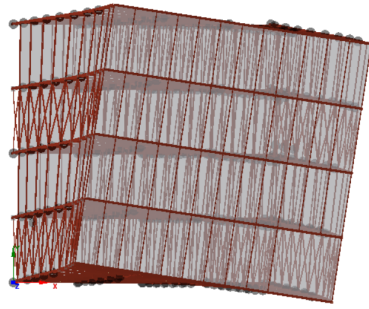


Figure 5.17: Deformed shape of the structure at failure state (plan perspective)

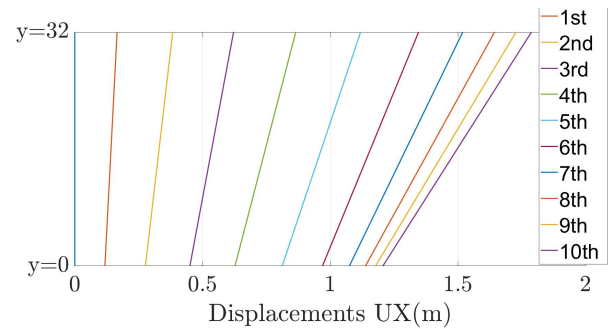


Figure 5.18: Corner columns' displacements of every storey level

Additionally, the response of damaged and undamaged elements is investigated. In the following figures the hysteretic curves of structural elements are illustrated. In Figure 5.19, the moment-rotation relation about the strong axis of a first floor column (damaged) and a second floor column (undamaged) is depicted. As it can be seen the first floor column reaches its plastic moment limit $M_{y,pl} = 1182kNm$ and the corresponding rotation $\theta_y = 0.006rad$. After that point the resistant of the column is significantly reduced, hence large rotations are observed with small increment of bending moments. On the other hand, the second floor column remains elastic through pushover analysis. However, the linear behaviour is a consequence of the first floor developed damages, which allows the structure to be rotated and therefore to dissipate the induced energy.

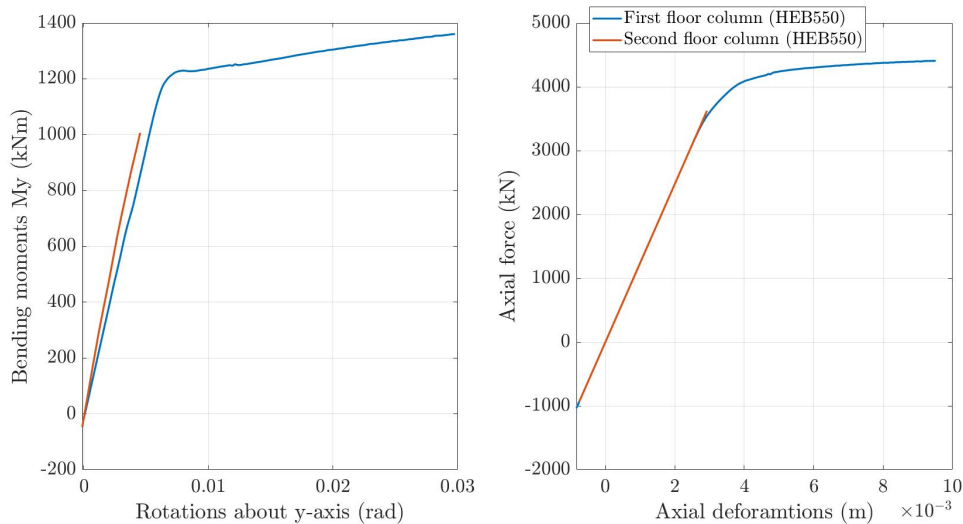


Figure 5.19: Hysteretic curves of damaged and undamaged column. The moment-rotation about the strong axis (left side) and axial force-axial deformation (right side) relations are depicted

Moreover, the axial force-axial deformations curve is illustrated. It can be seen that initially the columns are subjected to high compression. However, during pushover analysis and considering that the columns under investigation are located in the left side of the building (see Figure 5.15), large tensile forces are developed. Once more, the first floor column yields, while the second floor column remains linear.

In a similar way the moment-rotation relation of two primary beams is illustrated in Figure 5.20.

According to the previous example a damaged and an undamaged beam are compared. At this point, it has to be mentioned that the beams do not develop significant axial forces due to the rigid diaphragm effect. Therefore, the axial force-axial deformation plot is omitted. In this case a first floor's beam (damaged) and a eighth floor's beam (undamaged) are chosen. It is obvious that the first floor's beam is subjected to significant bending moments and rotations. Hence, it reaches the yielding point in which the bending moment amounts to $M_{y,pl} = 826kNm$ and the rotation $\theta_y = 0.011rad$.

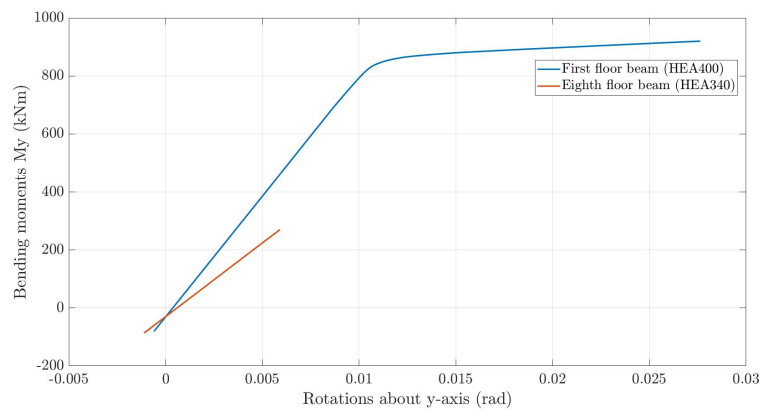


Figure 5.20: Hysteretic curves (moment-rotation) of damaged and undamaged beams

An interesting aspect is the response of the bracing system, see Figure 5.21. As it has been mentioned in Section 5.2 the bracing bars are simulated so that they can developed only axial tensile forces. Therefore only the bars under tension can resist the lateral forces. In Figure 5.21, it is obvious that yielding occurs only at those elements and their hysteretic curve can be seen in the same figure. In elements under compression the output gives some insignificant compression forces and deformations but their values are negligible since they are not influencing the global response of the structure. Moreover the effect of link elements is clearly depicted. For bars under compression, they allow the relative motion of one of the end nodes.

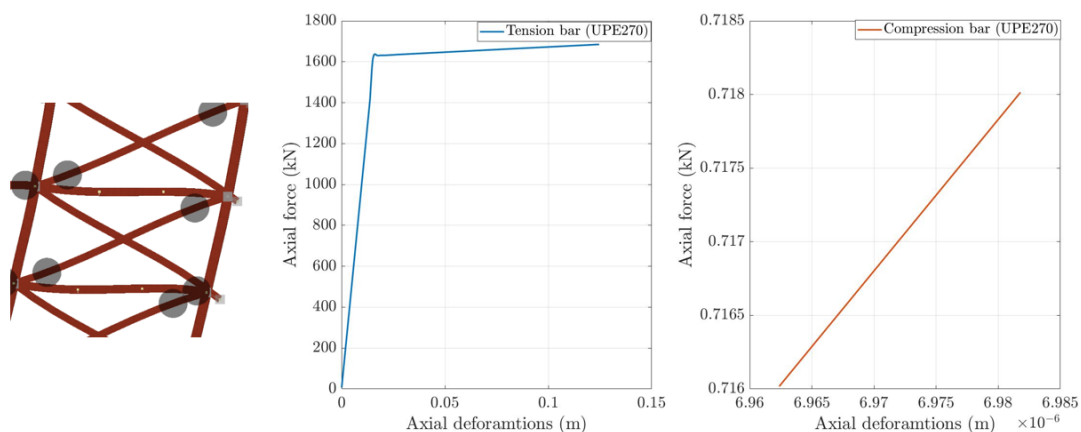


Figure 5.21: Hysteretic curves (moment-rotation) of damaged and undamaged beams

Moreover the effect of link elements can be seen in Figure 5.15. They allow the relative motion of the bars under compression so that they are not able to resist the lateral loading.

Y-direction

The capacity curve of the ten-storey steel building, in Y-direction, is illustrated in Figure 5.22. As it can be seen, the structure reaches the target displacements even for the most unfavourable limit state. The above indicates that the structure is safe and can resist the expected seismic actions in its life time. In comparison with X direction, the structural behaviour indicates a reduced capacity curve. The value of the base shear that the structure can resist in Y direction is significantly lower than in X direction. Moreover, the capacity of the structure to develop plastic deformations in this direction is limited. It can be explained by taking into consideration that in Y-direction only the bracing bars resist the induced loading, while in X-direction a considerable number of elements (beams, columns) are able to develop plastic deformations.

The maximum base shear that the structure can bear in Y-direction is $7163.70kN$ and the maximum distance that the top floor's center mass can be displaced is $0.42m$. By observing the idealized curve, it is obvious that the load which is required in order to form a collapse mechanism is equal to $7236kN$ and the corresponding displacement is $0.26m$.

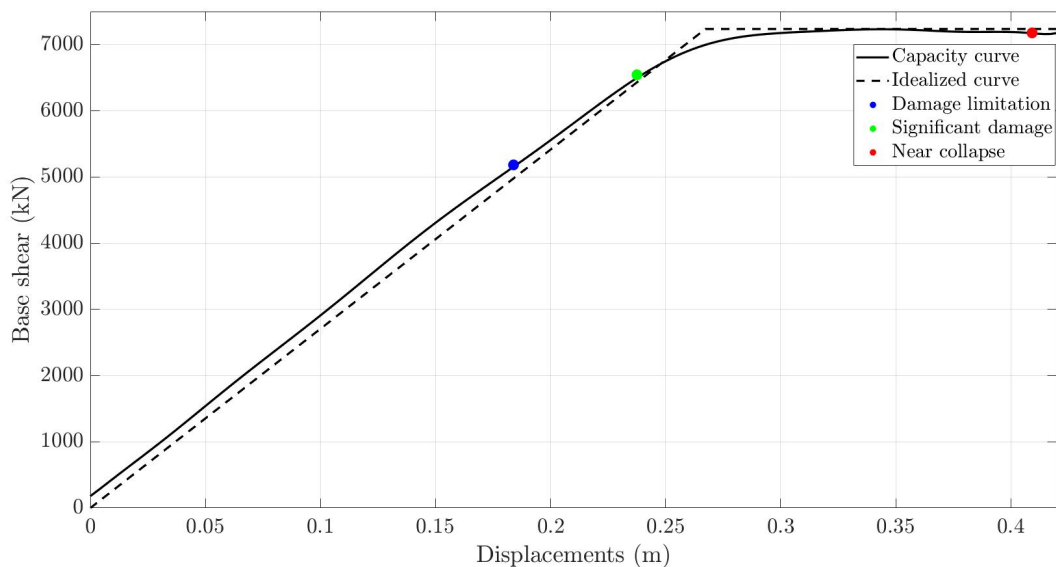


Figure 5.22: Capacity curve in Y-direction

Figure 5.23 visualises the deformed shape of the structure for both three limit states. Once again as in X-direction the developed damages are represented by black points. As damaged are defined the cross sections in which strains larger than 0.002 are obtained. This refers to the yielding point of uniaxial stress-strain curve of steel S355. The cross sectional stress-strain state of frame elements is obtained through integration of the nonlinear uniaxial response of the individual fibres in which the cross section has been subdivided.

For the damage limitation state, it is clear that there aren't any damages in the structural elements or even any significant drifts between the storey levels. As for the next limit state (**significant damage**) damages are developed in the bracing elements, as a result from the induced base shear. In the last limit state (**near collapse**) the structure is under severe damage in the bracing bars.

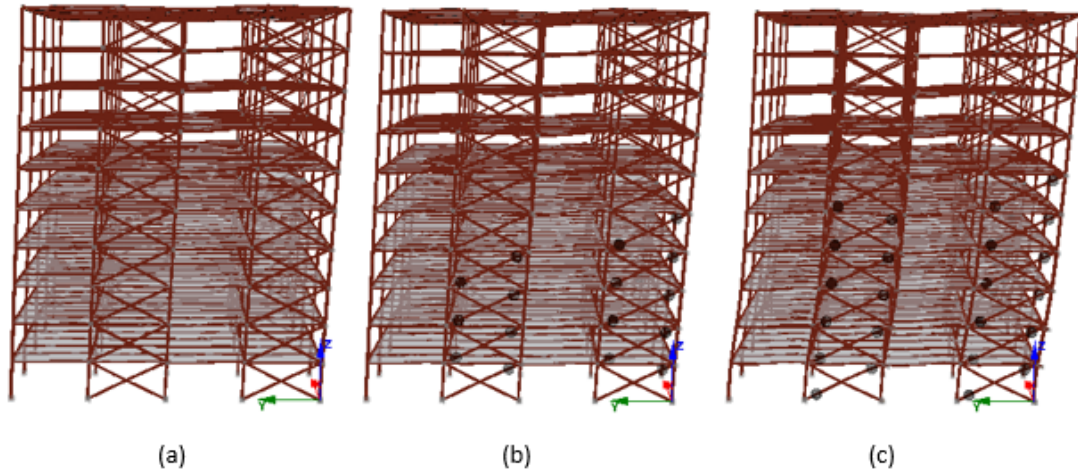


Figure 5.23: Deform shape in limit states:(a) Damage limitation, (b) Significant damage, (c) Near Collapse

The structure failure is occurred at top displacement of $0.42m$. This almost coincides with the last limit state (**near collapse**). The displacements at the center of mass in every level are illustrated in Figure 5.25 and the deformed shape at the structure's failure state can be seen in Figure 5.24. Moreover, it can be seen that the higher inter-storey drifts occur in lower storey-levels, while lower drifts are observed at the top of the structure. Hence it can be explained why there are not damages at the higher levels.

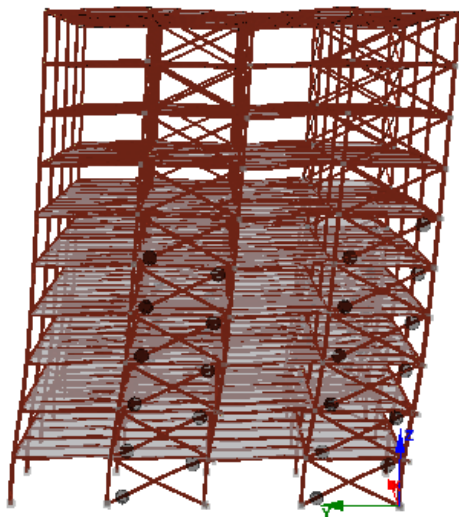


Figure 5.24: Deformed shape of the structure at failure state

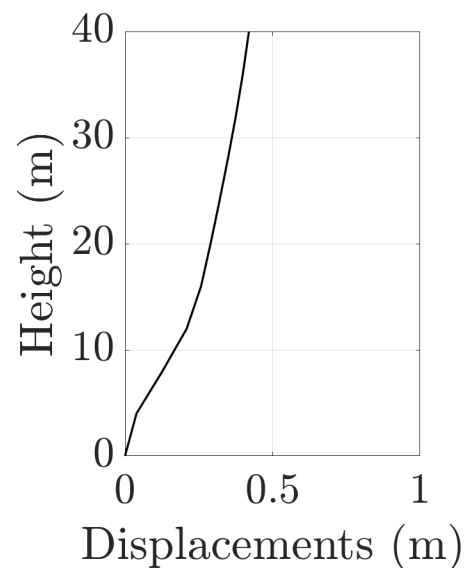


Figure 5.25: Displacements at the center of mass in every level

Additionally, in Figure 5.26 the plan deformed shape of the building is represented. On the right, Figure 5.27 illustrates the displacements in the Y-axis. A better illustration of the inter-storey drifts is given by this Figure. It is clear that the relative displacements are lower for the higher storeys, while the opposite is happening for the lower storeys.

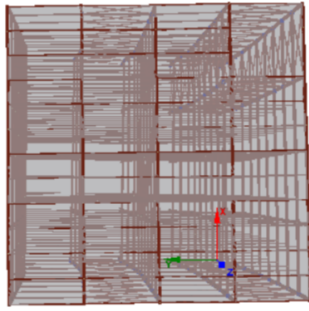


Figure 5.26: Deformed shape of the structure at failure state (plan perspective)

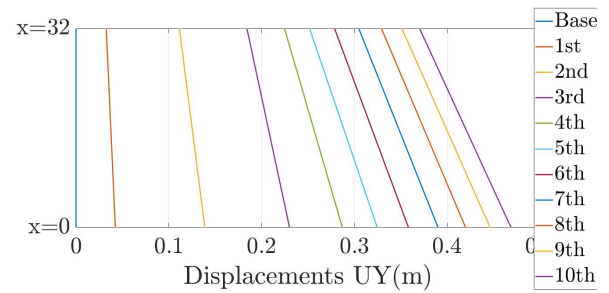


Figure 5.27: Corner columns' displacements of every storey level

5.4.4 Comparison between Model 1 and Model 2

In this section, a comparison of the results which are obtained out of nonlinear static analysis, for **Model 1** (tension only bracing bars) and **Model 2** (tension and compression bracing bars-reduced axial stiffness) is illustrated. More detailed results about nonlinear static analysis of **Model 2** can be found in Appendix G.

X-direction

In Figures 5.28 and 5.29 the capacity curves of **Model 1** and **Model 2**, respectively, are illustrated. It is obvious that the two models have identical behaviour. The maximum base shear in X direction is $12650kN$ for **Model 1** and $12778kN$ for **Model 2**. Additionally, the corresponding yielding displacements out of the idealized capacity curves amount to $0.612m$ and $0.609m$.

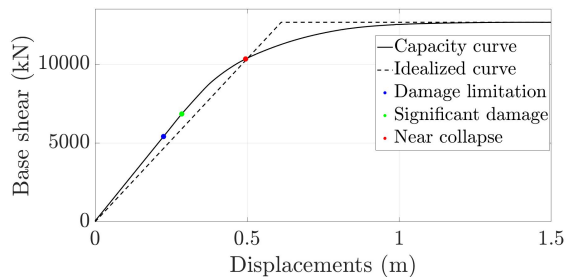


Figure 5.28: Capacity curve for **Model 1**

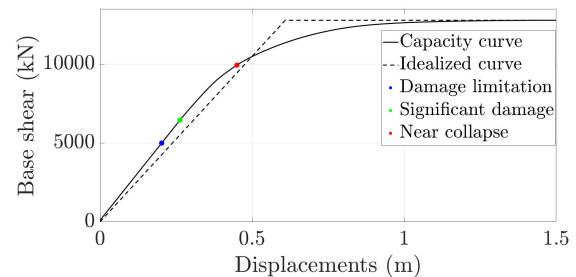


Figure 5.29: Capacity curve for **Model 2**

Moreover, view of the deformed shape of two models is given in Figures 5.30 and 5.31. It is obvious that the deformed shapes of **Model 1** and **Model 2** is perfectly matching.

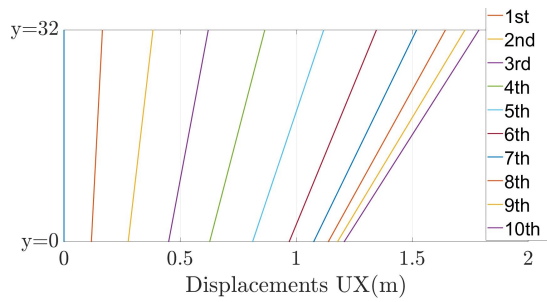


Figure 5.30: Corner columns' displacements of every storey level (**Model 1**)

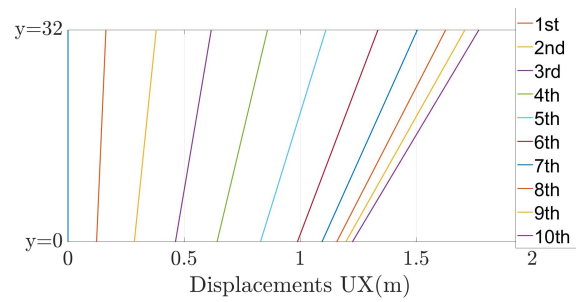


Figure 5.31: Corner columns' displacements of every storey level (**Model 2**)

Y-direction

Furthermore, identical behaviour is also observed in Y direction, see Figures 5.32, 5.34 for **Model 1** and Figures 5.33, 5.35 for **Model 2**. The deviation of maximum base shear forces between the two models and the corresponding yielding displacements deviation are 2% and 0.5% respectively.

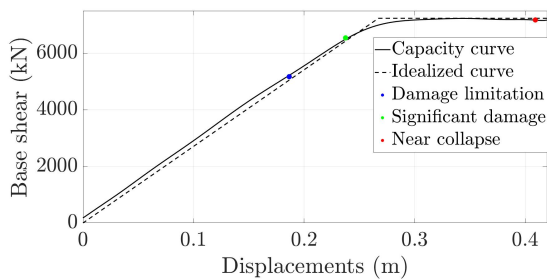


Figure 5.32: Capacity curve for **Model 1**

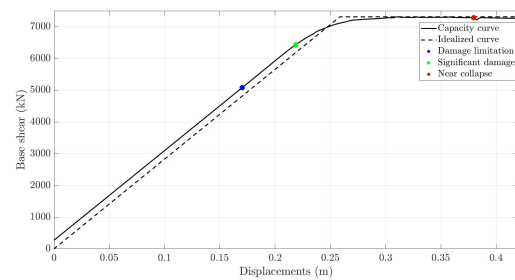


Figure 5.33: Capacity curve for **Model 2**

Finally the deformed shapes of **Model 1** and **Model 2**, in failure state, are represented in the following figures. It is obvious that the two models have the same response.

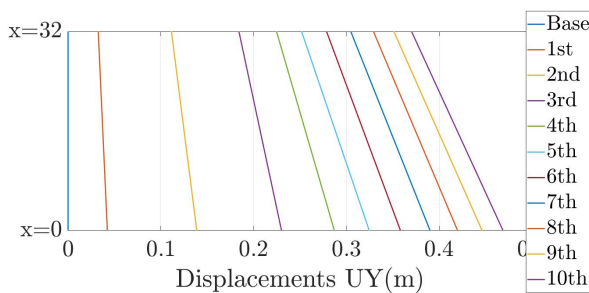


Figure 5.34: Corner columns' displacements of every storey level (**Model 1**)

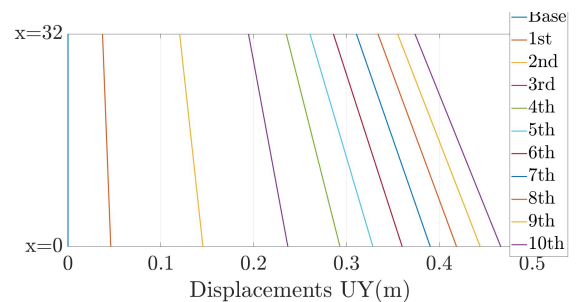


Figure 5.35: Corner columns' displacements of every storey level (**Model 2**)

5.5 Nonlinear time history analysis

In this section, the last purposed method by EN1998-1 [2004] is presented. This method is called nonlinear time history analysis and it is, computationally, the most advanced method of analysis. Consequently, it is computationally the most expensive method and this is the reason why only in recent years there has been a substantial growth of interest.

As it has been proved in Sections 5.3 and 5.4.4, **Model 1** and **Model 2** have identical behaviour. Moreover, **Model 1**, which makes use of link elements, significantly increases the computational time and the size of the output file. Therefore it is difficult to handle a nonlinear time history analysis of **Model 1** with conventional computational power. By taking into consideration the aforementioned reasons, it has been decided that only the **Model 2** (tension and compression in bracing bars-reduced axial stiffness) is investigated by means of nonlinear time history analysis. It is logically assumed that the two models will have identical output.

The finite element formulation of this method is presented in Equation 5.2.

$$[M]\{\ddot{D}\} + [C]\{\dot{D}\} + [K(D)]\{D\} = [R(t)] \quad (5.2)$$

In the framework of this project the simulation of nonlinear time history analysis has been done by means of:

- Consistent mass matrix
- Rayleigh damping model with damping coefficients $\alpha = 0.270$ and $\beta = 0.27$
- Implicit time integration with time step, $\Delta t = 0.01sec$
- Newton-Raphson iterative scheme.

5.5.1 Modified Northridge time history

In this case, the chosen time history has been recorded during Northridge earthquake in 1994. The magnitude of this earthquake was 6.7 in Richter scale, the peak ground acceleration was $0.57g$ and the total duration was $39.88sec$. However, the analysis is implemented only for the first $22sec$. After that point the accelerations are negligible and the signal fades out. The maximum spectral acceleration amounts to $2.00g$. The recorded acceleration time history and the corresponding response spectrum can be seen in Figures 5.36 and 5.37.

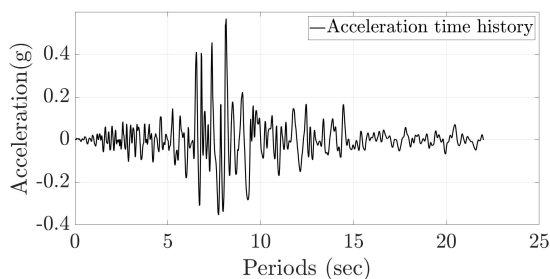


Figure 5.36: Accelerations time history of Northridge 1994

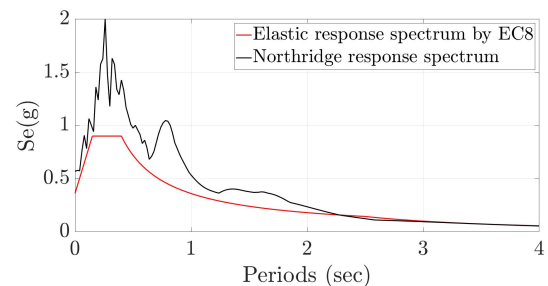


Figure 5.37: Elastic response spectrum of Northridge 1994 and [EN1998-1, 2004]

According to EN1998-1 [2004], the applied time history should be relevant with the expected earthquakes. Therefore, the response spectrum of the chosen time series should be similar with the response spectrum recommended by EN1998-1 [2004]. This requirement is satisfied by use of the commercial software *Seismomatch*. It is an application capable of adjusting earthquake accelerograms to match a specific target response spectrum, using the wavelets algorithm proposed by N.A.Abrahamson [1992] and Hancock J. [2006]. Hence, the Northridge time series and response spectrum are modified so that they match with the defined elastic response spectrum of EN1998-1 [2004].

The modified accelerogram and response spectrum can be seen in Figure 5.38 and 5.39. In this case, the accelerogram has been changed and the maximum peak ground acceleration it is equal to $0.34g$. Moreover the maximum spectral acceleration is reduced to $1.09g$.

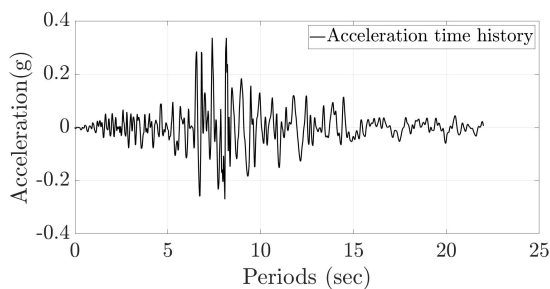


Figure 5.38: Modified accelerations time history of Northridge 1994

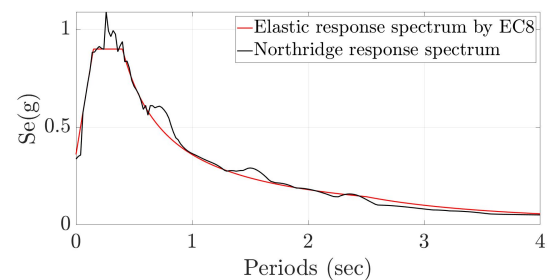


Figure 5.39: Modified elastic response spectrum of Northridge 1994 and [EN1998-1, 2004]

Structural response in X direction

The accelerations are applied to the restrain nodes of the supports, in X direction. In Figure 5.40, the displacements' time histories of center of mass of every storey level are illustrated. As it was expected the maximum displacements are observed at higher storey level, with a maximum value of $0.234m$ in time step equal to $17.60sec$. The maximum displacement does not occur simultaneously with the peak ground acceleration, but almost ten seconds later due to modest resonance phenomena.

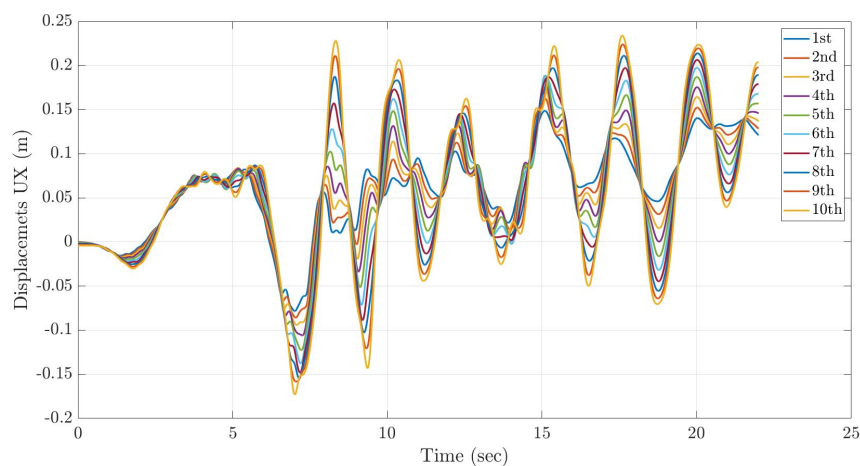


Figure 5.40: Displacements of the center of mass at every storey level

Moreover, in the right part of Figure 5.41 the deformed shape of the structure at every time step

is illustrated. In this case, every line represent the displacements of the building over the height at every time step. The plot is based on the displacements of the center of mass in every storey level, as they are depicted in Figure 5.40.

The upper left part of Figure 5.41 illustrates the deformed shape of the structure at the time step when the maximum relative displacement (inter-storey drift) occurs. The term relative displacement indicates the difference between the displacements of one storey level with the underlying one. The relative displacements can be seen also in the same plot. Finally the lower left part of Figure 5.41 illustrates the deformed shape of the structure as well as the relative displacement at the time when the maximum displacement occurs.

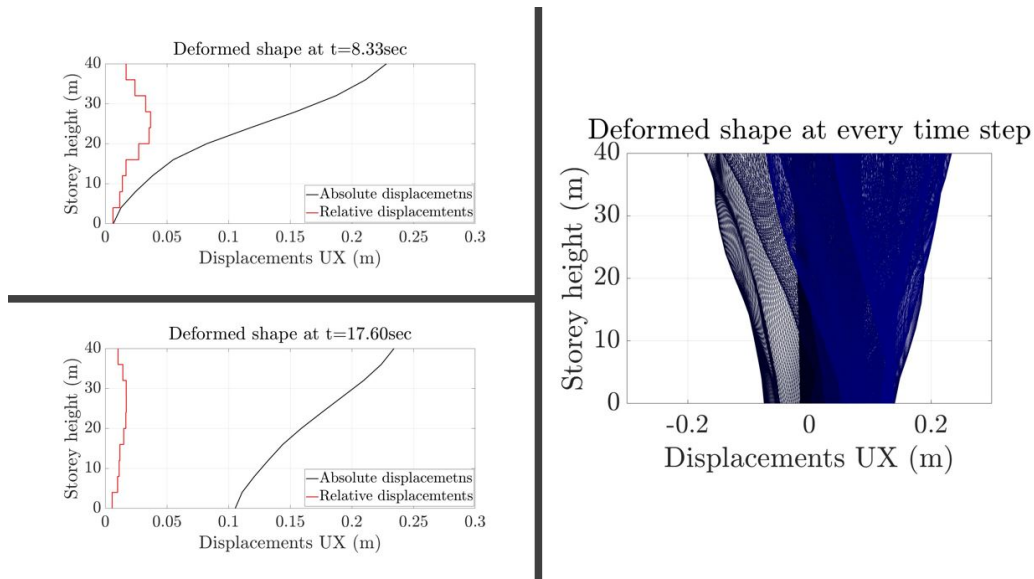


Figure 5.41: (Right) Deformed shape of structure at every time step, (Upper-left) Deformed shape when maximum relative displacement occurs, (Lower-left) Deformed shape when absolute maximum displacement occurs

Furthermore, the displacements' time histories of the corner columns' top nodes are illustrated in Figure 5.42. It is observed that most of the time, the two nodes are displaced equally. However, at the time steps of 9.41sec and 10.33sec there is a difference of 0.25m and 0.24m respectively. These differences indicate the development of torsional effects which are caused by the existence of the bracing system around the elevation shaft, in X direction.

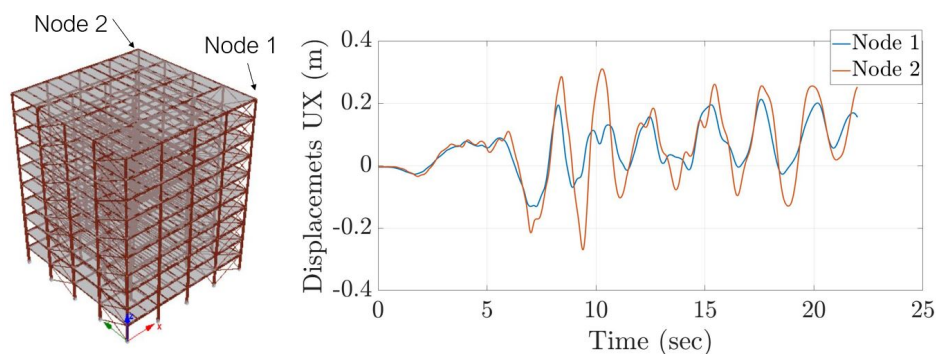


Figure 5.42: Displacements on top of the two corner columns

In addition, the total forces and bending moments which are developed at the supports of the structure are depicted in Figure 5.43. The total forces at the supports can be compared with the induced base shear force. As long as the accelerogram is applied in X direction it is consequent that mainly the support forces are developed in the same direction. Consequently the bending moment are mainly developed about the Y axis. However there are also supports forces in the Y direction due to the vibration of the structure in this direction. It has to be noticed that the developed bending moments about X axis are insignificant. It can be explained by considering that in this direction the weak axis of columns resist the motion. Hence, the columns are more "flexible" and they can not develop high bending moments.

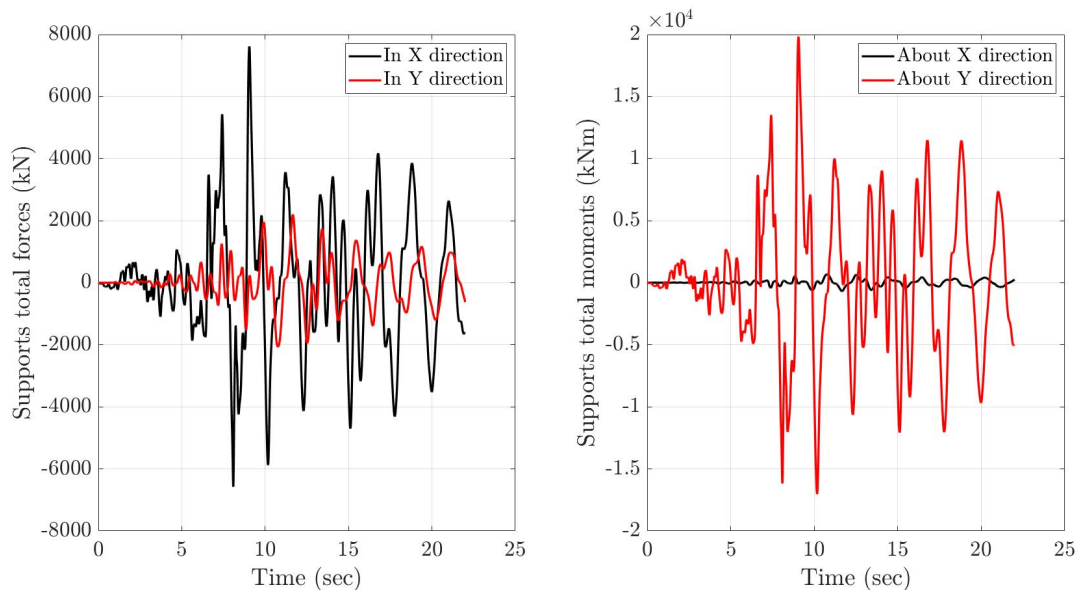


Figure 5.43: Total support forces and bending moments

The hysteretic curves of a column, primary beam and bracing bar are illustrated in Figure 5.44. As it can be seen, for the bracing bar and the beam, a linear elastic behaviour is observed. The column's hysteretic curves indicates a nonlinear behaviour due to varying axial forces. Therefore the geometric nonlinearity has a strong influence on column's hysteretic curve. However, no damages are observed in the structure as it can be seen in Figures 5.45 and 5.46. As damaged are defined those cross sections in which strains higher than 0.002 are calculated in the cross sectional fibers see Figure 5.3. This is the yielding point of uniaxial stress-strain curve of steel *S355*.

Therefore, in this case the induced energy of the earthquake is dissipated mainly by the motion of the structure. A small part of the energy is also dissipating by structural damping. No damages are observed in the structure, hence the there is no "need" of energy dissipation through material yielding.

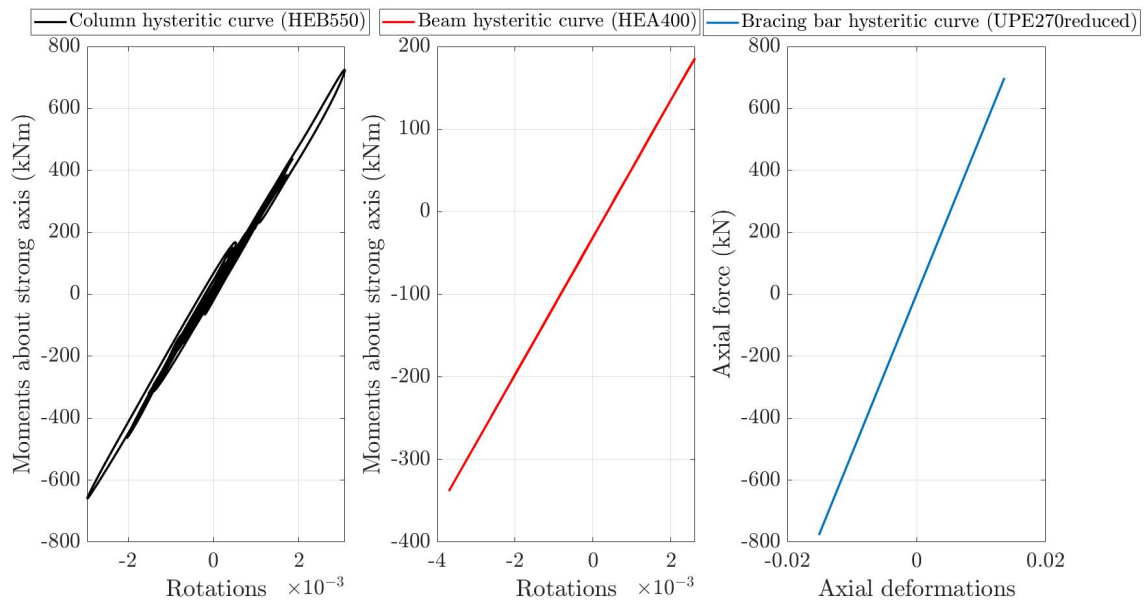


Figure 5.44: Hysteretic curves of column, beam and bracing bar

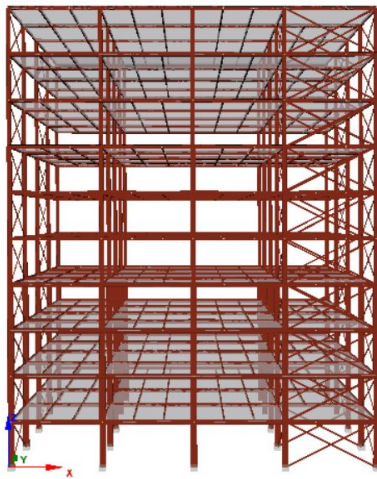


Figure 5.45: No damages occurrence in XZ plane (final state)



Figure 5.46: No damages occurrence in YZ plane, (final state)

Structural response in Y direction

In this case the accelerations are applied to the restrain nodes of the supports, in Y direction. As it can be seen in Figure 5.47 the structure is vibrated similarly as in X direction. However slightly higher displacements are calculated in this case. The maximum value reaches $0.32m$ at the time step of $17.60sec$. This can be explained by considering the response spectrum of the induced signal, see Figure 5.39, and the fundamental eigenperiod in Y direction, $T_2 = 1.87sec$. The induced signal contains marginally higher amount of energy in period equal to $T_2 = 1.87sec$, rather than in period equal to $T_1 = 2.00sec$, which is the fundamental eigenperiod in X direction. Hence, it can be explained why the structural vibrations are more intense in this case.

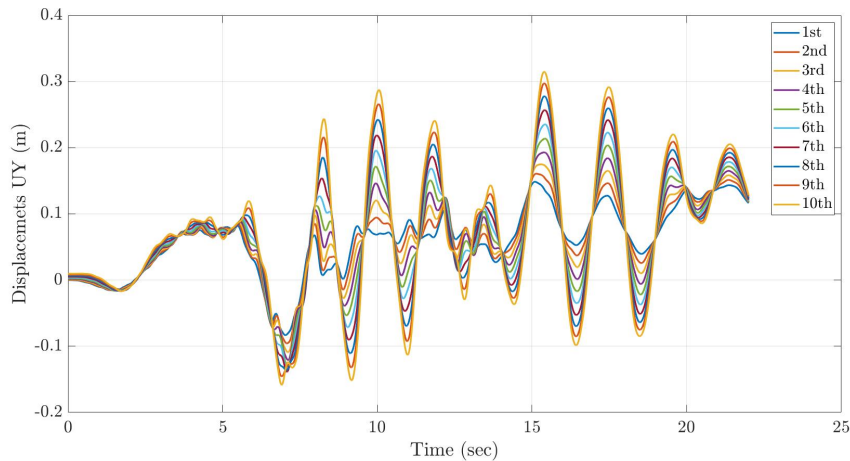


Figure 5.47: Displacements at the center of mass at every storey level

In line with X direction, the right part of Figure 5.48 illustrates the deformed shape of the structure at every time step. The upper left part depicts the deformed shape and the relative displacements of building at the time step when the maximum relative displacement (inter-storey drift) occurs, $t = 8.29\text{sec}$. This is also the time step when most of the damages occur, see Figure 5.53. Finally, in the lower left part the deformed shape and the relative displacements of the building are illustrated, at the time when the maximum displacement occurs.

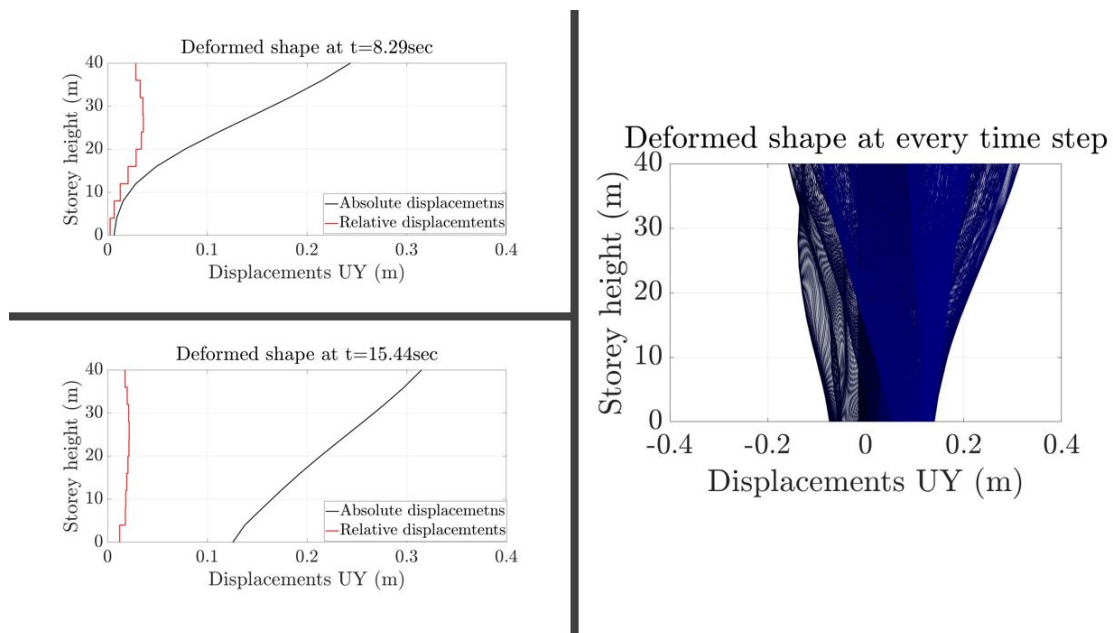


Figure 5.48: (Right) Deformed shape of structure at every time step, (Upper-left) Deformed shape when maximum relative displacement occurs, (Lower-left) Deformed shape when absolute maximum displacement occurs

Additionally, in Figure 5.49, the displacements time histories of the top nodes of two corner columns are depicted. As it can be seen the displacements are identical. In this case, torsional effects are not observed due to the fact that the lateral stiffness in Y direction is equally distributed over the plan of the building.

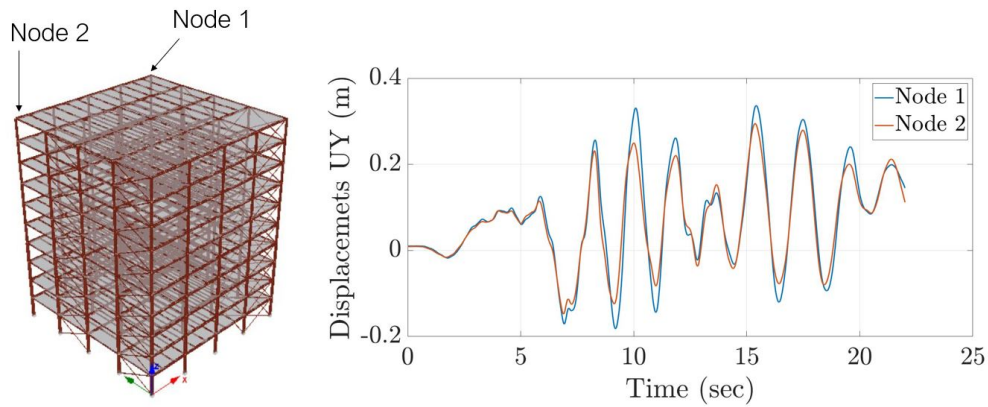


Figure 5.49: Displacements on top of the two corner columns

The supports total forces and moments can be seen in Figure 5.50. Since in this case, the induced accelerations are applied in Y direction, the developed support forces are higher in this direction. However, the maximum moments are still developed about Y axis, as in the previous case. It can be explained by considering again that the induced motion in Y direction is mainly resisted by bracing bars. Moreover, in this direction the weak axis of column is stressed. Therefore the columns can bear large rotation without developing significant bending moments. Contrary in X direction the motion is mainly resisted by moments which are developed about the strong axis of columns.

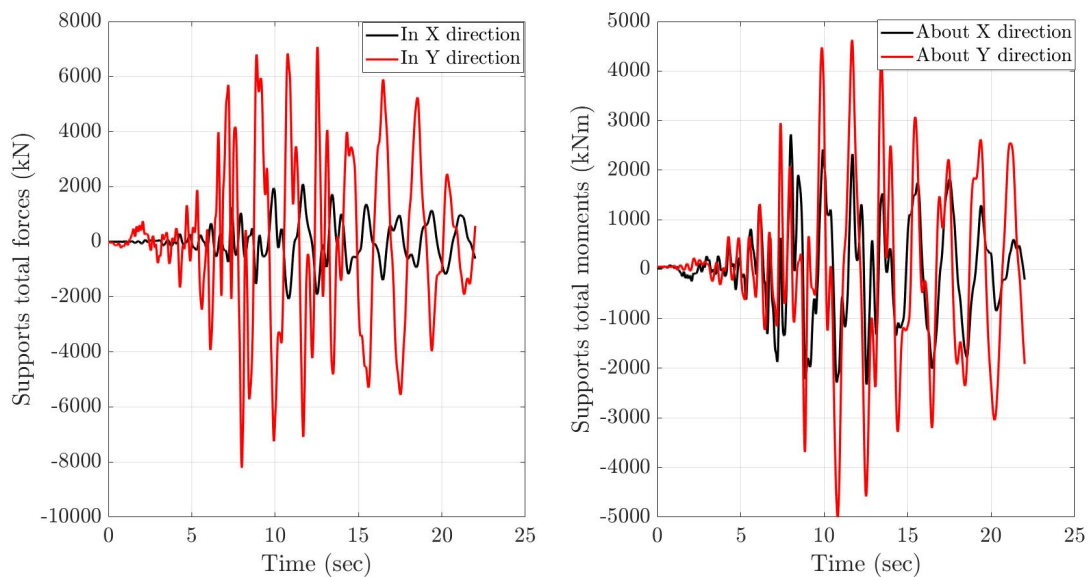


Figure 5.50: Total support forces and bending moments

The hysteretic curves of a column, a beam and a bracing bar can be seen in Figure 5.51. As it is obvious only the bracing bar has suffered damages. The hysteretic curve of these element displays that the element's yielding point under axial loading is 935kN with axial deformation of 0.019m . The area inside the hysteretic curve indicates the energy dissipation that this element has provided to the structure.

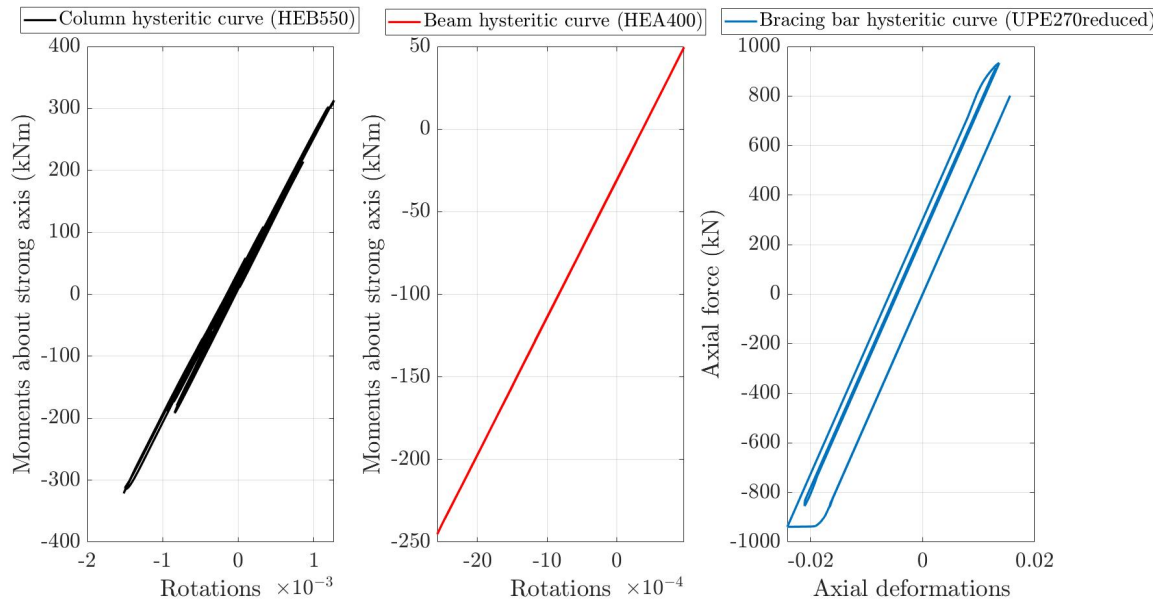
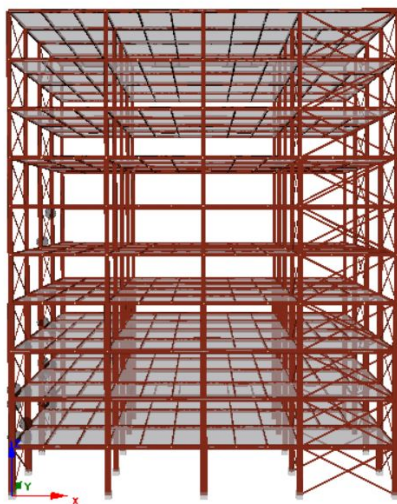
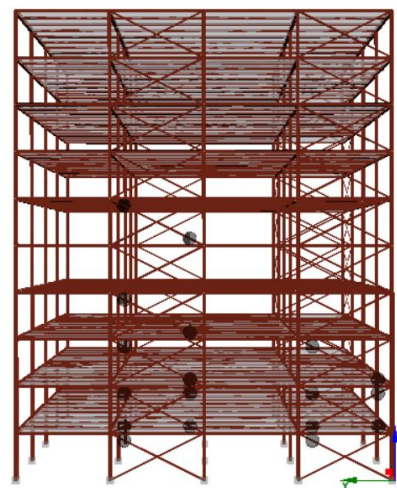


Figure 5.51: Hysteretic curves of column, beam and bracing bar

In Figures 5.52 and 5.53 the damages that the structure has experienced can be seen. In XZ plane there are not damages as it was expected. In YZ the bracing bars have experienced some damages (black marks), see Figure 5.53. However the overall behaviour of the structure is characterized as sufficient due to the fact that the yieldings are limited only to the bracing bars. This is the desirable behaviour for a concentrically braced frame, according to EN1998-1 [2004].

Figure 5.52: No damages occurrence in XZ plane (final state)Figure 5.53: Damages occurrence in YZ plane, (final state)

5.5.2 Original Northridge time history

In this Section, the original Northridge accelerogram, as it is illustrated in Figure 5.36, is applied in X and Y direction. More detailed results can be found in Appendix H.

A comparison between the original and modified accelerogram and response spectrum can be seen in

Figures 5.54 and 5.55. It is obvious that the two accelerograms are similar, but higher accelerations are contained in the original accelerogram.

By looking at the response spectrums it can be said that similar structural behaviour is expected. Even though the original response spectrum contains much higher spectral accelerations, in the range between 1.50 and 2.00 seconds, where the critical eigenperiods of the structure belong, the two spectrums are similar. However, slightly higher spectral accelerations are contained in the original response spectrum.

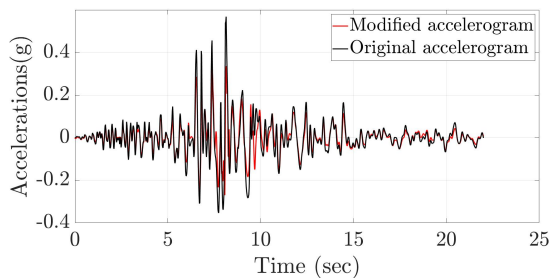


Figure 5.54: Comparison between original and modified accelerogram of Northridge earthquake

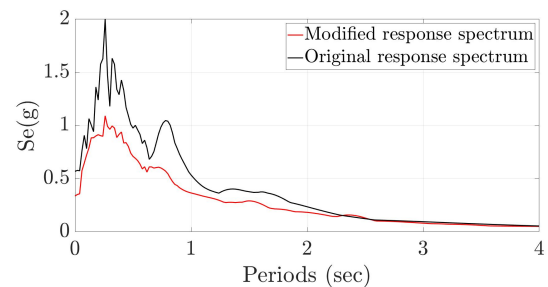


Figure 5.55: Comparison between original and modified response spectrum of Northridge earthquake

Structural response in X direction

In line with Section 5.5.1, initially the accelerations are applied to the restrained nodes of the model in X direction. In Figures 5.56 and 5.57 two perspectives of the structure, after nonlinear time history analysis implementation, are illustrated. The yieldings are depicted by black marks on the structural elements. In contrast with the modified Northridge time history, in this case damages occur in bracing bars and primary beams.

As it is expected, the yieldings occur in the bracing bars and the moment resisting frame which resist the motion in X direction, while the elements which resist the motion of the structure in Y direction remain linear elastic.

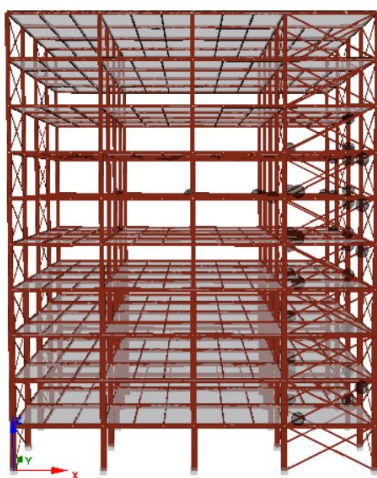


Figure 5.56: Damages occurrence in XZ plane (final state)

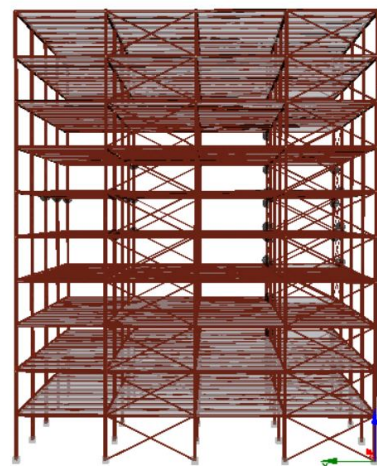


Figure 5.57: No damages occurrence in YZ plane, (final state)

The hysteretic curves of the damaged beams and bracing bars are illustrated in Figure 5.58. Moreover the hysteretic curve of the column is depicted in the same Figure. All columns remain linear elastic. However, their hysteretic curve is not a straight line due to existence of varying axial forces as it has been explained previously. As a result, the geometric nonlinearity has a strong influence.

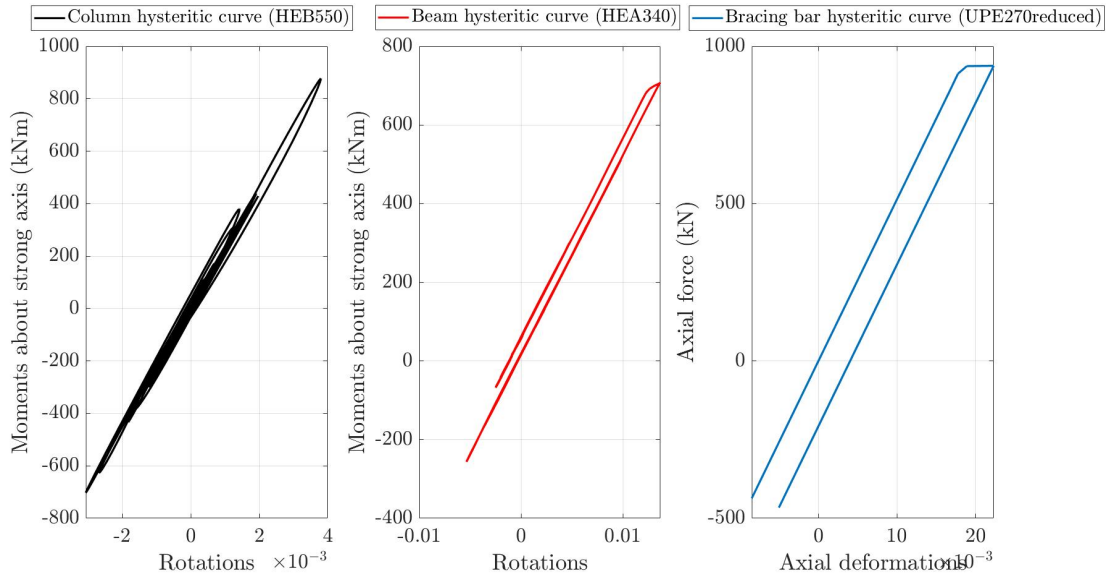


Figure 5.58: Hysteretic curves of column, beam and bracing bar

Structural response in Y direction

Thereafter, the accelerations are applied in Y direction. As it can be seen in Figure 5.60, extensive damages are calculated in the bracing bars of the concentrically braced frame (YZ plane). Moreover, high rotation values around the weak axis of first floor's columns are obtained. Therefore, the bracing bars of concentrically braced frame (YZ plane) are not sufficient to resist the induced motion and secure that the columns will remain linear elastic. Furthermore, damages are calculated on gravity beams (secondary beams) as it can be seen in Figure 5.60. These beams develop large rotations without developing bending moments due to the fact that they are simulated with moment releases.

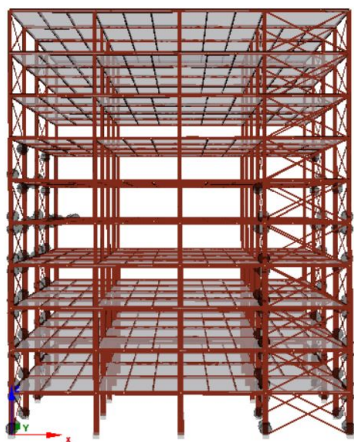


Figure 5.59: No damages occurrence in XZ plane (final state)



Figure 5.60: Damages occurrence in YZ plane, (final state)

The hysteretic curve are illustrated in Figure 5.61. It is obvious from the size of its hysteretic curve that large amount of energy is dissipated by bracing bars. All primary beams are remain linear elastic. It has to be noticed that the hysteretic curve of the chosen column is related with its strong axis.

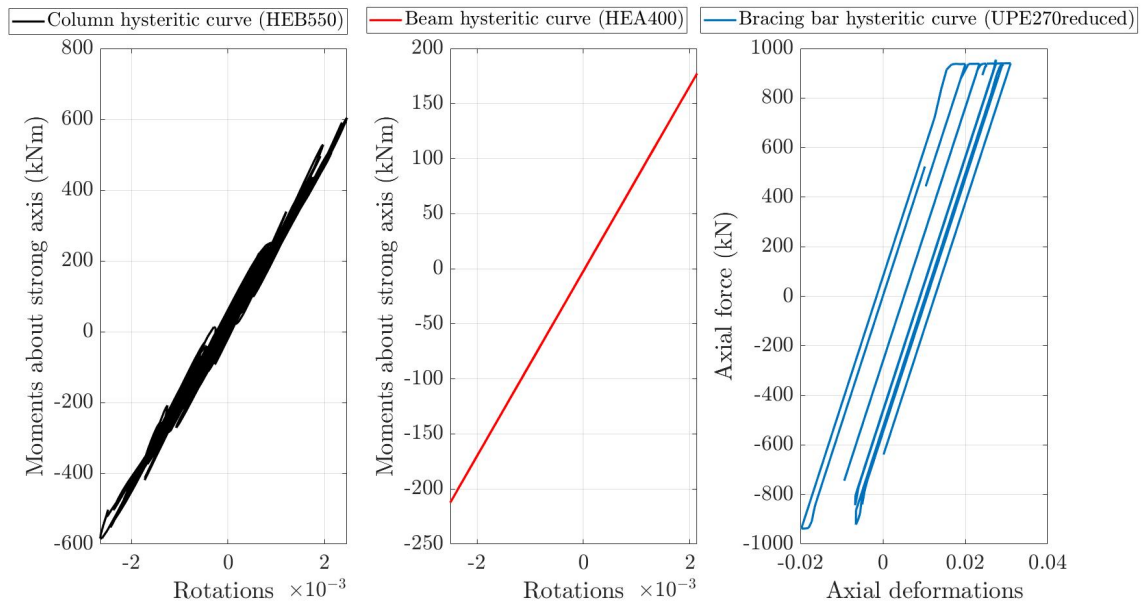


Figure 5.61: Hysteretic curves of column, beam and bracing bar

5.5.3 Artificially generated accelerogram

In this Section an artificially generated accelerogram is applied. For this reason, the *SeismoArtif* application is used. It is a software capable of generating artificial earthquake accelerograms matched to a specific target response spectrum. The purpose is to apply ground motion which strongly affects the structure. Therefore, the target response spectrum is chosen so that it contains high spectral accelerations in the range between 1.80 and 2.00 seconds, in which the critical eigenperiods of the structure, for X and Y directions, belong. This kind of response spectrum are defined according to New Mexican code, NMX-R-079-SCFI [2015]. According to this norm, long period earthquakes are expected in this region. The target response spectrum and the response spectrum of the artificially generated accelerogram are illustrated in Figure 5.62. Moreover the artificially generated accelerogram is depicted in Figure 5.63.

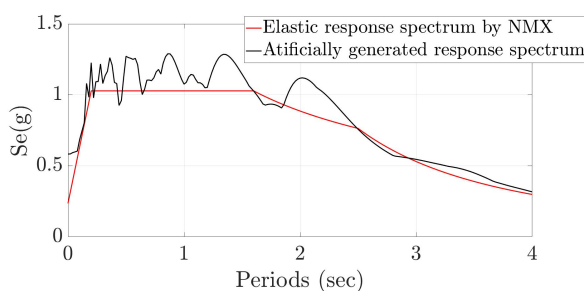


Figure 5.62: Target response spectrum and response spectrum of artificially generated accelerogram

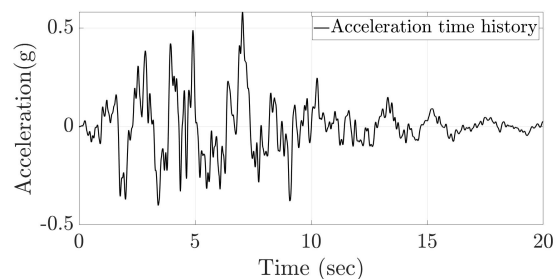


Figure 5.63: Artificially generated accelerogram

A comparison between the artificially generated and Northridge accelerograms can be seen in Figure 5.65. Furthermore the response spectrums of these to time histories are illustrated in Figure 5.64. From the last-mentioned figure, it is obvious that the artificial ground motion contains much higher energy in frequencies of interest. Even though, it doesn't contain higher accelerations than Northridge time history, see Figure 5.65, it is expected to be more destructive due to resonance phenomenon. The results are illustrated below. More detailed results can be found in Appendix H.

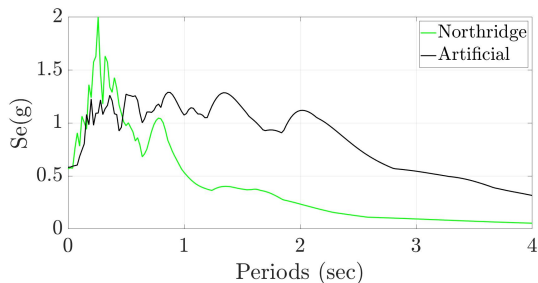


Figure 5.64: Comparison between artificial and Northridge response spectrum

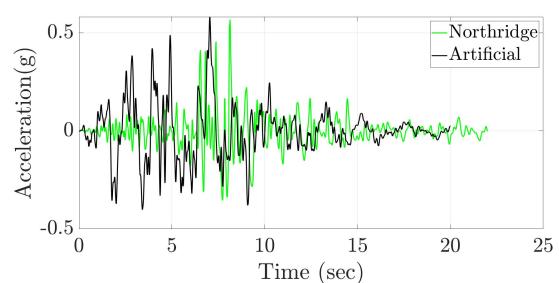


Figure 5.65: Comparison between artificial and Northridge acceleration time history

Structural response in X direction

The accelerations are applied in X direction. More detailed results can be found in Appendix H. Even from the time of 0.39sec the structural elements start yielding. The numerical solution can not proceed further than 16.52sec , hence it is considered that the structure has failed. Initially, the bracing bars which resist the motion in X direction are deformed plastically. Hereafter the damages occur to the primary beams and the first floor columns. Furthermore yieldings occur at the columns of higher levels. Finally the bracing bars that resist the motion in Y direction and the gravity beams (secondary beams) are yielding. The structure suffers significant damages which are depicted by black marks on the two perspective of the building in Figures 5.66 and 5.67.

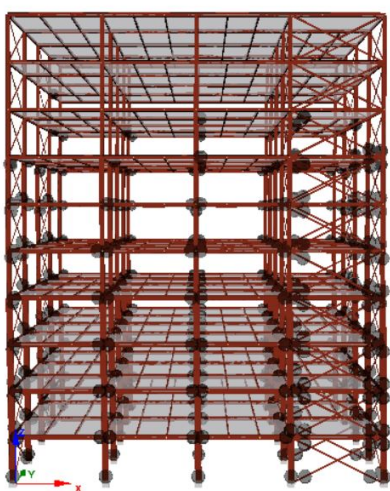


Figure 5.66: Damages occurrence in XZ plane (final state)



Figure 5.67: Damages occurrence in YZ plane, (final state)

Moreover, the structure need to dissipate a large amount of energy. This can be seen from the hysteretic curves of columns, beam and bracing bars in Figure 5.68. Almost all structural elements participate in the dissipation of energy by developing significant plastic deformations. The size of the hysteretic curve indicates the amount of energy that has been dissipated from this specific cross section.

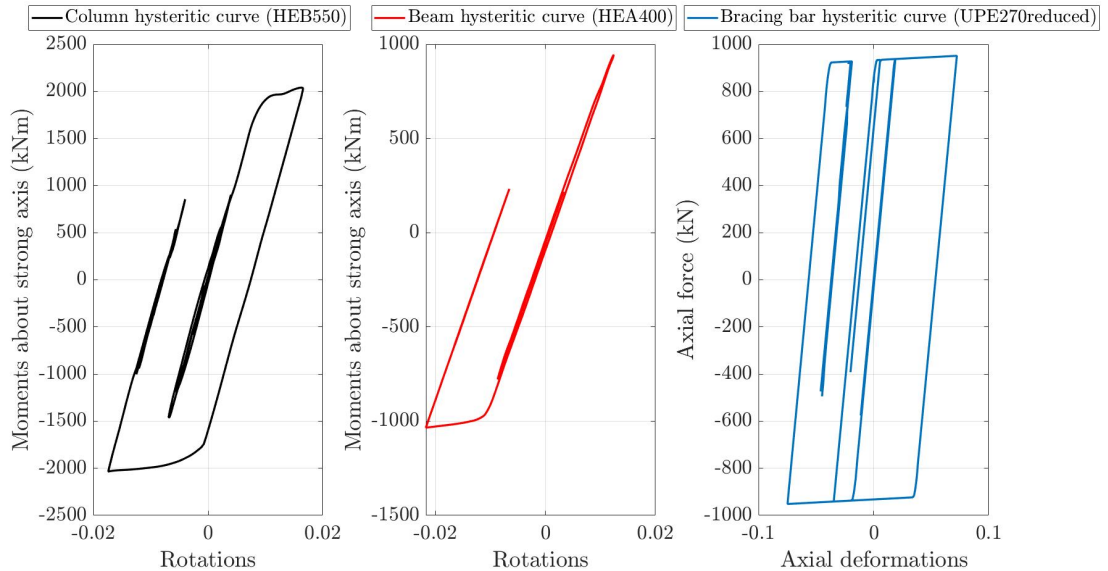


Figure 5.68: Hysteretic curves of column, beam and bracing bar

Structural response in Y direction

In this case the accelerations are applied in Y direction. More detailed results can be found in Appendix H. The nonlinear time history analysis runs until the 9th second. Thereafter, it is unable to converge to a solution. Hence, it is considered that the structure can not sustain the induced motion in the Y direction. In Figures 5.69 and 5.70 the yielding distribution is depicted. Extensive damaged in column bracing bars and secondary beams are observed. However the primary beams which are part of moment resisting frames remain linear elastic due to the fact that they are mainly affected from the motion in X direction.

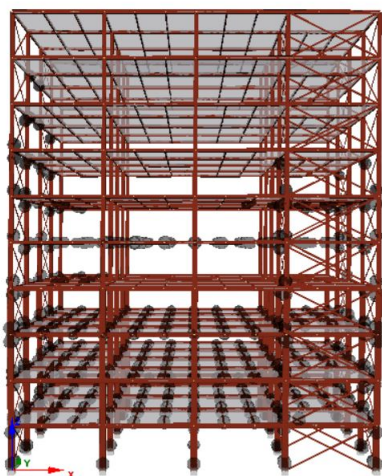


Figure 5.69: Damages occurrence in XZ plane (final state)

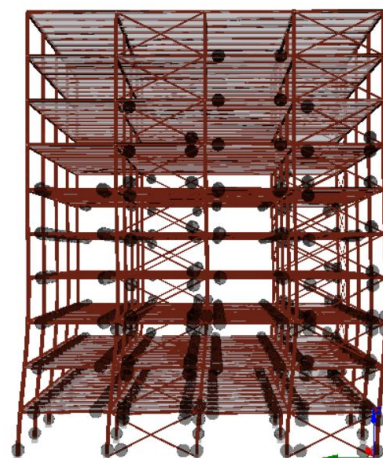


Figure 5.70: Damages occurrence in YZ plane, (final state)

In Figure 5.71 the hysteretic curves of a column about its strong axis (Y axis), of a primary beam and a bracing bar, part of concentrically braced frames (YZ plane), are illustrated.

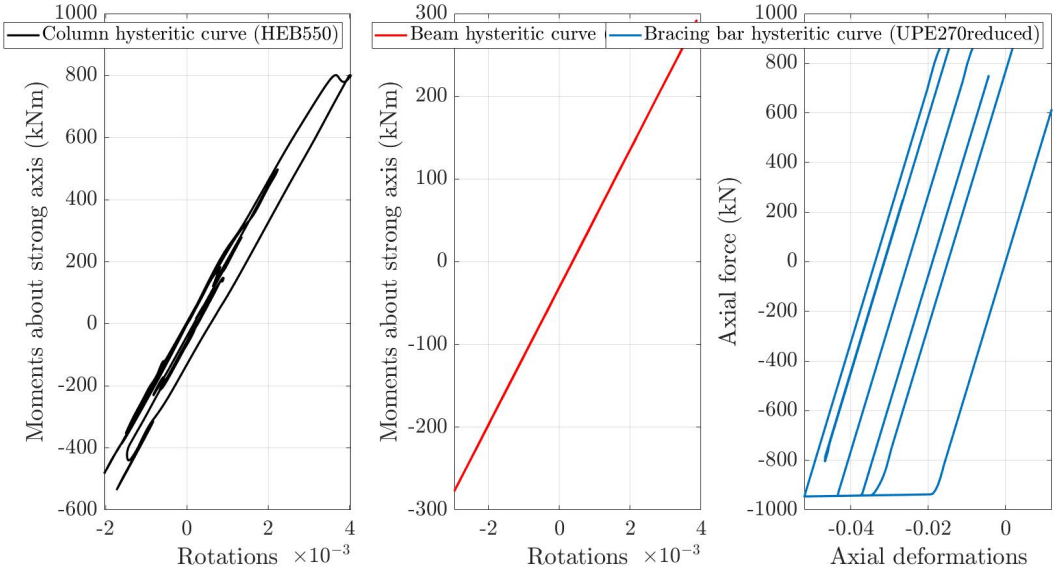


Figure 5.71: Hysteretic curves of column, beam and bracing bar

Base isolation 6

According to E.Kotrotsou [2015], base isolation as a technique of earthquake protection of structures was conceived more than 100 years ago. With this method, a flexible layer is introduced between the structure and its foundation in order to achieve decoupling of the two components. Therefore, the period of the structure is increased up to a larger value, so that resonance with earthquake excitations is avoided. As a result, the earthquake generated effects like floor acceleration, base shear and inters storey drifts are reduced. Then, the building can be designed for lower forces, contributing to a more economic efficient design. In other words, the purpose of seismically base isolated structures is to protect the structure against damages from earthquakes by reducing the earthquake forces rather than resisting them.

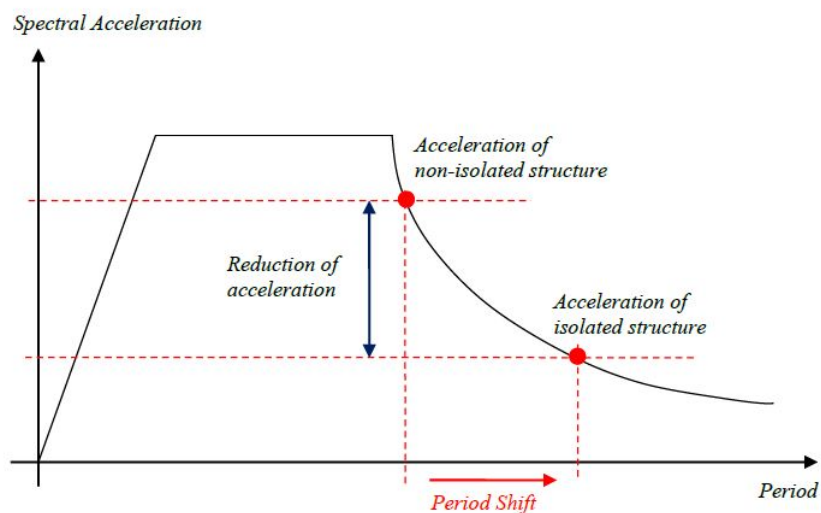


Figure 6.1: Period shift [D.Christianto, 2019]

This was initially achieved by using natural rubber bearings. The devices have evolved in time to provide stability and efficiency even in high shear strain rates, as well as high damping to avoid uncontrollable displacements. Seismic isolation devices could be classified as following:

- **Elastomeric bearings:** A further discretization for this kind of base isolation devices contains the following subcategories:
 - **Low-damping rubber** are natural rubber bearings with moderate energy dissipation capacities, which provide base-isolated buildings with damping ratios that range between 2% and 4% at 100% shear strain. To limit, displacements across the isolation interface, external supplemental damping devices are added, T.Fujita. [1998].

- **High-damping rubber:** bearings are composed of layers of an elastomeric compound, that provides energy dissipation under cycling loading, without the need for additional dampers. Due to this, the stress-strain behaviour is non linear and causes high horizontal stiffness for low shear strains that occur under service loading, maintaining forces and deformations in the elastic range. In a higher seismic event, the bearing develops nonlinear deformations, with reduced stiffness, and dissipates energy. The reduced horizontal stiffness results to the isolation of the structure. Damping ratios generally range between 10% and 20% of the critical one at 100% shear strain, D.N.Grant [2005]
- **Lead rubber:** bearings differ from low-damping rubber bearings only by the addition of a lead-plug core, see Figure 6.2. The elastomer provides the isolation component and the lead core provides the energy dissipation or damping component, due to the plastic deformation of the lead, T.Fujita. [1998].

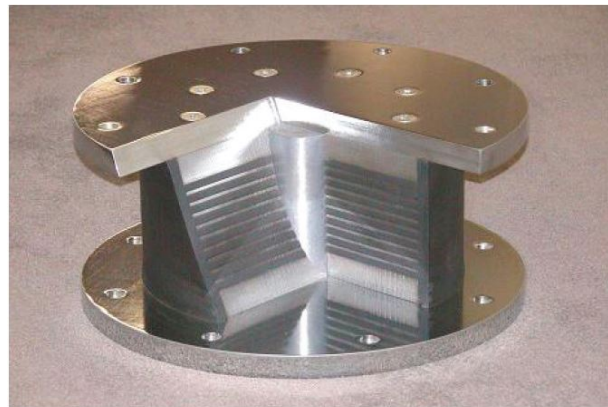


Figure 6.2: Lead rubber bearings [M.C.Constantinou, 2007]

- **Friction pendulum:** is a seismic isolation bearing, with a mechanism based on its concave geometry and surface friction properties, see Figure 6.3. The supported structure is administered into a pendulum motion as the base plate simultaneously glides on the concave dish and dissipates hysteretic energy via friction. Moreover, it ensures the re-centering property of the bearing. The radius of the concave contact surface and the friction coefficient are the parameters designed to give the Friction Pendulum bearings desirable dynamic properties.

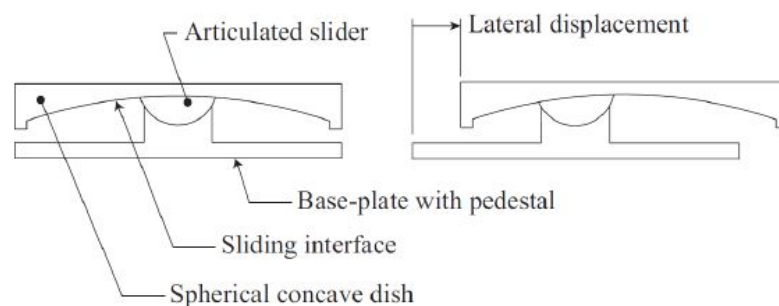


Figure 6.3: Friction pendulum bearings [G.P.Warn, 2012]

6.1 Modeling of elastomeric bearings

The simulation of elastomeric bearings is implemented with six discretized springs as it can be seen in Figure 6.4. There are three translational and three rotational degrees of freedom. In the framework of this project the response of each spring is considered self-governing and it is not influenced from the response of the other degrees of freedom.

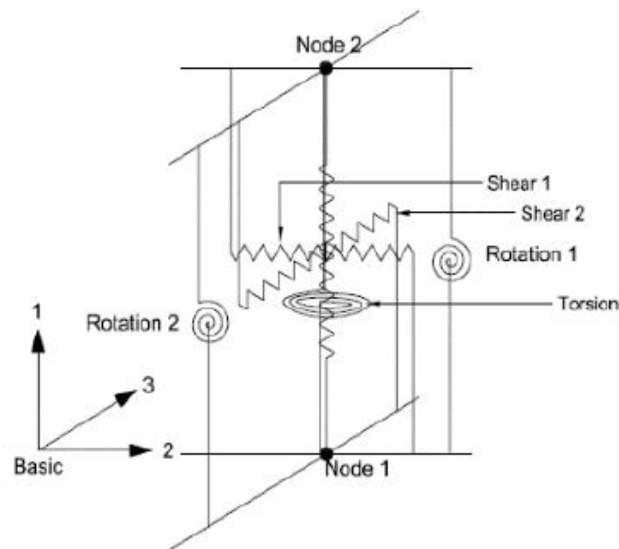


Figure 6.4: Modeling of elastomeric bearings [Kumar, 2018]

Furthermore, the elastomeric bearings are modeled by link elements. A constitutive model is assigned for every degree of freedom. In this project, it is considered that the elastomeric bearings are able to develop only shear deformations. For this reason, the constitutive model that is used for those degrees of freedoms is the bilinear kinematic model, see Figure 6.5, according to M.C.Constantinou [2007]. For the rest degrees of freedom a symmetric linear curve with high stiffness is used, see Figure 6.6. The high stiffness secure that there will be not deformation relative to those degrees of freedom.

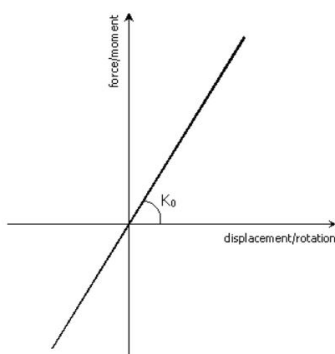


Figure 6.5: Linear constitutive model [Seismosoft, 2020]

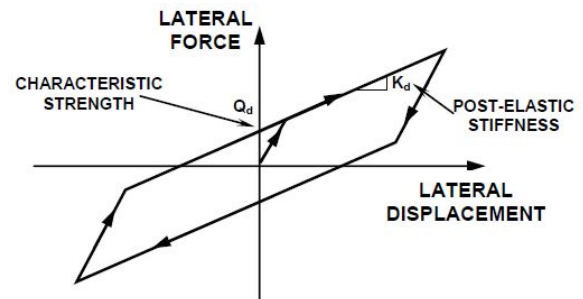


Figure 6.6: Bilinear constitutive model [M.C.Constantinou, 2007]

In the framework of this project five different lead rubber bearings have been chosen. The isolator's engineering properties are derived from the technical brochures of Dynamic Isolation Systems, Inc [2007] and they can be seen in Table 6.1.

Table 6.1: Elastomeric bearing's engineering properties

Isolator	Isolator Diameter D_i (mm)	Isolator Height H_i (mm)	Lead Diameter LD_i (mm)	Elastic stiffness K_E (kN/mm)	Yield stiffness K_D (kN/mm)	Characteristic Strength F_y (kN)
1st	305	125	100	2.0	0.2	65
2nd	405	175	125	3.0	0.3	110
3rd	520	175	180	4.0	0.4	180
4th	650	205	205	5.0	0.5	220
5th	750	230	255	7.0	0.7	265

Link elements are added between the restrained nodes of the supports and the bottom nodes of first floor's columns, see Figure 6.7. Even though link elements are illustrated with geometrical dimensions in Figure 6.7, it has to be noticed that link elements are zero length elements. Therefore they do not influence the geometry of the structure.

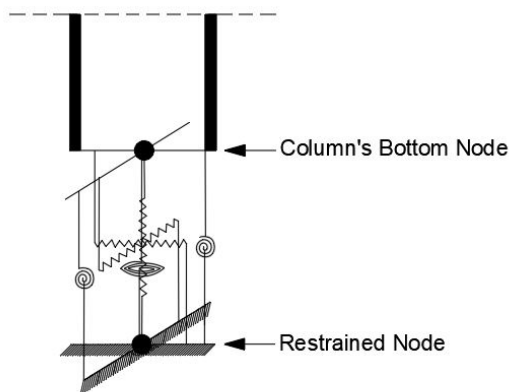


Figure 6.7: Elastomeric bearing simulation

6.2 Preliminary study of elastomeric bearings

In this case, the behaviour of a 2D framed structure with and without base isolation is investigated. The structure under investigation is a moment resisting frame, identical with the moment resisting frames of the ten-storey office building that has been analysed in Chapters 4 and 5. However, in this case elastic frame elements are used and the geometric nonlinearities are not included. Therefore the analysis is transformed to a linear elastic analysis. As a result of the reduction of the model to 2D framed structure and the analysis transformation to a linear elastic, the computational time is significantly reduced. Therefore a parametric study of the elastomeric engineering properties can be conducted.

Initially, a modal analysis is implemented and the mass of the frame is reduced so that the structure acquires the same dynamic characteristics as the 3D model of ten-storey office building. This is

understandable by comparing the eigenmodes and eigenperiods of the framed structure with the relevant periods of the 3D model, see Figure 6.8.

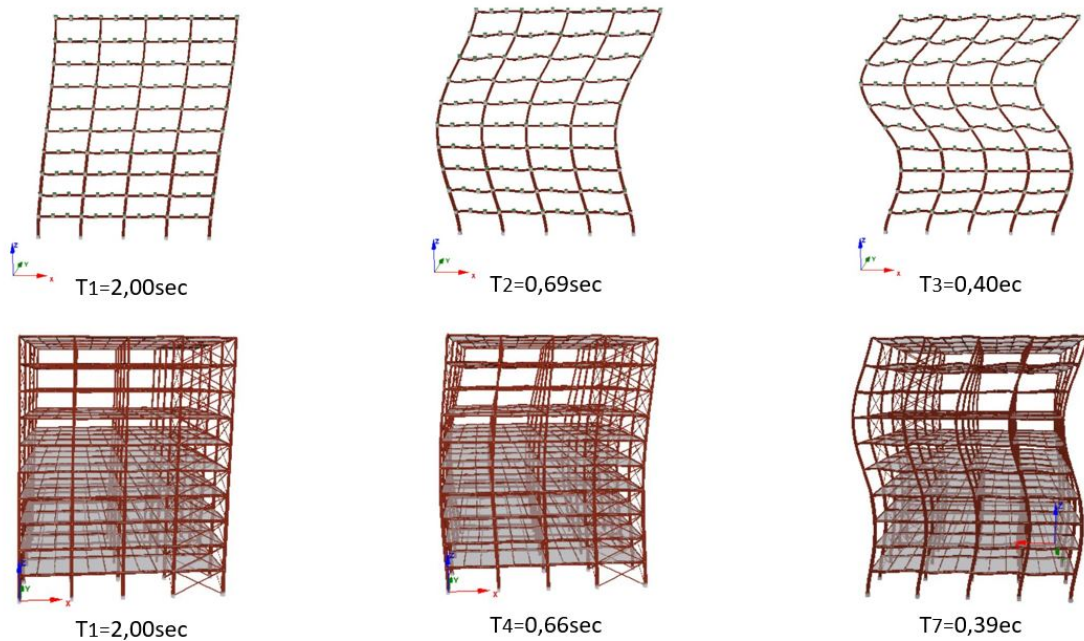


Figure 6.8: Eigenmodes' comparison

As it is illustrated, the 3D model's relative periods are the first the fourth and the seventh and their values are almost the same as the first, the second and the third period of the framed structure. Finally, the mass participation factor of the first three eigenmodes, of framed structure, is 91.52%. Therefore the first three eigenmodes are sufficient to describe the dynamic response of the structure according to EN1998-1 [2004].

Table 6.2: Framed structure's modal analysis results

Eigenmode	Frequency (Hz)	Period (sec)	Mass UX (%)
1st	0.50	2.00	73.44
2nd	1.45	0.69	13.43
3rd	2.50	0.40	4.65

Furthermore in this section, the artificially generated accelerogram, see Section 5.5.3, is used due to the fact that this is the more devastated for the structure. A linear elastic dynamic analysis is implemented for six different models. One of them is simulated as the fixed based frame while the rest are simulated with elastomeric bearings. The engineering properties of the elastomeric bearings varying according to Table 6.1.

Initially, the maximum absolute accelerations and displacements, of center of the mass, of every storey level are calculated. Moreover, the storeys' relative displacements are calculated, see Figure 6.9.c. For example, the maximum relative displacement between ground level and first floor is $0.08m$, between first floor and second floor $0.16m$ etc. As it can be seen in the same figure, the red line represents the envelopes of those magnitudes. The same procedure is implemented for all the cases and the results can be seen in Figure 6.10.

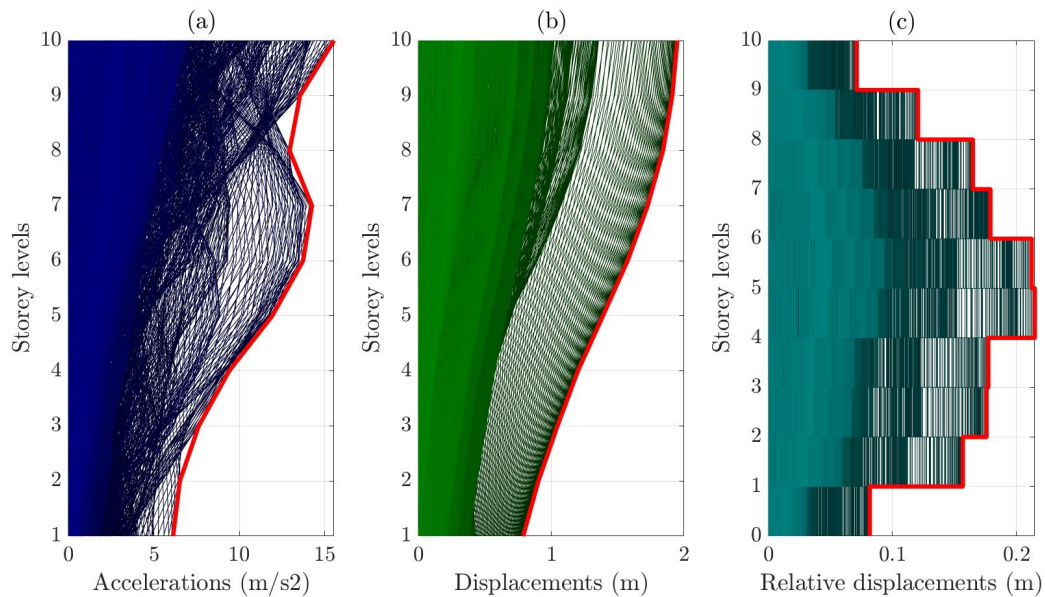


Figure 6.9: (a) Storeys' accelerations envelope, (b) Storeys' displacements envelope, (c) Storeys' relative displacements envelope

As it was expected, the seismic isolation of the frame is significantly affect the structural response and provides beneficial results. By looking at Figure 6.10, it is obvious that accelerations, displacements and storeys' relative displacements of isolated frames are significantly reduced compared to the fixed based frame responses. By comparing only the isolated frames' responses, it can be said that as the lateral stiffness of the elastomeric bearings is increased the less beneficial their effects are. However, even for the stiffer case (5th Isolator) the structural response is significantly better than the fixed based frame's response.

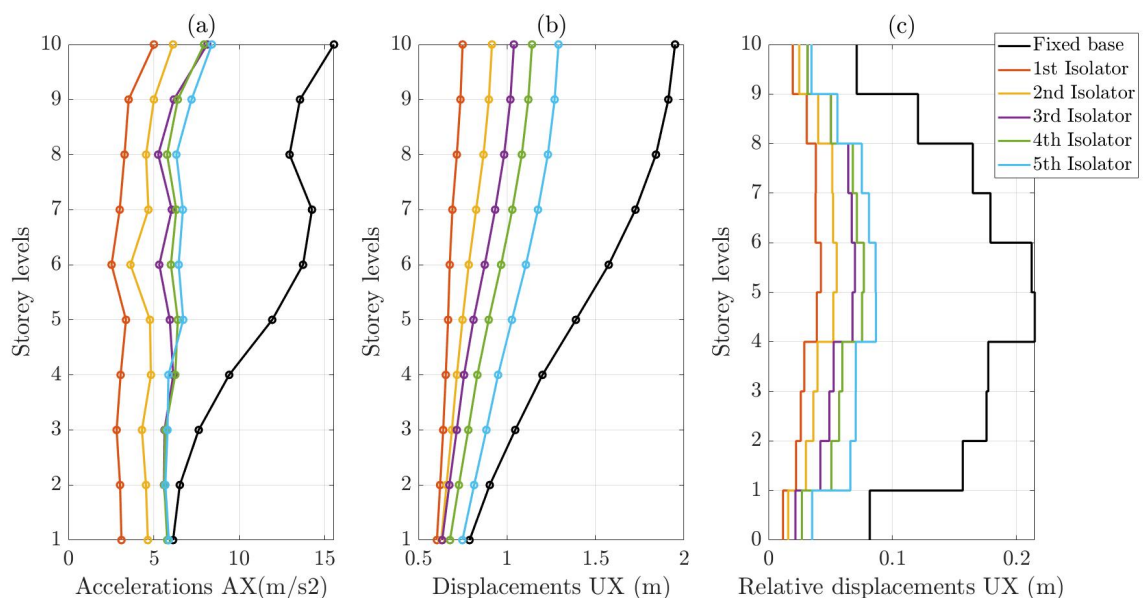


Figure 6.10: Fixed based frame: (a) Storey accelerations' envelope, (b) Storey displacements' envelope, (c) Storey relative displacements' envelope

Accordingly, the same behaviour is observed at the supports' total forces and total bending moments. For the fixed base case, the maximum force and bending moment amounts to $5533kN$ and $21050kNm$ respectively, while for the 5th elastomeric bearing case, they are calculated $2611kN$ and $9420kNm$ respectively. For the rest of the cases, as the elastomeric bearing's lateral stiffness is reduced, the developed forces and bending moments are reduced accordingly.

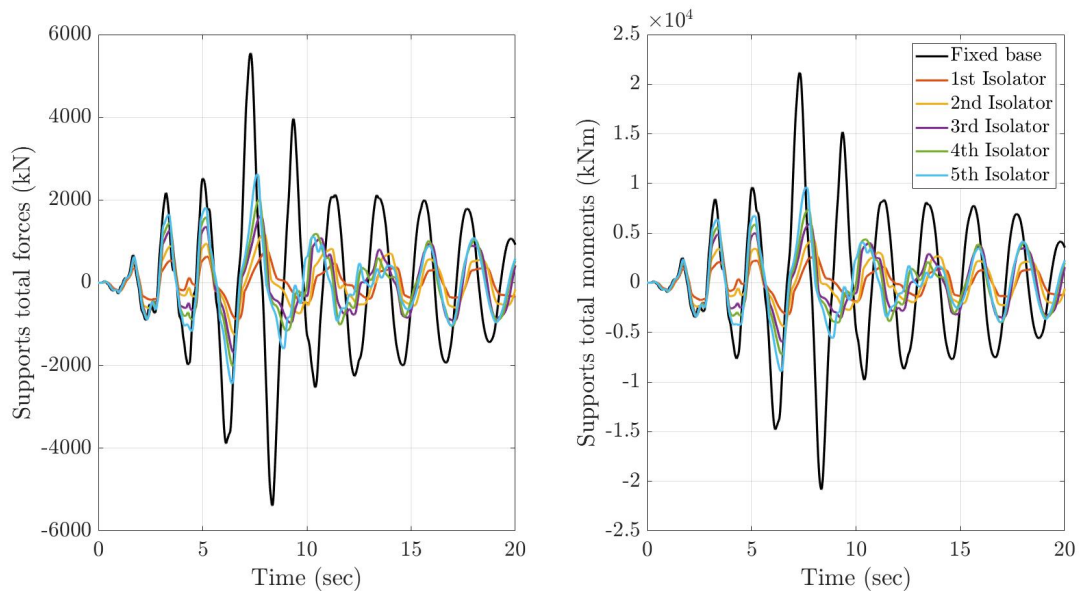


Figure 6.11: Total supports' forces and bending moments

In Figure 6.12 the elastomeric bearings' hysteretic curves are illustrated. The decision of the appropriate type of elastomeric bearings mainly depends on the initial stiffness of the device, as well as its yielding point. The initial stiffness should be high enough so that the presence of elastomeric bearings do not affect the serviceability of the structure. Furthermore, it has to be secured that the yielding point can be reached under moderated or high seismic actions so that the elastomeric bearing's stiffness to be reduced. In this way the desired flexibility is provided only when it is necessary.

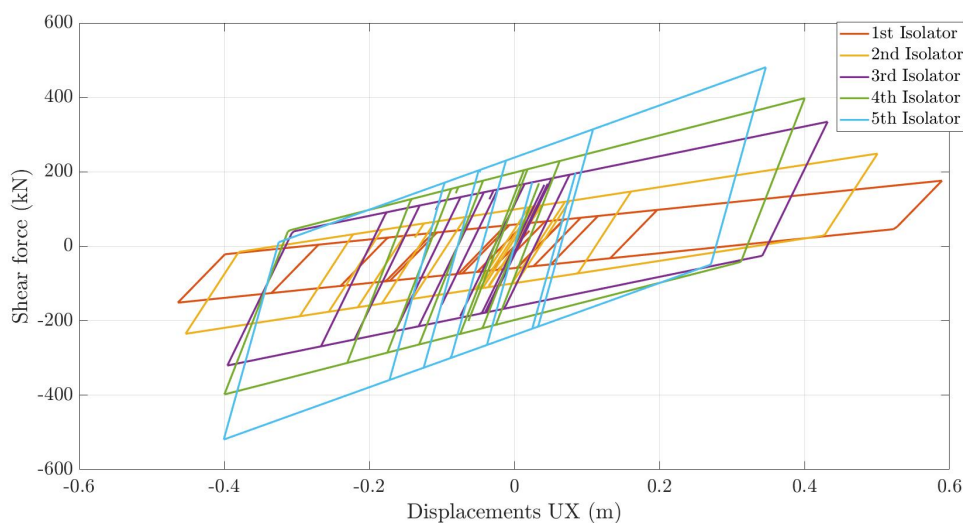


Figure 6.12: Elastomeric bearings' hysteretic curves

6.3 3D model with elastomeric bearings

In this section, elastomeric bearings are added in the 3D model of the ten-storey office building that has been used in Chapters 4 and 5. A nonlinear dynamic time history analysis is implemented and the results are compared with the fixed base structure response. The artificially generated accelerogram is applied, see Section 5.5.3. Under the effect of this accelerogram, the fixed base structure develops significant damages and the solution is unable to converge until the final state. Hence, it is considered that the fixed base structure can not sustain the applied accelerations.

The engineering properties of elastomeric bearings are randomly chosen to be the same as the 3rd isolator in Table 6.1. Therefore, the elastic stiffness, yield stiffness and characteristic strength are equal to $4.0kN/m$, $0.4kN/m$ and $180kN$ respectively.

6.3.1 X direction

Initially, the accelerations are applied to the restrained nodes in X direction. A comparison between the fixed base and isolated model is implemented. More detailed results about fixed base structure's response can be found in Section 5.5.3 and Appendix H.3.

As it can be seen in Figure 6.13, the oscillation of the isolated structure is significantly lower than the fixed base structure's oscillation. In absolute values, the maximum displacement for the isolated structure amounts to $0.9m$ while in the other case it is $1.31m$. For the fixed base structure the maximum amplitude of the oscillation is equal to $1.90m$. At the same time the maximum amplitude of oscillation for the isolated structure amounts to $1.20m$. However, the most important information out of Figure 6.13 is that in the first case the solution can not converge at the time-step of $16.51sec$ while in the second one the analysis is able to converge until the final state. Therefore, it is considered that the fixed base structure can not sustain the applied accelerogram and at the time step of $16.51sec$ there is structural collapse. On the other hand the isolated structure can sustain the applied accelerations until the final state.

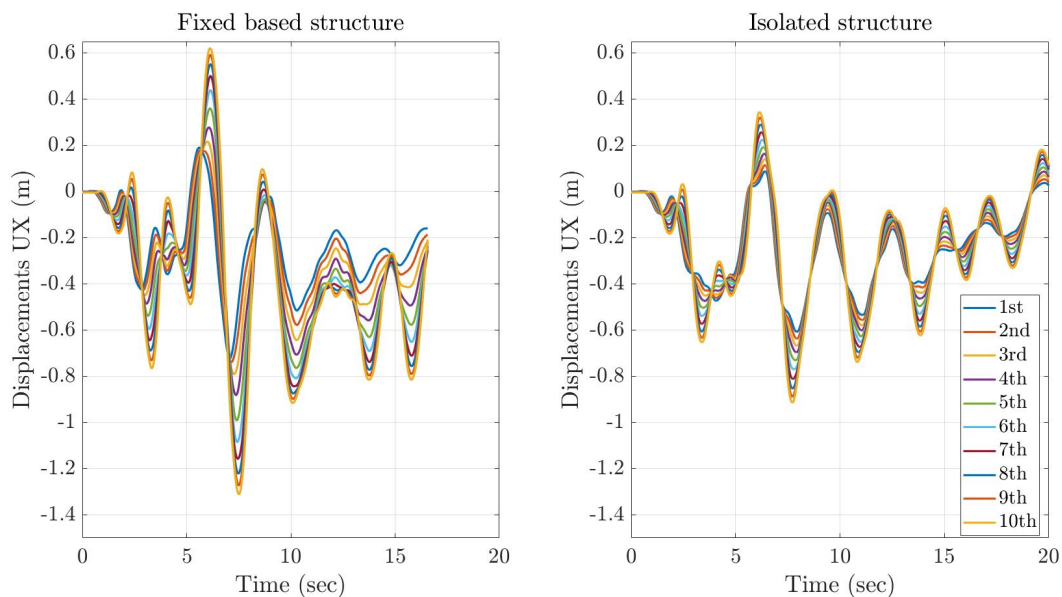


Figure 6.13: Displacements time history comparison

Furthermore, it can be seen in Figure 6.13 that the relative displacement between storey levels are larger for the fixed base structure. A more detailed comparison can be seen in Figure 6.14. It is obvious that the relative displacements for the fixed base structure are almost three times higher than the relative displacement of the isolated structure. In the first case the maximum relative displacement is equal to $0.14m$, while in the second case it amounts to $0.05m$. This is an important beneficial effect of base isolation as the high relative displacements between storey levels cause significant damages to the structure.

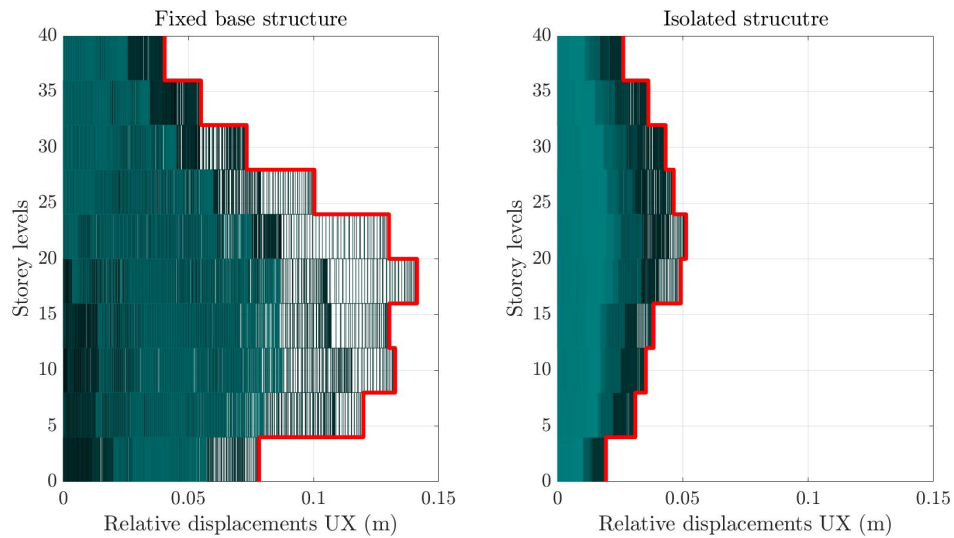


Figure 6.14: Relative displacements comparison

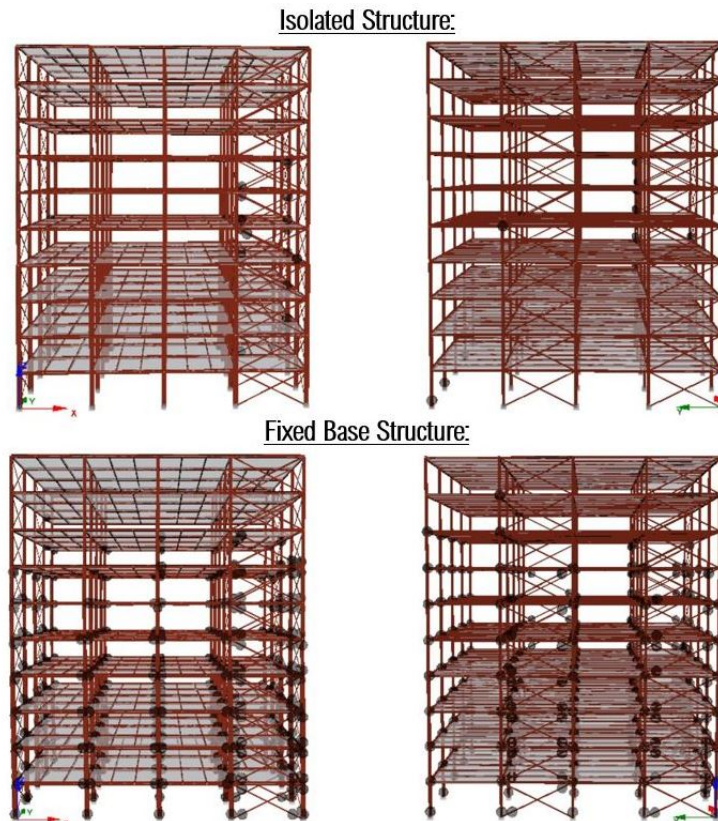


Figure 6.15: Damages occurrence for the two models

In Figure 6.15, the damages occurrence is illustrated. For every model two perspectives are depicted, in XZ and YZ plane. The black marks on the structure depict the damages and imply that in those points the strains are calculated equal or larger than 0.002 which is the yielding point of uniaxial stress-strain curve for steel *S355*. As it is obvious, the fixed base structure is experienced severe damages. Contrary, the isolated structure is experienced only limited plastic deformations which mainly occur at the bracing bars of the structure. Therefore, under this specific seismic actions in X direction, it is obvious that the elastomeric bearings have a beneficial contribution on the structural response.

6.3.2 Y direction

In this case, the accelerations are applied to the restrained nodes in line with the Y direction. As it can be seen in Figure 6.16 the numerical solution of the isolated structure is able to converge until the final state, while the solution of the fixed base structure is unable to converge at the time step of 9.35sec. Extensive plastic deformations are observed at this time step and therefore it is considered that the structure can not sustain further the applied accelerations.

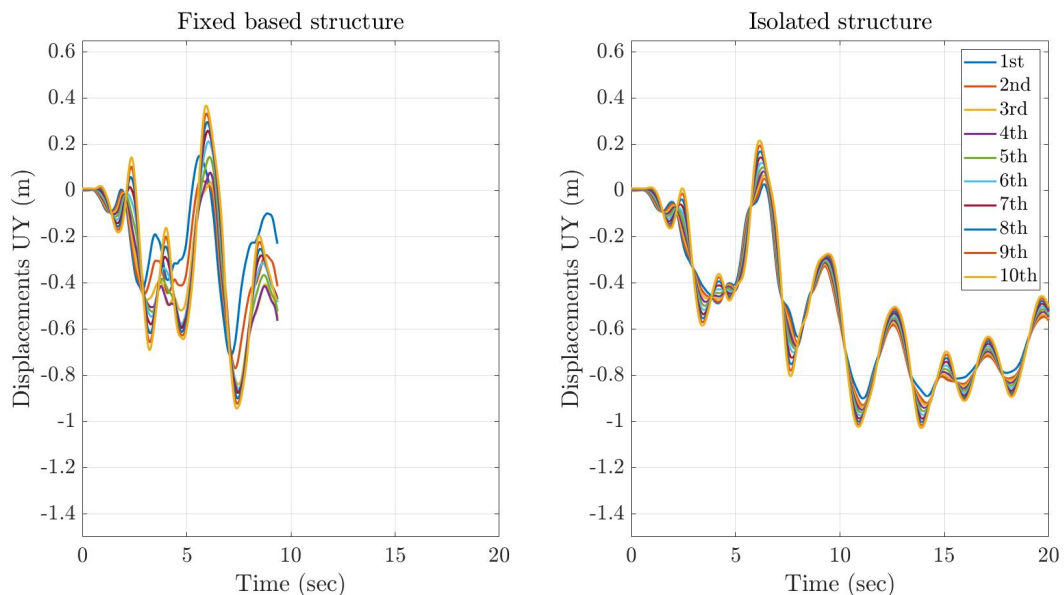


Figure 6.16: Displacements time history comparison

In Figure 6.17 the relative displacements at the center of mass between every storey level can be seen. It is clear that there is a significant increment of the relative displacement between ground and first storey-level, which is equal to $1.33m$. Therefore, it can be said that there is formation of soft storey mechanism. According to capacity design concept, it is of significant importance the avoidance of soft storey mechanism. Hence, in this case the use of elastomeric bearings is not as beneficial as in X direction. The formation of soft storey mechanism is possible to cause structural collapse. Even if the structure do not collapse the damages which are caused from the soft storey mechanism are difficult to be repaired.

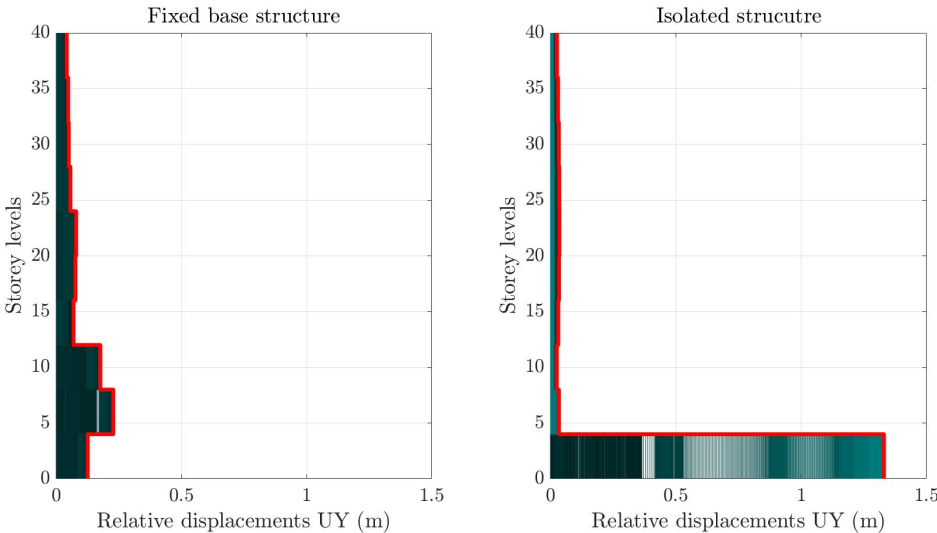


Figure 6.17: Relative displacements comparison

In Figure 6.18, the damages occurrence for the fixed base and isolated structure can be seen. By looking at the YZ perspective of the isolated structure it is obvious that first floor’s column have undergone extensive structural damages. The only exception are the concentrically brace columns which remain linear elastic.

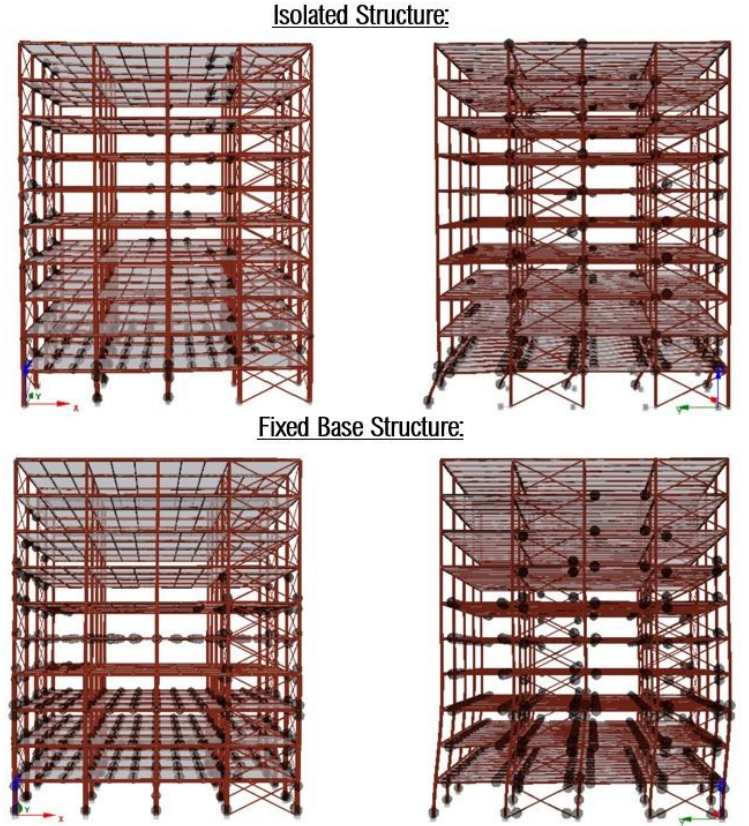


Figure 6.18: Damages occurrence for the two models

6.4 Perspectives of base isolation design

For a detailed design of a base isolated structure more aspects need to be taken into account. Initially, it has to be investigated whether or not the initial stiffness of the bearings is sufficient in order to avoid undesirable motion of the structure, under service loading. Furthermore, the axial capacity of the elastomeric bearings has to be higher than the expected axial loading under earthquake effect. However, it is not easy to predict the expected axial loading due to the fact that it varies when the engineering properties of the elastomeric bearing device changes. Therefore, several cases need to be examined.

Moreover, the response of elastomeric bearings, in reality, is strongly influenced by the weight or axial load they carried, A.K. Chopra [2004]. Such influence is important since axial loads vary in an earthquake due to overturning. The prior or post-yield lateral stiffness as well as the yielding strength might be modified. As a result the stability of the structure is significantly affected.

Therefore, these aspects need to be considered and a further investigation in these directions need to be done when a base isolated structure is designed.

Conclusion 7

The main purpose of this project is to design and examine the behaviour of a ten-storey steel structure under earthquake effects. The total height of the building is 40 meters, while its length in two principal horizontal directions is 32 meters. The beam and the columns are made out of steel (*S355*) while the slabs are made out of reinforced concrete (*C20/25*).

For the design of the structure, the Robot software by Autodesk is used which is a proficient tool for steel structures design, according to EC3 and EC8. The structure is consisted of moment resisting and concentrically braced frames. A modal analysis is performed so that the eigenmodes and eigenfrequencies to be calculated and also the finite element model to be validated. In addition, the eigenperiods are confirmed with the Rayleigh method. Then, the regularity criteria are investigated. Furthermore, two linear elastic analysis are implemented according to EC8. The modal response spectrum analysis and the equivalent static method of analysis are performed. By comparing the results from both methods as it concerns the base shear a large difference is observed. This is mainly caused due to simplified approach of the equivalent static method and the crude approximation of the fundamental eigenperiods. It has also to be mentioned that the equivalent static method takes into consideration only the two principal eigenmodes and it neglects the influence of higher eigenmodes, while the modal response spectrum takes into consideration seven eigenmodes. For all the above the modal response spectrum analysis is considered as more accurate method. Finally, the cross sectional dimensions are validated according to EC3 and EC8 and the capacity design provisions are investigated.

The advantage of the aforementioned linear elastic methods is that they do not demand expensive computational capacity. However, they use simplified methods to describe the nonlinear behaviour of the structure, which is of significant importance when earthquakes are considered. As a result, they might lead to an overestimation of the structural dimensions. Moreover, in case of irregular buildings, the nonlinear behaviour can be wrongly predicted due to the fact that those methods consider equally distributed plasticity to the structure.

In the next step the response assessment of the ten-storey building is implemented by means of nonlinear analysis. The finite element software Seismostruct is used for both static and dynamic nonlinear analysis. For the nonlinear static (pushover) analysis two models are used which are explained in Chapter 5. Both in X-direction and Y-direction the two models appear to have almost identical behaviour (capacity curves and yielding displacements). Moreover, the structural response in X direction indicates that the structure can easily resist even the higher events in its lifetime. Therefore, a more sophisticated design, with reduced cross sectional dimensions might was possible. However, this is not the case in Y direction.

Furthermore, a nonlinear time history analysis is applied to the model. This is the most advanced method computationally. Three different accelerograms are used : Modified Northridge, Original Northridge and Artificially generated. In the first case, Northridge's recorded accelerogram is

modified so that its response spectrum matches with the elastic response spectrum as it is defined in EC8. Again, the analysis indicates that the cross sectional dimension could have been reduced. A similar behaviour is observed with the original Northridge accelerogram, even though it contains slightly higher spectral accelerations. The Artificially generated accelerogram is created by use of *SeismoArtif* a software capable to generate earthquake matched to a specific target response spectrum. In this case, a response spectrum which is defined in the New Mexican norm is chosen. The main target is to apply a ground motion which would strongly affect the structure (high spectral accelerations in range 1.80 and 2.00 seconds). In this way, it is clearly stated that the earthquake design should be implemented according to the local seismic expectations. As a result, the artificially generated accelerogram is more destructive for the structure.

Then, the effect of a base isolation system is investigated. With this method, a flexible layer is introduced between the structure and its foundation in order to achieve decoupling of the two components which results in an increase of eigenperiods, so that resonance with earthquake excitation is avoided. In this project the use of lead-rubber elastomeric bearings is selected. Chapter 6 explains analytically the modeling of the selected elastomeric bearings. Initially a 2D framed structure, with and without seismic isolation, is subjected to the artificially generated accelerogram. The seismic isolation of the frame significantly affects the structural response and provides beneficial results. The accelerations and the displacements of isolated frames are significantly reduced compared to the fixed based frame responses. Finally, elastomeric bearings are added in the 3D model of the ten-storey office building. Once again the artificially generated accelerogram is applied. In X direction the isolated structure is experienced only limited plastic deformations which mainly occur at the bracing bars of the structure. So it is obvious that the the elastomeric bearings have beneficial effects on the structural behaviour. On the contrary, in Y direction the structural response indicates soft floor mechanism.

Further research can be made by extended parametric study of the structural irregularities and their affect to the dynamic response of the structure. Additionally, the influence of semi-rigid steel connection between beams columns and bracing bars can be considered. Moreover, the structure-foundation dynamic interaction can be investigated. Furthermore, a more detailed investigation of the base isolation techniques, as well as consideration of elastomeric bearings' coupled degrees of freedom can be done.

Bibliography

- A.K. Chopra, 2004.** J.M. Kelly A.K. Chopra, K. L.Ryan. *Experimental observation of axial load effects in isolation bearings*. 13th World Conference on Earthquake Engineering Vancouver, B.C., Canada August 1-6, No. 1707, 2004.
- Alessia Di Cuiaa, 2017.** Flavia De Lucaa Raffaele De Risia Silvia Caprili Walter Salvatore Alessia Di Cuiaa, Luca Lombardia. *Linear Time-History Analysis for EC8 design of CBF structures*. Procedia Engineering, 199, 2017.
- Anaxagoras Elenas, 2014.** Petros Alvanitopoulos Ioannis Andreadis Katerina Mallousi Anaxagoras Elenas, Eleni Vrochidou. *HHT-Based Artificial Seismic Accelerograms Generation*. version. 1, p. 477–485, 2014.
- Arnold, 2015.** Christopher Arnold. *EARTHQUAKE EFFECTS ON BUILDINGS*, 2015.
- Chopra, 2012.** Anil K. Chopra. *Dynamics Of Structures Theory and Applications to Earthquake Engineering*. ISSN: 0-13-285803-7. Pearson Education, 4 ed. edition, 2012.
- Chopra A. K. & Goel R. K., 2000.** Chopra A. K. & Goel R. K. *Building period formulas for estimating seismic displacements*. Earthquake Spectra, 16(2), 2000.
- Christensen, 2019.** Richard Christensen. *Physical Ductility*, 2019.
- D.Christianto, 2019.** E.Leonardy W.H.Lim M.Theodora D.Christianto, D.Surachmat. *Analysis of Damping Ratio in Passive Control Devices with Graded Sand as Fillers in the Shaft Section*. IOP Conference Series: Materials Science and Engineering towards a Resilient World, 2019.
- D.N.Grant, 2005.** F.Auricchio D.N.Grant, G. L.Fenves. *Modelling and analysis of high-damping rubber bearings for the seismic protection of bridges*. Research Rep. ROSE, 2005.
- Dynamic Isolation Systems, Inc, 2007.** Dynamic Isolation Systems, Inc. *Seismic Isolation for buildings and bridges*. <http://www.dis-inc.com/index.html>, 2007. Downloaded: 10-05-2020.
- E.Kotrotsou, 2015.** M.Hill I.Ioannou E.Kotrotsou, Y.D.Aktas. *Seismic Reliability of Elastomeric Base Isolators*. Conference: SECED 2015 Earthquake Risk and Engineering towards a Resilient World, 2015.
- Elghazouli, 2003.** Ahmed Y. Elghazouli. *Seismic design procedures for concentrically braced frames*, 2003.
- Elghazouli, 2017.** Ahmed Y. Elghazouli. *Seismic design of buildings to Eurocode 8*. ISBN-13: 978-1-4987-5159-9. CRC Press, Taylor and Francis Group, 2 ed. edition, 2017.
- EN1990, 2002.** CEN European Standard EN1990. *EN1990: Basis of structural design*, 2002.
- EN1991-1-1, 2002.** CEN European Standard EN1991-1-1. *EN1991-1-1: Actions on structures, Part 1-1: General actions — Densities, self-weight, imposed loads for buildings*, 2002.

- EN1993-1-1, 2005.** CEN European Standard EN1993-1-1. *EN1993-1-1: Design of steel structures, Part 1-1: General rules, and rules for buildings*, 2005.
- EN1998-1, 2004.** CEN European Standard EN1998-1. *EN1998-1: Design of structures for earthquake resistance, Part 1: General rules, seismic actions and rules for buildings*, 2004.
- Erdey, 2007.** Charles K. Erdey. *Earthquake Engineering*. ISBN-13: 978-0-470-04843-6 (cloth). John Wiley and Sons, Inc., Hoboken, New Jersey, first edition, 2007.
- G.P.Warn, 2012.** K.L.Ryan. G.P.Warn. *A review of seismic isolation for buildings: historical development and research needs*. Buildings, 2(3), 2012.
- Hancock J., 2006.** Abrahamson N.A. Bommer J.J. Markatis A. McCoy E. Mendis R. Hancock J., Watson-Lamprey J. *An improved method of matching response spectra of recorded earthquake ground motion using wavelets*. Journal of Earthquake Engineering, 10, 2006.
- Krabbenhøft, 2002.** Kristian Krabbenhøft. *Basic Computational Plasticity*, 2002. Department of Civil Engineering Technical University of Denmark.
- Kumar, 2018.** Manish Kumar. *Elastomeric seismic isolation bearings - Modelling, analysis and design*, 2018.
- L.Damkilde, 2018.** L.Damkilde. *Introduction to Structural Dynamics*, 2018.
- Luis S. da Silva, 2010.** Helena Gervasio Luis S. da Silva, Rui Simoes. *Design of steel structures*. ISBN: 978-92-9147-098-3. ECCS – European Convention for Constructional Steelwork, first edition, 2010.
- M. Bosco, 2014.** E.M. Marino P.P. Rossi M. Bosco, A. Ghersi. *A Capacity Design Procedure For Columns of Steel Structures with Diagonals Braces*. The Open Construction and Building Technological Journal, 8, 2014.
- M. J. N. Priestly, 1992.** T. Paulay M. J. N. Priestly. *Seismic Design of Reinforced Concrete and Masonry Buildings*. ISBN: 9780470172841. John Wiley & Sons, Inc, 1 ed. edition, 1992.
- Martinelli, 1996.** Perotti F. Martinelli, Mulas M. G. *The seismic response of concentrically braced moment-resisting steel frames*. Earthquake engineering & structural dynamics, Vol. 25, 1996.
- M.C.Constantinou, 2007.** Y.Kalpakidis D.M.Fenz G.P.Warn M.C.Constantinou, A.S.Whittaker. *Performance of Seismic Isolation Hardware Under Service and Seismic Loading*. ISSN 1520-295X. Technical Report MCEER-07-0012, University at Buffalo, The State University of New York, 1 ed. edition, 2007.
- Muhammad Tayyab Naqash, 2014.** Salim Khoso Muhammad Tayyab Naqash, Khalid Mahmood. *An Overview on the Seismic Design of Braced Frames*. American Journal of Civil Engineering, Vol. 2, No. 2, 2014.
- N.A.Abrahamson, 1992.** N.A.Abrahamson. *Non-stationary spectral matching*. Seismological Research Letters, 63, 1992.
- NMX-R-079-SCFI, 2015.** Seguridad Estructural de la Infraestructura Fisica Educativa. Requisitos. Direccion General de Normas NMX-R-079-SCFI. *Norma Mexicana, Escuelas.*, 2015.

- P. Bisch, 2012.** H. Degee P. Fajfar M. Fardis P. Franchin M. Kreslin A. Pecker P. Pinto A. Plumier H. Somja G. Tsionis P. Bisch, E. Carvalho. *Eurocode 8: Seismic Design of Buildings Worked examples*. ISBN: 978-92-79-23068-4. Publications Office of the European Union, 1st edition, 2012.
- Pettinga and Priestley, 2008.** Didier Pettinga and Nigel Priestley. *Accounting for P-Delta effects in structures when using direct displacement-based design*. The 14th World Conference on Earthquake Engineering, October 2008, 2008.
- R.D.Cook, 2002.** Michael E. Plesha R.J.Witt R.D.Cook, D.S.Malkus. *Concepts and Applications of Finite Element Analysis*. John Wiley and Sons, Inc, fourth edition, 2002.
- Seismosoft, 2020.** Seismosoft. *SeismoStruct 2020 – A computer program for static and dynamic nonlinear analysis of framed structures*. <https://seismosoft.com/>, 2020. Downloaded: 28-02-2020.
- Seth Stein, 2005.** Michael Wyssession Seth Stein. *An Introduction to Seismology, Earthquakes, and Earth Structure*. ISBN 0-86542-078-5. Blackwell Publishing Ltd., first edition, 2005.
- T.A. Adagunodo, 2015.** L.A. Sunmonu T.A. Adagunodo. *Earthquake: A terrifying of all natural phenomenal*. Journal of Advances in Biological and Basic Research, 8, 2015.
- T.Fujita., 1998.** T.Fujita. *Seismic isolation of civil buildings in Japan*. Progress in Structural Engineering and Materials, 1(3), 1998.
- W.F. Chen, 2005.** E.M. Lui W.F. Chen. *Handbook of Structural Engineering*. CRC Press, second edition edition, 2005.

Part II

Appendix

Analysis Methods A

In this chapter the recommended approaches of earthquake design and response assessment, according to EN1998-1 [2004], are described. Initially, an introduction to the response spectrum concept is given and then the four different methods of analysis are analysed.

A.1 Elastic response spectrum

The three out of four recommended approaches make use of response spectrum. Therefore, its concept has to be introduced. A significant advantage of response spectrum is that seismic signals that looks different in time domain representation may actually contain similar frequencies and therefore result to similar response spectrum Elghazouli [2017]. Most of the seismic design norms represent the earthquake effects as lateral forces applied on the structure or as maximum accelerations corresponding to each critical eigenmode, see Section A.3. The forces and the accelerations are determined from the response spectrum which represent the maximum acceleration, velocity or displacement of single degree of freedom structures under the expected ground excitation. The maximum response is plotted as functions of the eigenperiods, see Figure A.1.

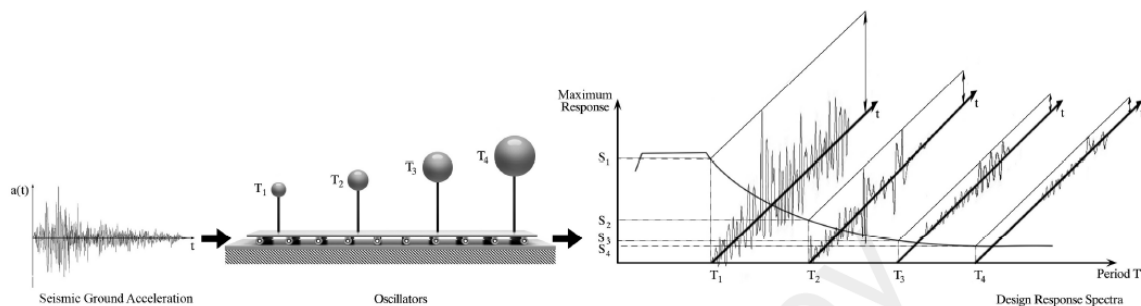


Figure A.1: Concept of design response spectrum [Anaxagoras Elenas, 2014]

Initially, the structural response is considered elastic. Therefore the starting point is the determination of the horizontal elastic response spectrum. In this point, it has to be mentioned that the vertical ground excitation is taken into account only in special cases. Therefore, in this project only the horizontal actions are considered. According to EN1998-1 [2004], there are two categories of spectra, as it can be seen in Figures A.2 and A.3. The first one is used for areas of high seismicity, earthquake magnitudes higher than 5.5, while the second one is used for areas of moderate seismicity.

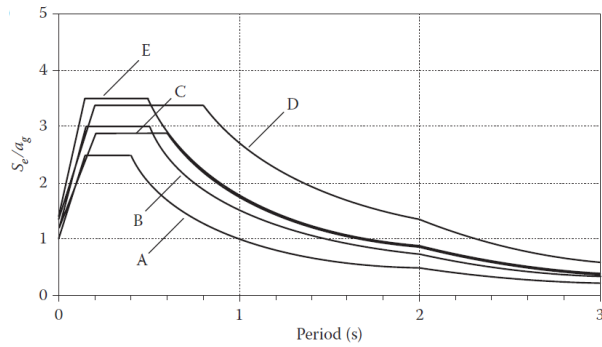


Figure A.2: Elastic response spectrum type 1, [EN1998-1, 2004]

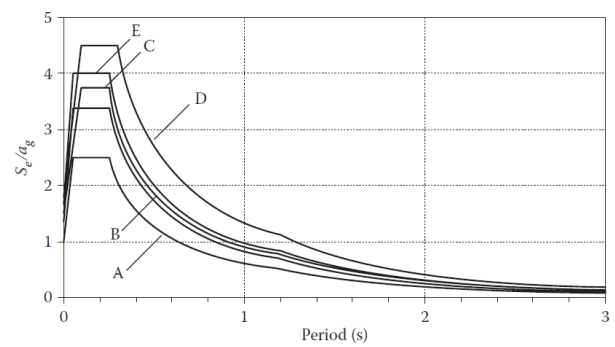


Figure A.3: Elastic response spectrum type 2, [EN1998-1, 2004]

The horizontal axis represents the natural periods of the single degree of systems and the vertical axis represents the spectral acceleration of the elastic structure, S_e , normalized by the peak ground acceleration, a_g . Moreover, as it can be seen there are five categories corresponding to different soil profiles. The classification of the soil profiles is done according to Table B.1 which can be found in Appendix B. The elastic response spectrum is calculated according to the following equations:

$$\begin{aligned}
 S_e(T) &= a_g \cdot S \cdot \left[1 + \frac{T}{T_B} \cdot (\eta \cdot 2.5 - 1) \right] & \text{for } 0 \leq T \leq T_B \\
 S_e(T) &= a_g \cdot S \cdot \eta \cdot 2.5 & \text{for } T_B \leq T \leq T_C \\
 S_e(T) &= a_g \cdot S \cdot \eta \cdot 2.5 \cdot \frac{T_C}{T} & \text{for } T_C \leq T \leq T_D \\
 S_e(T) &= a_g \cdot S \cdot \eta \cdot 2.5 \cdot \frac{T_C \cdot T_D}{T^2} & \text{for } T_D \leq T \leq 4
 \end{aligned} \tag{A.1}$$

where a_g is the peak ground acceleration, S is the soil factor and η is the damping factor. The values of S , T_B , T_C and T_D , for response spectrum type 1 and type 2, can be found in Appendix B. The peak ground acceleration varies in respect to the seismic zone of the region under consideration.

A.2 Ductility and design spectrum

Designing structures to remain elastic in large earthquakes turns out to uneconomic and might infeasible solutions. According to earthquake design concept, the structural response can be inelastic. Therefore, it is expected that the structure, under earthquake effects, can be deformed plastically, so that a part of the induced energy is dissipated. Ductility is the ability of the structure to develop plastic deformations without losing its bearing capacity. The ductility index is determined as follows:

$$\mu = \frac{d_u}{d_y} \tag{A.2}$$

where:

d_u | displacement at the fracture
 d_y | displacement at the yielding

The plasticity index depends on:

- the material of the structure. Structures made out of steel have higher plasticity index than structures made out of masonry.
- the statical indeterminacy. The higher the degree of indeterminacy the higher the plasticity index due to the fact that the stresses and the strains can be redistributed in many elements without structural collapse.

The ductility of a structure depends on the response of its elements. Under cyclic loading, the response of an element is described as ductile when the hysteresis loops are constant in respect to the maximum force and the width of loops, see Figure A.4. Contrariwise the element is characterised as brittle when it loses its bearing capacity and the width of the loops is reduced, see Figure A.5.

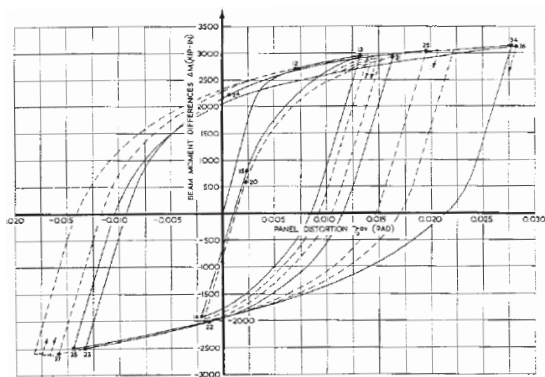


Figure A.4: Force–deformation relations for structural steel, [Chopra, 2012]

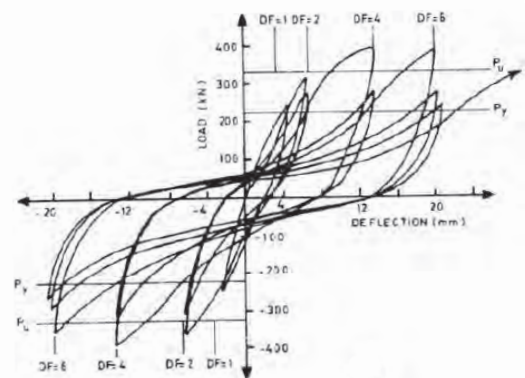


Figure A.5: Force–deformation relations for masonry, [Chopra, 2012]

According to EN1998-1 [2004], the ability of the structure to dissipate energy through plastic deformations can be taken into account by applying an elastic analysis but with a force reduction. This can be done by introducing the behaviour factor q . This is the ratio between the peak force that would be developed in a single degree of freedom structure if its response was only elastic, F_{el} and the yield force of the system, F_y .

$$q = \frac{F_{el}}{F_y} \quad (\text{A.3})$$

The value of the behaviour factor q is determined according to EN1998-1 [2004], based on the structural material and the static system of the structure. Furthermore, the structures are categorized in three different levels according to their ductility. Designing a structure against earthquake effects, the ductility class of the structure should be specified in advance. Usually, in regions of higher seismicity the structures are designed to have dissipative structural behaviour, therefore medium or high ductility structures, while in regions of lower seismicity the structures are designed with low ductility.

Table A.1: Elastic response spectrum values type 2, [EN1998-1, 2004]

Structural ductility class	Range of values of behaviour factor
DCL: Low ductility	≤ 1.5
DCM: Medium ductility	≤ 4 , see Table 6.2 [EN1998-1, 2004]
DCH: High ductility	see Table 6.2 [EN1998-1, 2004]

Table A.2: Elastic response spectrum values type 2, [EN1998-1, 2004]

The behaviour factor \mathbf{q} is used in order to reduce the elastic response spectrum values. This results to the design spectrum according to EN1998-1 [2004]. The most common approach to design structures, by taking into account the non-linear response, is to apply a linear elastic structural analysis but with reduced design forces as it is explained later in this chapter. The applied forces are outcome of the design spectrum, see Figure A.6 This approach is useful in regular structures where plasticity is uniformly distributed. In more complex cases, this approach is unreliable and more advanced methods should be used, such as nonlinear static or time history analysis.

Design spectra, based on the type 1 elastic response spectrum and soil type C for a range of different behaviour factors can be seen in Figure A.6. In most of the period's ranges the design spectra are a factor of \mathbf{q} times lower than the values of the elastic spectrum, as it can be seen from the following equations:

$$\begin{aligned}
 S_d(T) &= a_g \cdot S \cdot \left[\frac{2}{3} + \frac{T}{T_B} \cdot \left(\frac{2.5}{q} - \frac{2}{3} \right) \right] & \text{for } 0 \leq T \leq T_B \\
 S_d(T) &= a_g \cdot S \cdot \frac{2.5}{q} & \text{for } T_B \leq T \leq T_C \\
 S_d(T) &= a_g \cdot S \cdot \frac{2.5}{q} \cdot \frac{T_C}{T} & \text{for } T_c \leq T \leq T_D \\
 S_d(T) &= a_g \cdot S \cdot \frac{2.5}{q} \cdot \frac{T_C \cdot T_D}{T^2} & \text{for } T_D \leq T \leq 4
 \end{aligned} \tag{A.4}$$

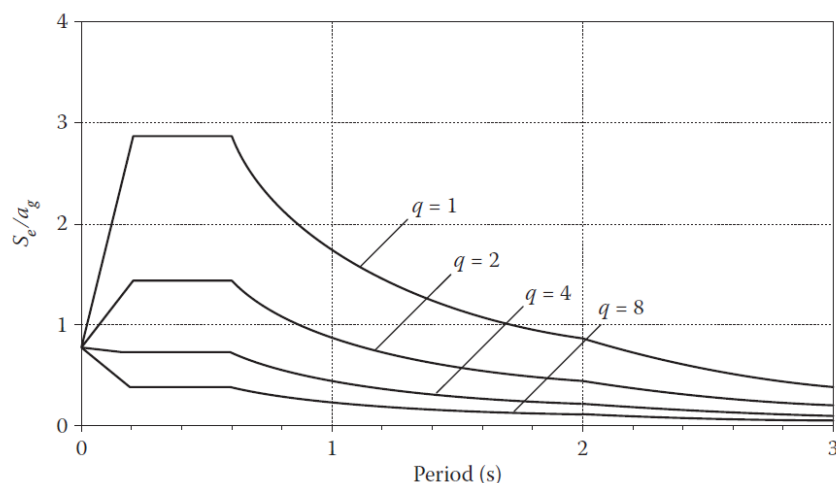


Figure A.6: Design response spectra (type 1 spectrum, soil type C), [Elghazouli, 2017]

A.3 Modal response spectrum analysis

In general, modal response spectrum analysis is a dynamic method of analysis, which is consisted out of a continuity of static analysis. Even though a static analysis is implemented, the dynamic nature of the structure is taken into account through free vibration analysis while the ground motion characteristics are taken into account by use of the response spectrum. It is an approximate method and the results are not expected to be the same as a dynamic time history analysis. However, it is considered sufficient for designing purposes due to its small computational cost. However, the disadvantage of this method is that approximate solutions are given for the combination of the modal responses since the principal of superposition can not be applied. The main steps of this procedure can be summarised as follows:

- Free vibration analysis
- Decide the number of the eigenmodes
- Compute the modal properties, read the spectral acceleration and compute the desired response parameters
- Combine the modal contributions

Initially, a free vibration analysis should be implemented, so that the natural frequencies and the eigenmodes to be determined, see R.D.Cook [2002].

$$[M]\{\ddot{D}\} + [K]\{D\} = 0 \quad (\text{A.5})$$

A system of N degrees of freedom is able to be vibrated in N different modes which occur in particular frequencies and they are independent of external loading. The following figures illustrates the four eigenmodes of a four-storey framed structure with stiff floors.

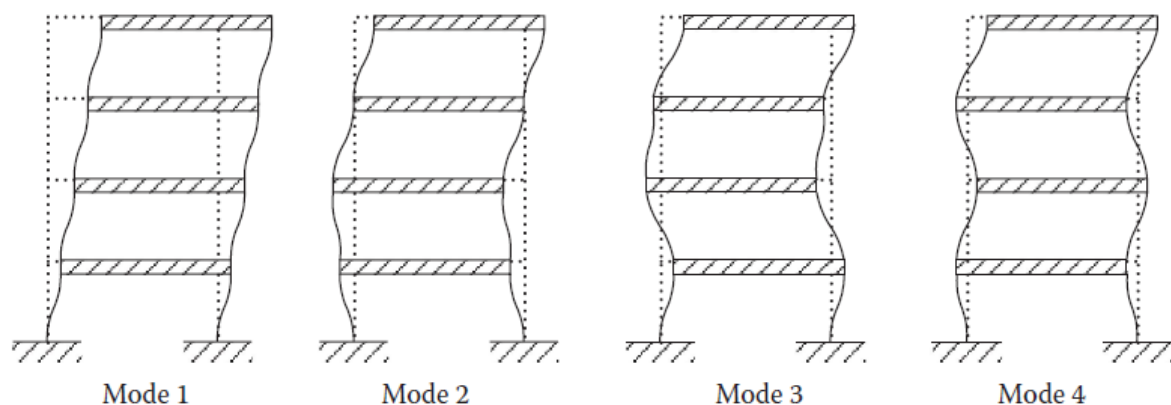


Figure A.7: Mode shapes of a four-storey building [Elghazouli, 2017]

Eigenmode is called the deformed shape of the structure when the structure is subjected to a harmonic loading with frequency equal to the specific eigenfrequency. The motion of the structure at any time can be written as the sum of the modal response. Each eigenmode activates a part of the total mass of the structure which is called modal mass.

According to EN1998-1 [2004], an approximate formula can be used so that the first eigenfrequency can be calculated.

$$T_1 = C_t H^{0.75} \quad (\text{A.6})$$

where T_1 is the first eigenfrequency in seconds, H is the height of the building in meters, and C_t is a constant which varies according to the structure's formulation.

Since the natural frequencies and the eigenmodes have been determined the equation of motion can be analysed as a set of N uncoupled equations by using the principle of modal superposition, see R.D.Cook [2002].

$$D = \bar{D}_1 Z_1 + \bar{D}_2 Z_2 + \dots + \bar{D}_N Z_N \quad (\text{A.7})$$

After some modification the equation of motion can be written in terms of modal coordinates Z_i

$$\ddot{Z}_i + 2\xi\omega_i\dot{Z}_i + \omega_i^2 Z = \frac{L_i}{M_i} \ddot{x}_g \quad (\text{A.8})$$

where ξ is the damping ratio, ω_i is the i^{th} eigenfrequency, \ddot{x}_g is the ground acceleration, $L_i = \sum_j m_j \bar{D}_{ij}$ and $M_i = \sum_j m_j \bar{D}_{ij}$. The index i refers to the eigenmode and the index j to the degree of freedom. Therefore, the factor L_i is an excitation factor which indicates the sensitivity of the i^{th} eigenmode to the induced ground motion and M_i is the modal mass. *The dimensionless factor L_i/M_i is the ratio of the response of a multi degree of freedom structure in a particular mode to that of a single degree of freedom system with the same mass and period*, Elghazouli [2017].

For each eigenmode, the spectral acceleration, corresponding to the specific eigenfrequency, can be found from the design response spectrum. Since this value is compatible for a single degree of system, it has to be scaled by the factor L_i/M_i . Finally, the horizontal forces on mass j^{th} in mode i^{th} are determined by simply multiply the aforementioned acceleration by the corresponding mass.

$$F_{ij}(\text{max}) = \frac{L_i}{M_i} S_{di} \bar{D}_{ij} m_j \quad (\text{A.9})$$

As long as the nodal forces has been determined, static analysis can be implemented. Moreover, the total horizontal force on the structure, which is called base shear, of i^{th} eigenmode is calculated by summing all the nodal forces:

$$F_{bj}(\text{max}) = \frac{L_i^2}{M_i} S_{di} \quad (\text{A.10})$$

The ratio L_i^2/M_i defines the amount of mass participation in the structural response of the particular eigenmode. It is often called participation factor. If this ratio is calculated and summed for all the eigenmodes of the structure, the result will be equal with the total mass of the structure.

In order to obtain the structural response the aforementioned procedure should be implemented for all the eigenmodes of the structure, which are as many as the degrees of freedom. It is obvious that this procedure demands significant computational time. In practice only a small subset of the eigenmodes is used, due to the fact that the participation factors are small for higher eigenmodes, Elghazouli [2017]. According to EN1998-1 [2004] it is sufficient to include modes, so that the sum of the effective masses is at least 90% of the total mass or to include all the eigenmodes with effective modal mass higher than 5%.

In some cases it is hard to fulfil the above-mentioned criteria. Therefore, EN1998-1 [2004] recommends the following expressions where n is the storeys' number and T_i is the i^{th} eigenfrequency.

- $k \geq 3\sqrt{n}$
- $T_i \leq 0.20sec$

Since the maximum modal responses don't occur simultaneously, the combination of them for the decided number of eigenmodes is done by simple rules, according to EN1998-1 [2004]. If the differences between every couple of eigenfrequencies are larger than 10% of the longer period, then the eigenmodes can be considered as independent. In this case, the *SRSS* method can be used. Therefore, the peak overall response, exE , of the peak modal responses E , is calculated with the following equation, where k is the number of the chosen eigenmodes.

$$exE = \pm \sqrt{\sum_{i=1}^k E_i^2} \quad (\text{A.11})$$

On the other hand, when the independent condition is not fulfilled, a more sophisticated procedure combination rule is used. This procedure is called *complete quadratic combination (CQC)* and is based on the estimation of a correlation coefficient, ε_{ij} , between two dependent eigenmodes, see Chopra [2012].

$$exE = \pm \sqrt{\sum_{i=1}^k \sum_{j=1}^k \varepsilon_{ij} E_i E_j} \quad (\text{A.12})$$

A.4 Equivalent static analysis

A simplified method, approximate the dynamic response of the structure by considering only the the first eigenmode. This method can be applied if the structure obey the regularity criteria, see Chapter 3 and it can be reasonably assumed that the structural response, under earthquake effects, coincides with its fundamental lateral eigenmode. Therefore, a simply static analysis procedure can be used, without considering the dynamic behaviour of the system. This procedure has been the main method of earthquake design, for many years, due to its computational simplicity.

According to EN1998-1 [2004], initially the fundamental natural period of the structure should be determined. This can be done either by some simplified semi-empirical formulas, see Equations A.6, or by free vibration analysis. Then it has to be verified if the equivalent static analysis is permitted which requires $T_1 < 2sec$. If this condition or regularity criteria are not met, modal response spectrum analysis must be used, see Section A.3.

Having determined the fundamental natural period of the structure, the spectral acceleration can be read from the design response spectrum. Then the base shear is calculated from the following equation:

$$F_b = \lambda m S_d \quad (\text{A.13})$$

where m is the total mass of the structure, S_d is the spectral acceleration, and λ is a constant which value is 0.85 for buildings of more than two storeys with $T_1 < 2T_C$ and is 1.0 for all the other cases. Furthermore, the base shear has to be distributed over the height of the building in proportion to each floor's mass and the shape of the eigenmode. For some simple cases of regular buildings, EN1998-1 [2004] allows the assumption that the first eigenmode is a straight line, the displacements are directly proportional to height. Therefore the base shear can be distributed according to the following equation:

$$F_k = F_b \frac{z_k m_k}{\sum_j z_j m_j} \quad (\text{A.14})$$

where z is the storey height. Finally, the response of the structure is calculated by linear static analysis with lateral forces as it can be seen in Figure A.8.

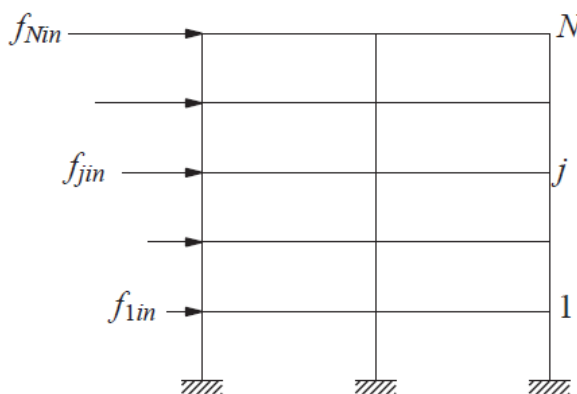


Figure A.8: Equivalent static forces for the i th frame associated with response of the building in its n th natural mode, [Chopra, 2012]

A.5 Nonlinear static analysis

Pushover analysis is a non-linear static analysis that can be used in order to estimate seismic structural deformations. According to this method, a structure is subjected to gravity loading and a monotonic displacement-controlled lateral load pattern which continuously increases through elastic and inelastic behavior until the ultimate condition is reached. It can be said that the lateral load represents the range of base shear which is caused by an earthquake load. A pushover curve (base shear against top displacement) can then be plotted. This curve describes the deformation capacity of the structure and is also well known as capacity curve. In order to determine the necessary demands of a structure which is subjected to an earthquake, this must be equated to the demand curve. The next step is to reexamine the non-linear static analysis in order to determine the

member forces and deformations at that specific point. The advantage of this method in comparison with the linear analysis and ductility modified response spectra is that it is based on a more accurate estimation of the distributed yielding within a structure, rather than an assumed, uniform ductility. However, it has to be mentioned that the pushover analysis has no strict theoretical basis, so if the assumed load distribution is incorrect, it may be inaccurate. There are several different pushover analysis which vary according to (i) the choices of load patterns to be applied and (ii) the method of simplifying the pushover curve for design use. The method which is used by the EN1998-1 [2004] can be analysed below:

Two pushover analyses are performed, using two different lateral load distributions. The most unfavourable results from those two different distributions, should be used for the design purposes. In the first case, the acceleration distribution is assumed proportional to the fundamental mode shape. The inertia force F_k can be obtained by the formula:

$$F_k = \frac{m_k \bar{D}_k}{\sum_j m_j \bar{D}_j} F_b \quad (\text{A.15})$$

where F_b is the base shear (which is increased steadily from zero until failure), m_k the k th storey mass and \bar{D}_k the mode shape coefficient for the k th floor. In case that the fundamental mode shape is linear, then \bar{D}_k is proportional to storey height z_k . In the second case the acceleration is assumed constant with height. The inertia forces are then obtained by the following formula:

$$F_k = \frac{m_k}{\sum_j m_j} F_b \quad (\text{A.16})$$

The variation of base shear F_b with top displacement d and maximum displacement d_m gives the output from the above analysis. This can be transformed to an equivalent single degree of freedom system by using the following relations:

$$F^* = \frac{F_b}{\Gamma}, \quad d^* = \frac{d}{\Gamma} \quad (\text{A.17})$$

where

$$\Gamma = \frac{\sum m_i \bar{D}_i}{\sum_i m_i \bar{D}_i^2} \quad (\text{A.18})$$

The Single degree of freedom pushover curve is expected to be somehow linear, due to the formation of successive plastic hinges as the lateral load intensity is increasing up to the point of the formation of a collapse mechanism. In order to determine the seismic demand from a response spectrum it is mandatory to simplify this to an equivalent elastic-perfectly plastic curve as shown in Figure A.9 The load required to cause formation of a collapse mechanism is denoted as F_y^* and d^*y indicates the yield displacement. By making use of the above, the initial elastic period of the idealised system can be estimated:

$$T^* = 2\pi \sqrt{\frac{m^* d_y^*}{F_y^*}} \quad (\text{A.19})$$

By taking into account the relation between the initial elastic period of the idealised system T^* and the period at the end of the constant-acceleration part of the design response spectrum T_C the target displacement of the Single degree of freedom system under the design earthquake can be estimated:

$$\begin{aligned} d_t^* &= S_e \left(\frac{T^*}{2\pi}\right)^2 & \text{for } T^* \geq T_C \\ d_t^* &= S_e \left(\frac{T^*}{2\pi}\right)^2 \frac{1}{q_u} \left[1 + (q_u - 1) \frac{T_C}{T^*}\right] & \text{for } T^* < T_C \end{aligned} \quad (\text{A.20})$$

where $q_n = (S_e / (F_y^* / m^*))$ and $m^* = \sum_{j=1}^n m_l \phi_i$

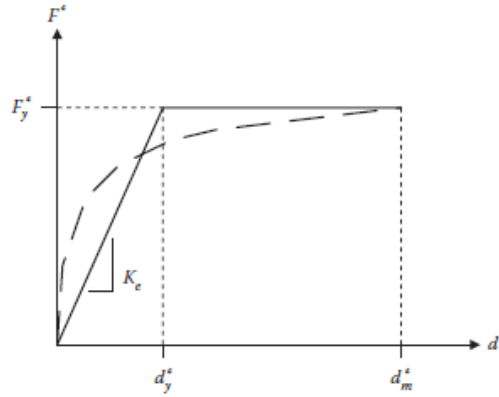


Figure A.9: Idealisation of pushover curve in EC8, [Elghazouli, 2017]

In Figures A.10 and A.11 the equation A.19 is visualized schematically, where the design response spectrum has been plotted in acceleration against displacement format rather than the more normal acceleration versus period. If T^* is greater than T_C , the target displacement is based on the equal displacement rule for elastic and inelastic systems. For shorter period structures, a correction is applied to account for the more complex interaction between behaviour factor and ductility. By using the equation A.16 the target displacement can be transformed from a single degree of freedom system to a multi degree of freedom system, and the forces and deformations in the structure can be checked by considering the point in the pushover analysis which corresponds to this displacement value. The benefit of using the procedure recommended by EN1998-1 [2004] is that it is a simple and explicit method but from the other side it is probably too conservative.

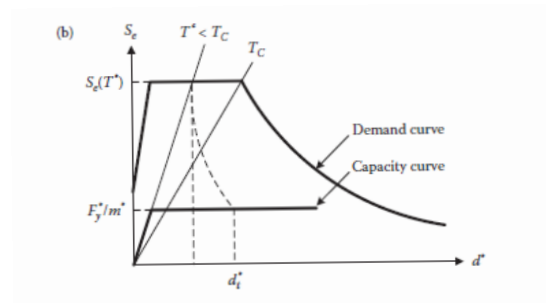


Figure A.10: Determination of target displacement in pushover analysis for short period, [Elghazouli, 2017]

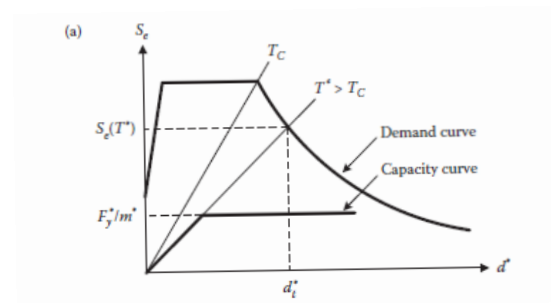


Figure A.11: Determination of target displacement in pushover analysis for long period, [Elghazouli, 2017]

A.6 Non-linear time history analysis

Another option is the use of non-linear dynamic analysis. According to this method, a non-linear model of the structure is analysed under a ground acceleration time history whose frequency content fits the design spectrum. The time history is defined as a series of data points at time intervals of the order of 0.01 s, and by using a stepwise procedure which is known as direct integration, the analysis is implemented. By enveloping and smoothing spectra which corresponds to different earthquake time histories the design spectra can be determined. This follows that there are several time histories which are well matched with the spectrum. These can either be recorded or artificially generated by making use of programs such as SIMQKE, for generating suites of spectrum-compatible accelerograms. The different spectrum-compatible time histories can give as a result different structural responses, so it is crucial to perform multiple analysis in order to be sure of achieving representative results. The mean result can be used if at least seven different analysis have been performed, otherwise the most severe result is the one which should be used. It is important to be mentioned that the earthquake time histories should be chosen in way so that the time domain characteristics such as duration and number of cycles, are relevant to the regional seismicity and local ground conditions.

EC8 table B

Ground type	Description of stratigraphic profile	Parameters		
		$V_{s,30}(m/s)$	N_{SPT}	$c_u(KPa)$
A	Rock or other rock-like geological formation, including at most 5m of weaker material at the surface	> 800	-	-
B	Deposits of very dense sand, gravel, or very stiff clay, at least several tens of meters in thickness, characterized by a gradual increase of mechanical properties with depth.	360 – 800	> 50	> 250
C	Deep deposits of dense or medium-dense sand, gravel or stiff clay with thickness from several tens to many hundreds of meters.	180 – 360	15 – 50	70 – 250
D	Deposits of loose-to-medium cohesionless soil (with or without some soft cohesive layers), or of predominantly soft-to-firm cohesive soil.	< 180	< 15	< 70
E	A soil profile consisting of surface alluvium layer with $v_s > 800m/s$.	-	-	-

Table B.1: Ground types [EN1998-1, 2004]

<i>Groundtype</i>	S	$T_B(sec)$	$T_C(sec)$	$T_D(sec)$
A	1.00	0.15	0.40	2.50
B	1.20	0.15	0.50	2.50
C	1.15	0.20	0.60	2.50
D	1.35	0.20	0.80	2.50
E	1.40	0.15	0.50	2.50

Table B.2: Elastic response spectrum values type 1, [EN1998-1, 2004]

<i>Groundtype</i>	<i>S</i>	<i>T_B(sec)</i>	<i>T_C(sec)</i>	<i>T_D(sec)</i>
A	1.00	0.10	0.25	1.50
B	1.25	0.10	0.30	1.50
C	1.40	0.15	0.35	1.50
D	1.60	0.15	0.45	1.50
E	1.70	0.10	0.35	1.50

Table B.3: Elastic response spectrum values type 2, [EN1998-1, 2004]

Modal response spectrum analysis results



C.1 Second load combination

Second load combination is defined as: $1.00G + 0.3Q + E_{Edx} - 0.3E_{Edy}$

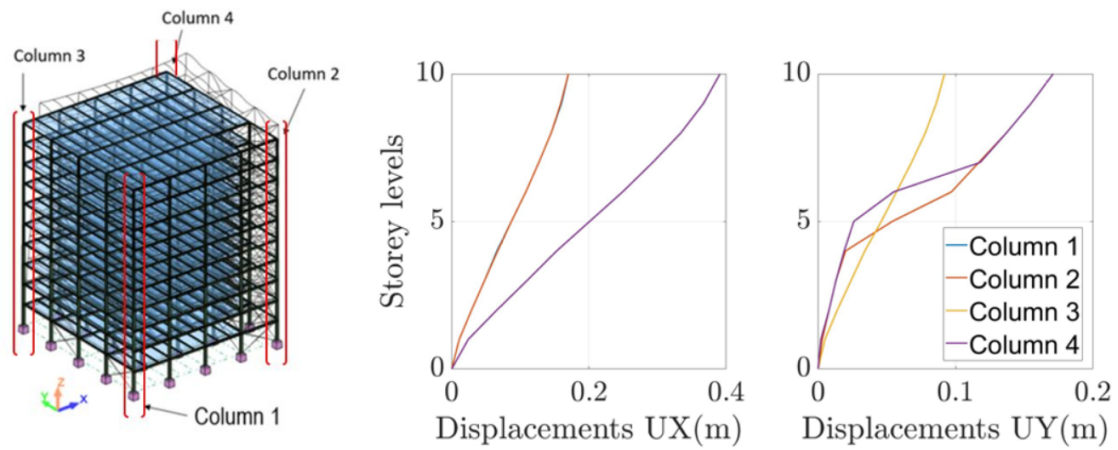


Figure C.1: Corner columns' displacements for the first combination ($1.00G + 0.3Q + E_{Edx} - 0.3E_{Edy}$)

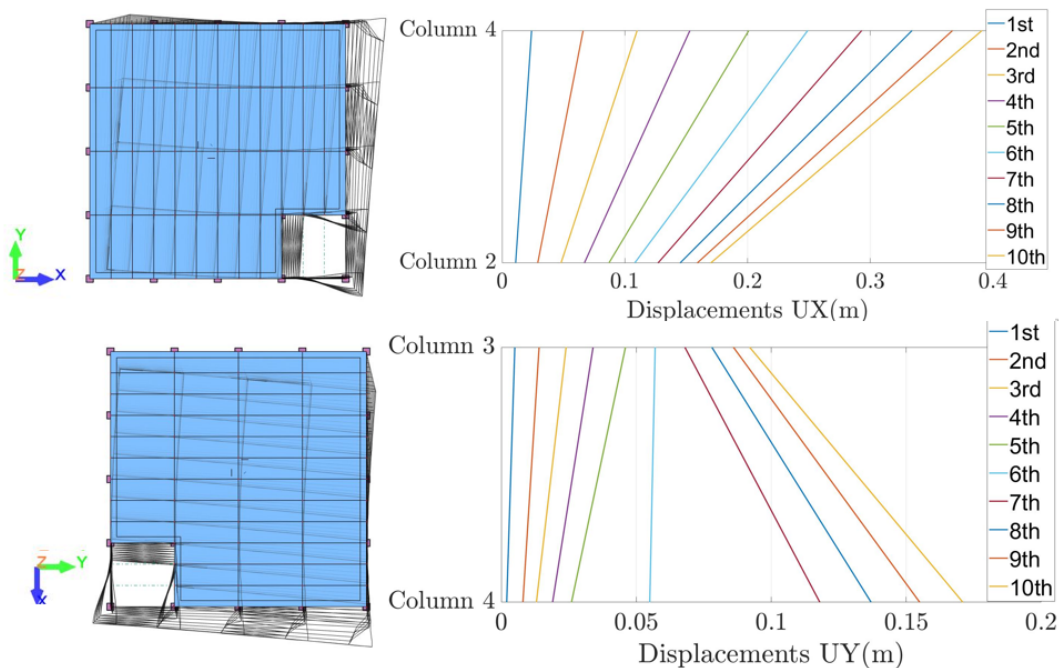


Figure C.2: Corner columns' displacements in plan, for the first combination ($1.00G + 0.3Q + E_{Edx} - 0.3E_{Edy}$)

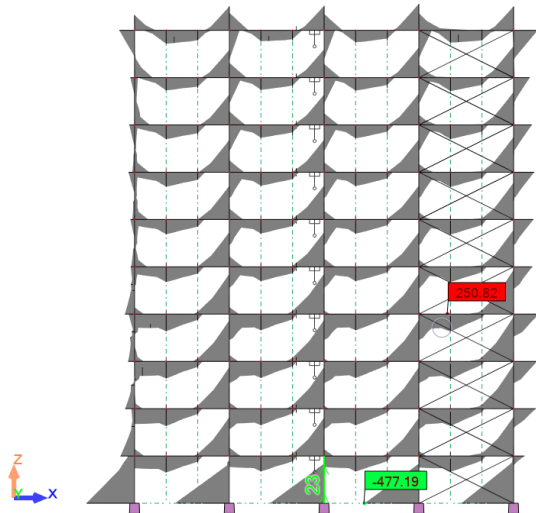


Figure C.3: Bending moments in X-direction out of the load combination $1.00G + 0.3Q + E_{Edx} - 0.3E_{Edy}$

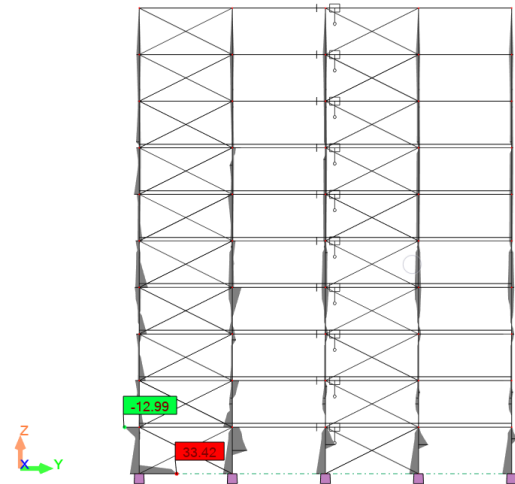


Figure C.4: Bending moments in Y-direction out of the load combination $1.00G + 0.3Q + E_{Edx} - 0.3E_{Edy}$

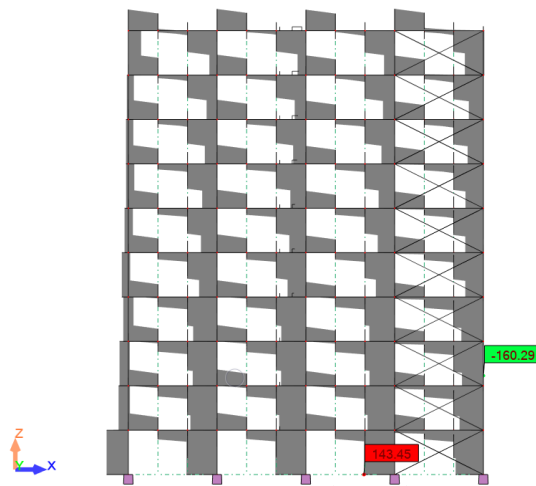


Figure C.5: Shear forces in X-direction out of the load combination $1.00G + 0.3Q + E_{Edx} - 0.3E_{Edy}$

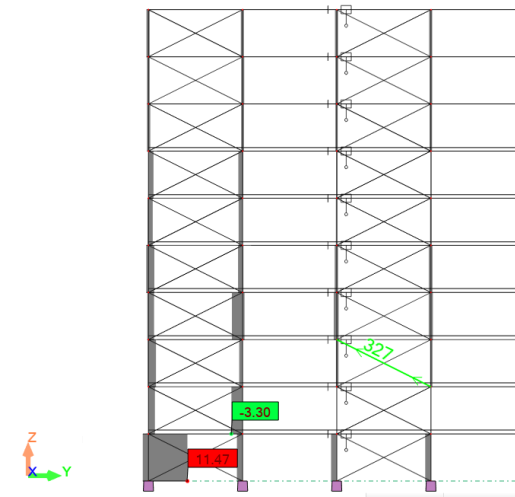


Figure C.6: Shear forces in Y-direction out of the load combination $1.00G + 0.3Q + E_{Edx} - 0.3E_{Edy}$

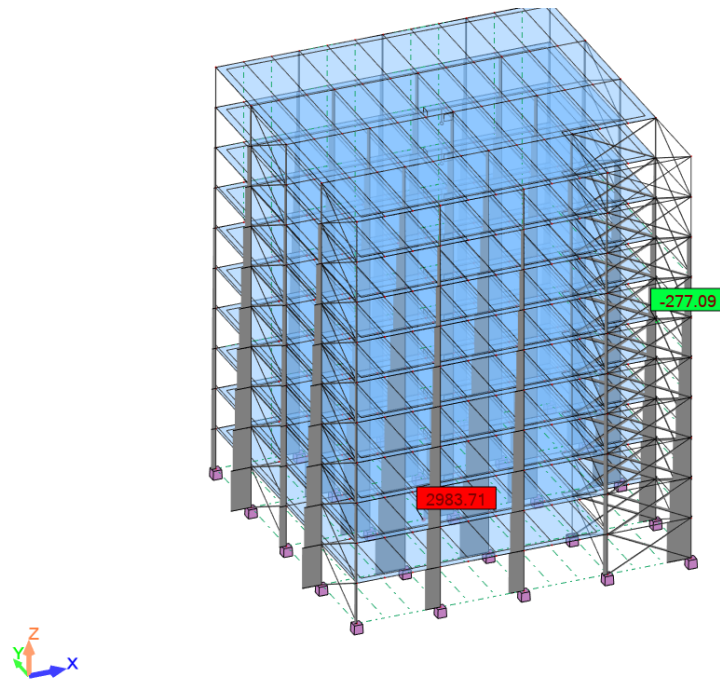


Figure C.7: Axial forces out of load combination $1.00G + 0.3Q + E_{Edx} - 0.3E_{Edy}$

C.2 Third load combination

Third load combination is defined as: $1.00G + 0.3Q + 0.3E_{Edx} + E_{Edy}$

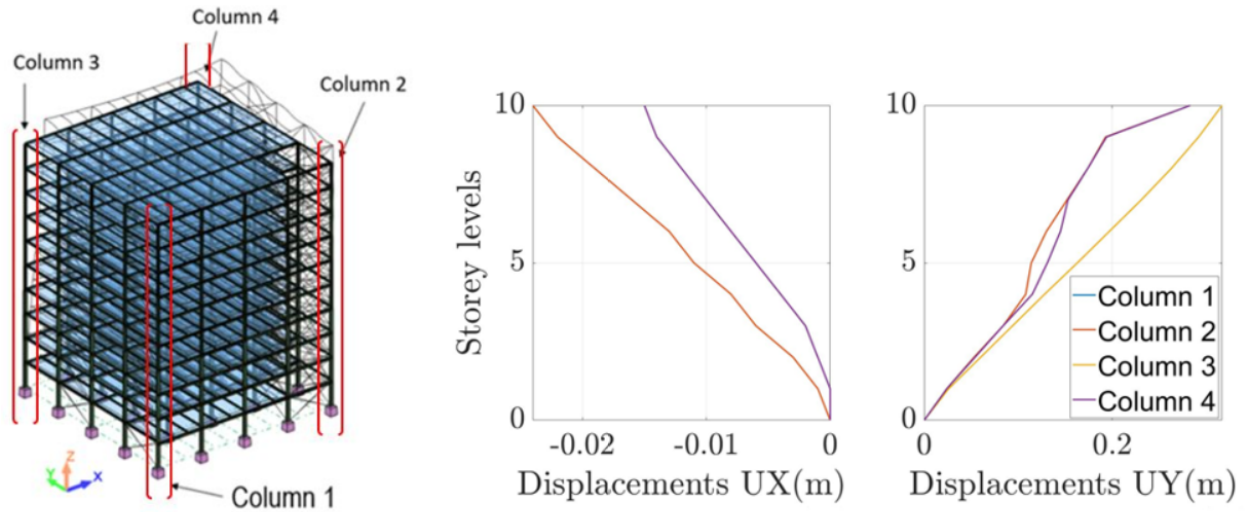


Figure C.8: Corner columns' displacements for the first combination ($1.00G + 0.3Q + 0.3E_{Edx} + E_{Edy}$)

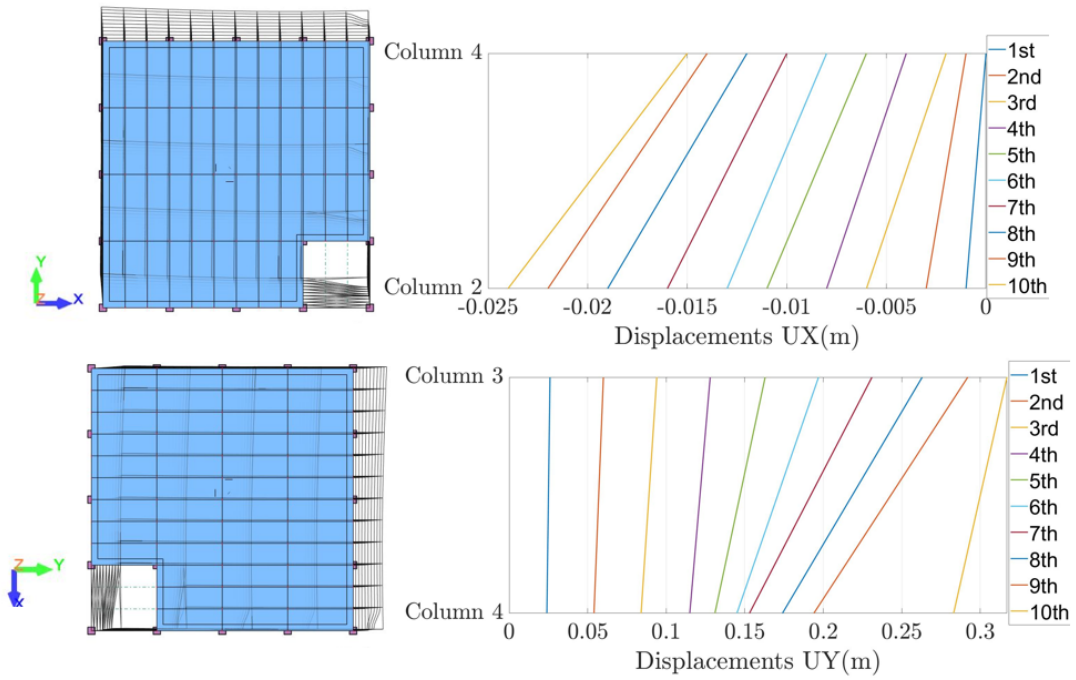


Figure C.9: Core columns' displacements in plan, for the first combination ($1.00G+0.3Q+0.3E_{Edx}+E_{Edy}$)

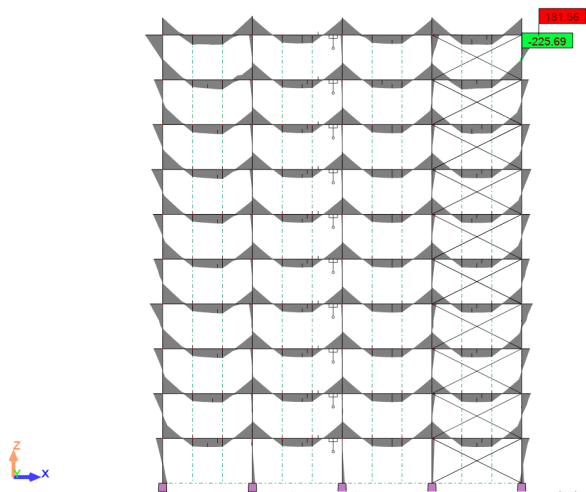


Figure C.10: Bending moments in X-direction out of the load combination $1.00G+0.3Q+0.3E_{Edx}+E_{Edy}$

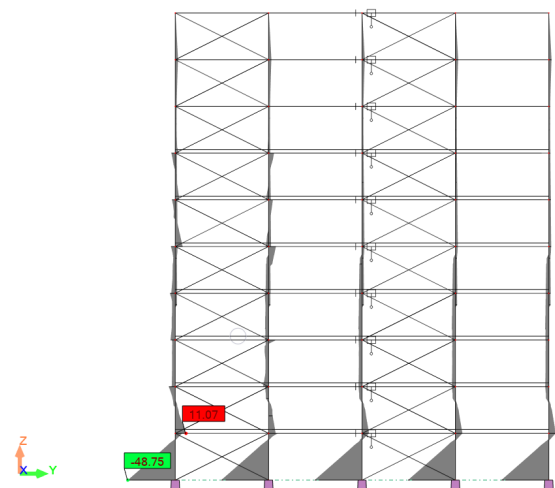


Figure C.11: Bending moments in Y-direction out of the load combination $1.00G+0.3Q+0.3E_{Edx}+E_{Edy}$

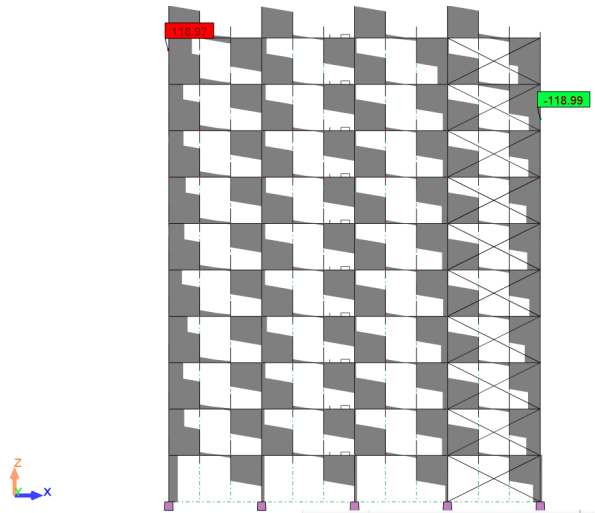


Figure C.12: Shear forces in X-direction out of the load combination $1.00G + 0.3Q + 0.3E_{Edx} + E_{Edy}$

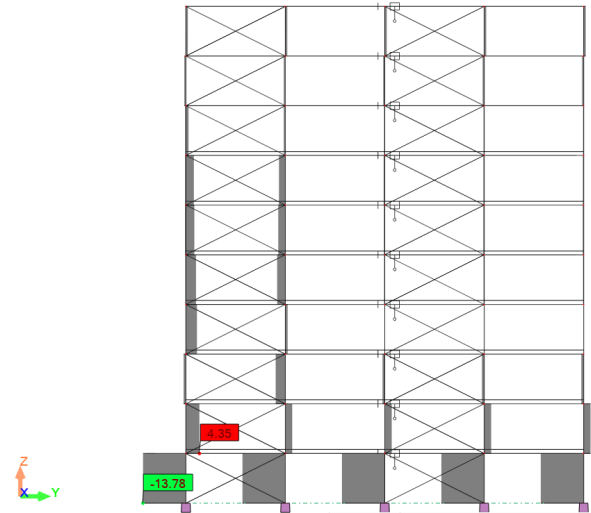


Figure C.13: Shear forces in Y-direction out of the load combination $1.00G + 0.3Q + 0.3E_{Edx} + E_{Edy}$

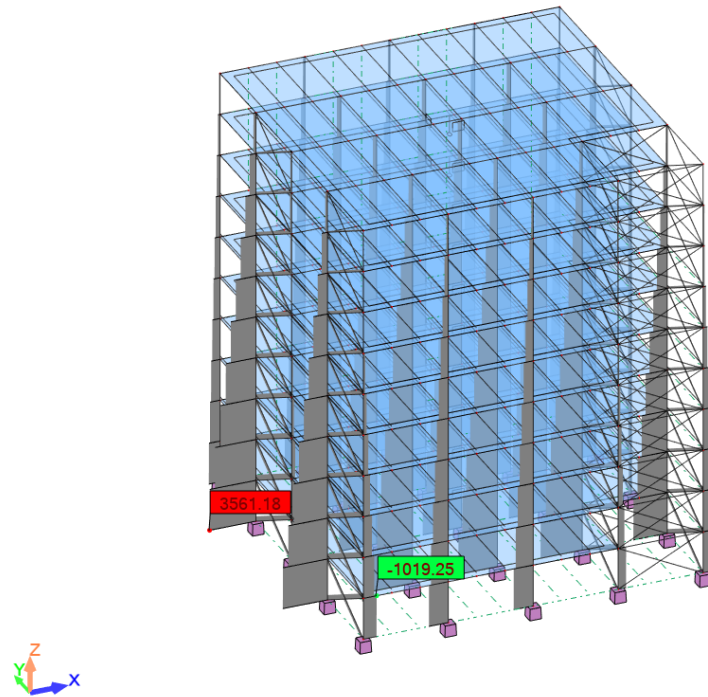


Figure C.14: Axial forces out of load combination $1.00G + 0.3Q + 0.3E_{Edx} + E_{Edy}$

C.3 Fourth load combination

Fourth load combination is defined as: $1.00G + 0.3Q + 0.3E_{Edx} - E_{Edy}$

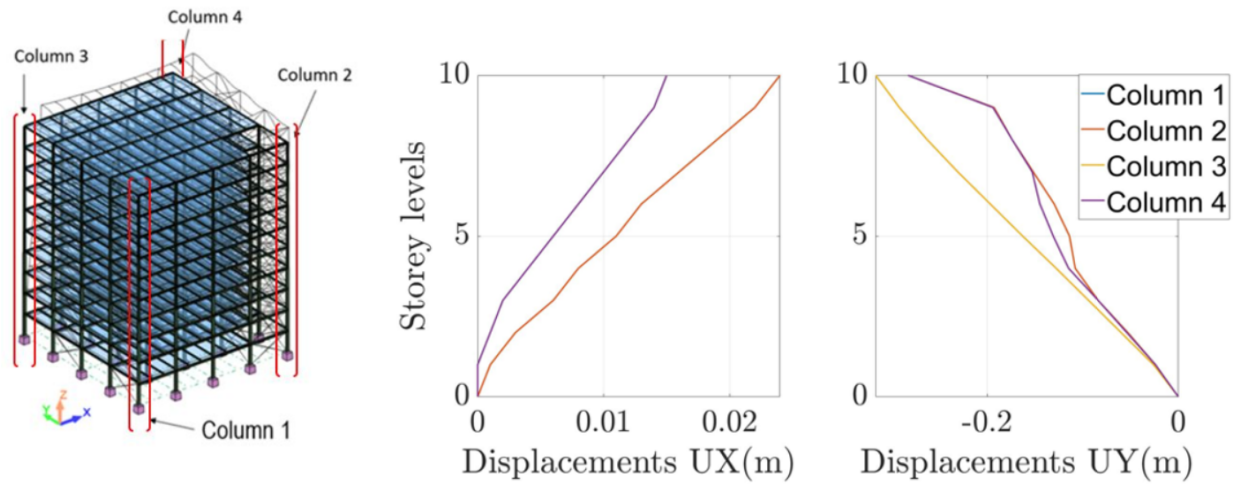


Figure C.15: Corner columns' displacements for the first combination ($1.00G + 0.3Q + 0.3E_{Edx} - E_{Edy}$)

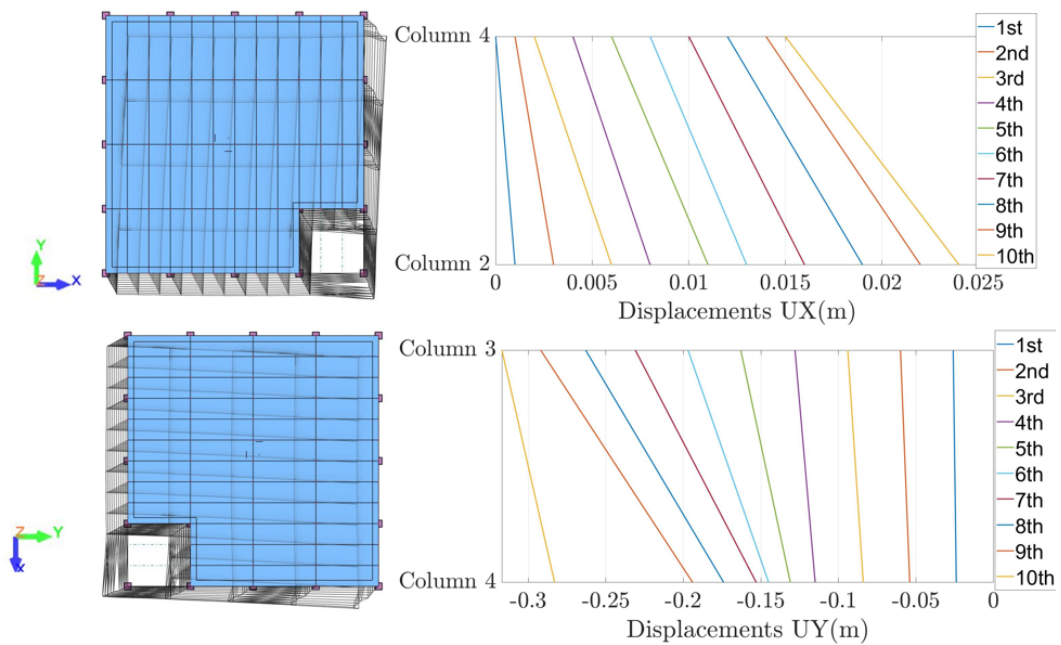


Figure C.16: Corner columns' displacements in plan, for the first combination ($1.00G + 0.3Q + 0.3E_{Edx} - E_{Edy}$)

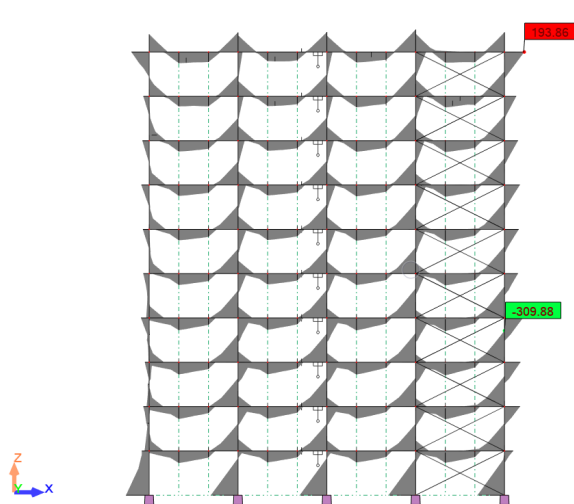


Figure C.17: Bending moments in X-direction out of the load combination $1.00G + 0.3Q + 0.3E_{Edx} - E_{Edy}$

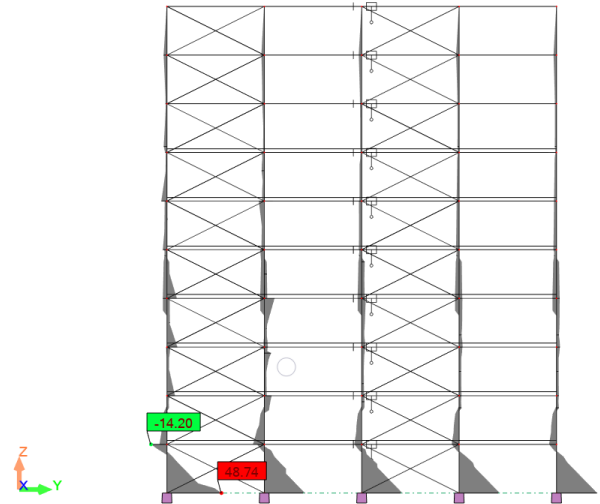


Figure C.18: Bending moments in Y-direction out of the load combination $1.00G + 0.3Q + 0.3E_{Edx} - E_{Edy}$

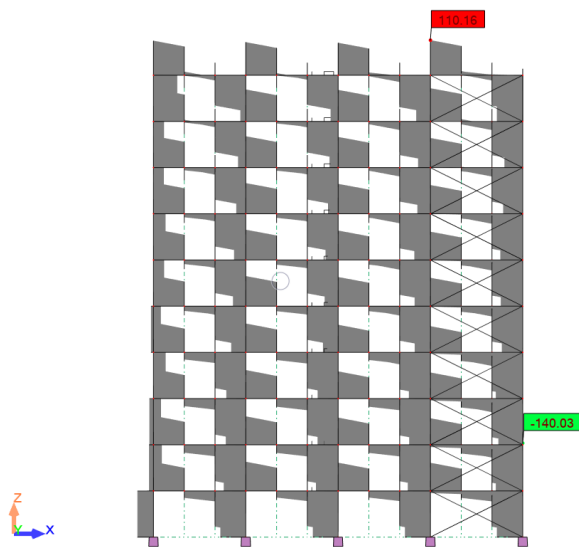


Figure C.19: Shear forces in X-direction out of the load combination $1.00G + 0.3Q + 0.3E_{Edx} - E_{Edy}$

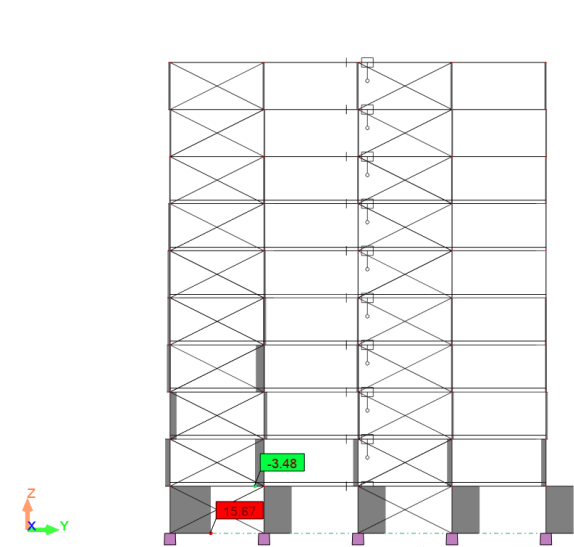


Figure C.20: Shear forces in Y-direction out of the load combination $1.00G + 0.3Q + 0.3E_{Edx} - E_{Edy}$

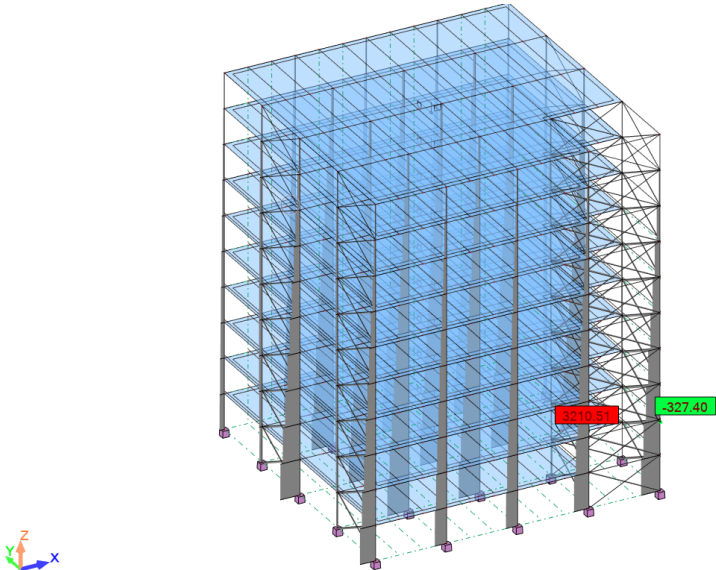


Figure C.21: Axial forces out of load combination $1.00G + 0.3Q + 0.3E_{Edx} - E_{Edy}$

Equivalent static method of analysis results D

D.1 Second load combination

Second load combination is defined as: $1.00G + 0.3Q + E_{Edx} - 0.3E_{Edy}$

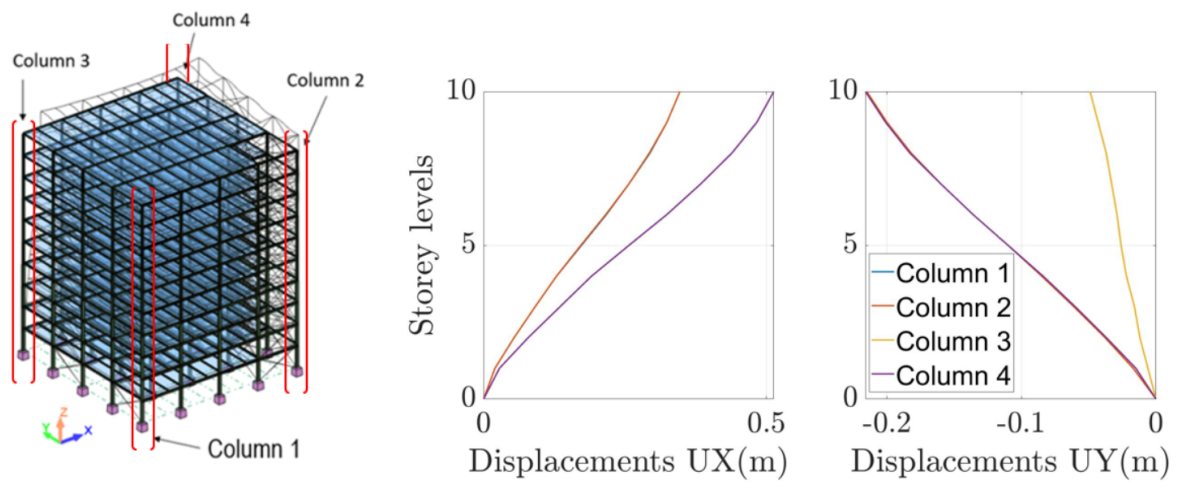


Figure D.1: Corner columns' displacements for the first combination ($1.00G + 0.3Q + E_{Edx} + 0.3E_{Edy}$)

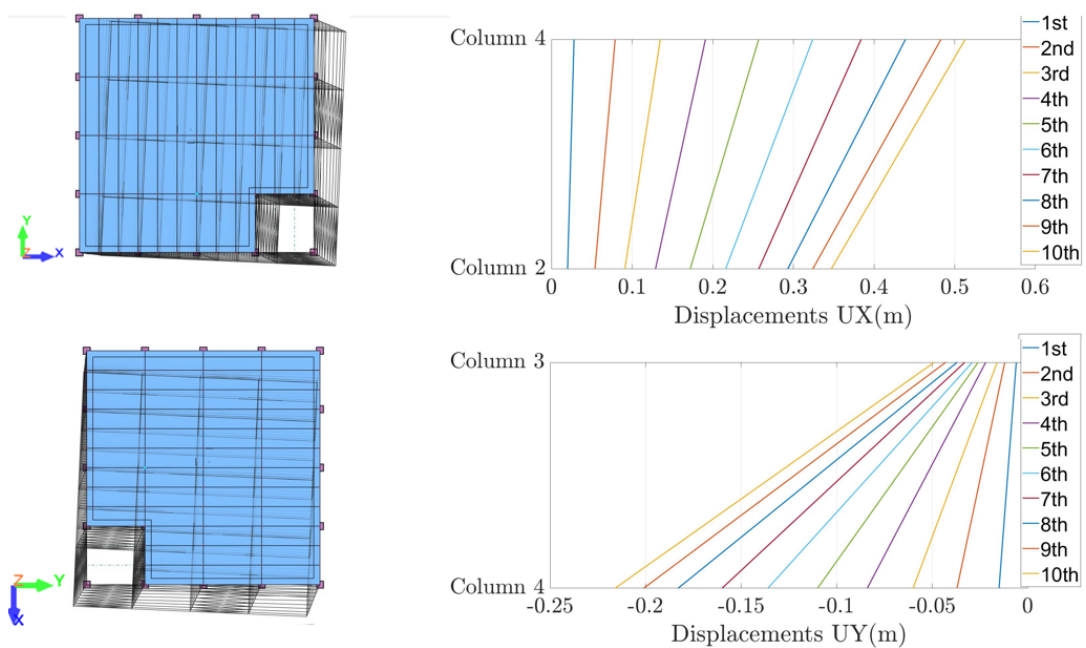


Figure D.2: Corer columns' displacements in plan, for the first combination ($1.00G + 0.3Q + E_{Edx} + 0.3E_{Edy}$)

D.2 Third load combination

Third load combination is defined as: $1.00G + 0.3Q + 0.3E_{Edx} + E_{Edy}$

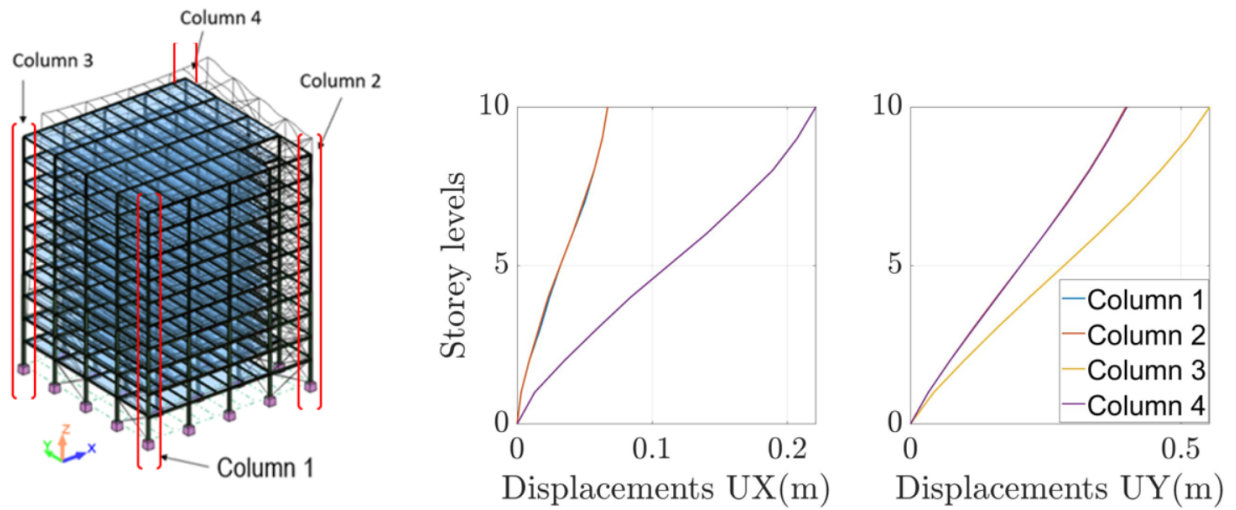


Figure D.3: Corner columns' displacements for the first combination ($1.00G + 0.3Q + E_{Edx} + 0.3E_{Edy}$)

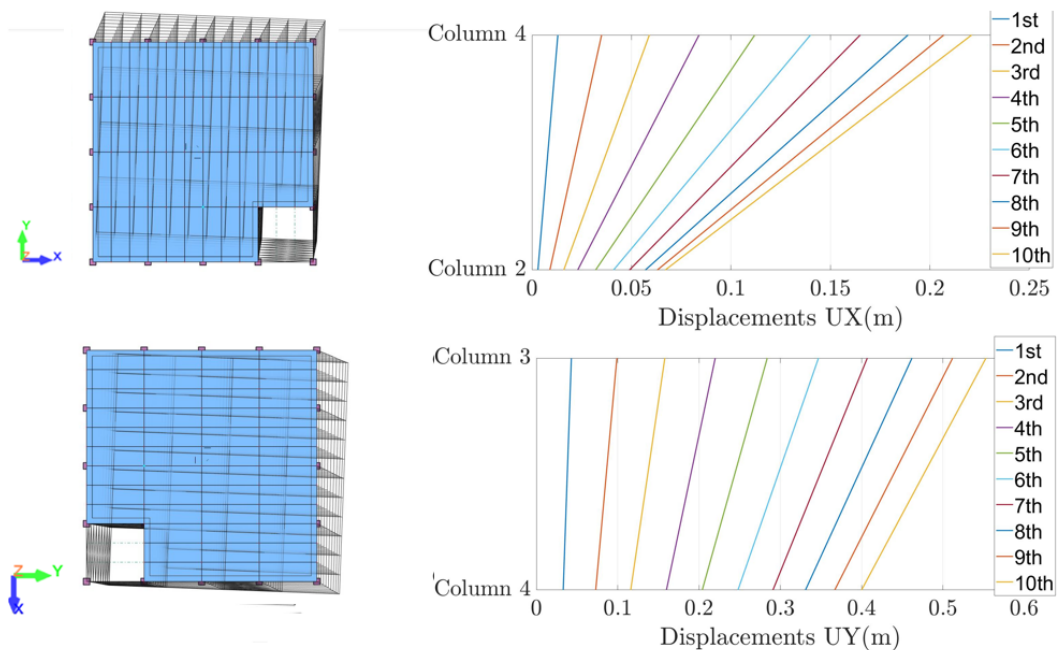


Figure D.4: Corner columns' displacements in plan, for the first combination ($1.00G + 0.3Q + E_{Edx} + 0.3E_{Edy}$)

D.3 Fourth load combination

Fourth load combination is defined as: $1.00G + 0.3Q + 0.3E_{Edx} - E_{Edy}$

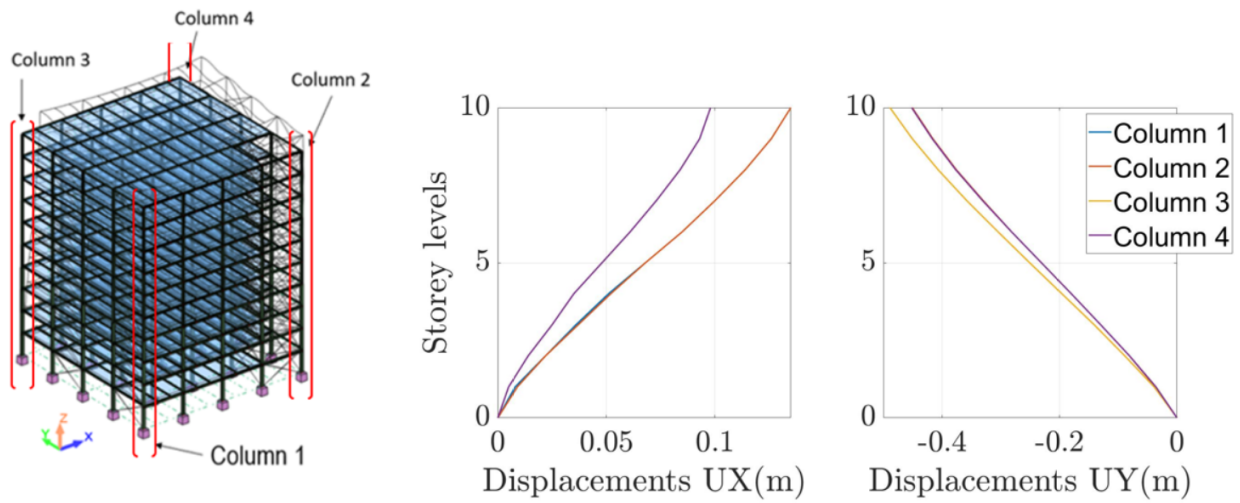


Figure D.5: Corner columns' displacements for the first combination ($1.00G + 0.3Q + E_{Edx} + 0.3E_{Edy}$)

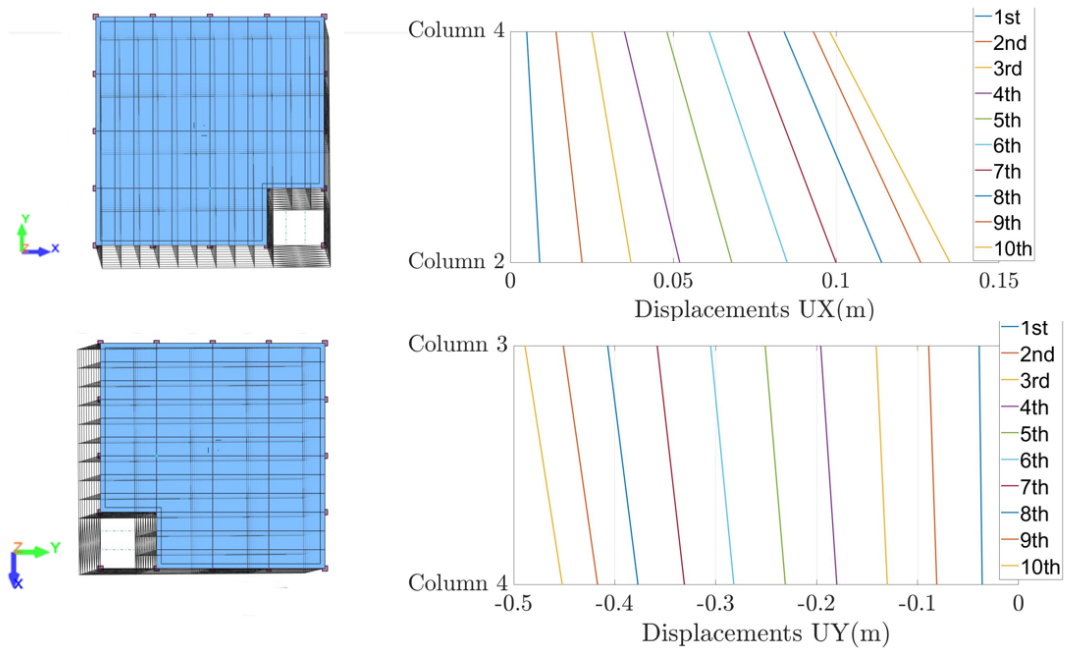


Figure D.6: Corer columns' displacements in plan, for the first combination ($1.00G + 0.3Q + E_{Edx} + 0.3E_{Edy}$)

Calculation note



CODE: EN 1993-1-2005/A1:2014, Eurocode 3: Design of steel structures.
ANALYSIS TYPE: Member Verification

CODE GROUP:
MEMBER: 5 Column_5 POINT: 1 COORDINATE: x = 0.00 L = 0.00 m

LOADS:
Governing Load Case: 11 COMB6 (1+7)*1.00+2*0.30

MATERIAL:
S 355 (S 355) fy = 355.00 MPa



SECTION PARAMETERS: HE 550 B

h=55.0 cm	gM0=1.00	gM1=1.00	
b=30.0 cm	Ay=188.36 cm ²	Az=100.07 cm ²	Ax=254.06 cm ²
tw=1.5 cm	Iy=136691.00 cm ⁴	Iz=13076.90 cm ⁴	Ix=679.00 cm ⁴
tf=2.9 cm	Wply=5590.85 cm ³	Wplz=1341.16 cm ³	

INTERNAL FORCES AND CAPACITIES:

N _{Ed} = 1196.21 kN	My _{Ed} = -459.41 kN*m	Mz _{Ed} = -3.76 kN*m	Vy _{Ed} = -0.65 kN	
N _{c,Rd} = 9019.06 kN	My _{Ed,max} = -459.41 kN*m		Mz _{Ed,max} = 5.11 kN*m	Vy _{1,Rd} = 3859.79 kN
N _{b,Rd} = 6914.82 kN	My _{c,Rd} = 1984.75 kN*m	Mz _{c,Rd} = 476.11 kN*m	Vz _{Ed} = 130.15 kN	
	MN _{y,Rd} = 1984.75 kN*m	MN _{z,Rd} = 476.11 kN*m	Vz _{T,Rd} = 2050.77 kN	
	Mb _{Rd} = 1984.75 kN*m		Tt _{Ed} = 0.02 kN*m	
			Class of section = 1	



LATERAL BUCKLING PARAMETERS:

z = 0.00	Mcr = 11227.22 kN*m	Curve,LT = b	XLT = 0.99
L _{cr,low} = 4.00 m	Lam _{LT} = 0.42	fi _{LT} = 0.57	XLT _{mod} = 1.00

BUCKLING PARAMETERS:



About y axis:

L _y = 4.00 m	Lam _y = 0.23
L _{cr,y} = 4.00 m	X _y = 0.99
Lam _y = 17.24	k _{yy} = 0.75



About z axis:

L _z = 4.00 m	Lam _z = 0.73
L _{cr,z} = 4.00 m	X _z = 0.77
Lam _z = 55.75	k _{yz} = 0.51

Torsional buckling:

Curve _T = b	alfa _T = 0.34
L _t = 4.00 m	fi _T = 0.72
N _{cr,T} = 28803.09 kN	X _T = 0.86
Lam _T = 0.56	Nb _{T,Rd} = 7727.85 kN

Flexural-torsional buckling

Curve _{TF} = b	alfa _{TF} = 0.34
N _{cr,TF} = 177067.55 kN	fi _{TF} = 0.53
N _{cr,TF} = 177067.55 kN	X _{TF} = 0.99
Lam _{TF} = 0.23	Nb _{TF,Rd} = 8936.85 kN

Figure E.1: Calculation note of column 5

VERIFICATION FORMULAS:

Section strength check:

$N_{Ed}/N_{c,Rd} = 0.13 < 1.00$ (6.2.4.(1))
 $My_{Ed}/MN_{y,Rd} = 0.23 < 1.00$ (6.2.9.1.(2))
 $Mz_{Ed}/MN_{z,Rd} = 0.01 < 1.00$ (6.2.9.1.(2))
 $(My_{Ed}/MN_{y,Rd})^2 + (Mz_{Ed}/MN_{z,Rd})^2 = 0.06 < 1.00$ (6.2.9.1.(6))
 $Vy_{Ed}/Vy_{T,Rd} = 0.00 < 1.00$ (6.2.6-7)
 $Vz_{Ed}/Vz_{T,Rd} = 0.06 < 1.00$ (6.2.6-7)
 $\tau_{xy,Ed}/(fy/(\sqrt{3}) * gM0) = 0.00 < 1.00$ (6.2.6)
 $\tau_{xz,Ed}/(fy/(\sqrt{3}) * gM0) = 0.00 < 1.00$ (6.2.6)

Global stability check of member:

$\lambda_{y} = 17.24 < \lambda_{max} = 210.00$ $\lambda_{z} = 55.75 < \lambda_{max} = 210.00$ STABLE
 $N_{Ed}/\text{Min}(N_{b,Rd}, N_{T,Rd}, N_{b,TF,Rd}) = 0.17 < 1.00$ (6.3.1)
 $My_{Ed,max}/Mb_{Rd} = 0.23 < 1.00$ (6.3.2.1.(1))
 $N_{Ed}/(Xy * N_{Rk}/gM1) + kyy * My_{Ed,max}/(XLT * My_{Rk}/gM1) + kyz * Mz_{Ed,max}/(Mz_{Rk}/gM1) = 0.31 < 1.00$ (6.3.3.(4))
 $N_{Ed}/(Xz * N_{Rk}/gM1) + kzy * My_{Ed,max}/(XLT * My_{Rk}/gM1) + kzz * Mz_{Ed,max}/(Mz_{Rk}/gM1) = 0.27 < 1.00$ (6.3.3.(4))

Section OK !!!

Figure E.2: Calculation note of column 5 (Verification formulas)

Verification example of tension only elements



In this example a steel frame with a bracing bar is modeled. The bracing bar is connected with the frame in the upper right part, while in the other end is linked with the support by use of link element as they are described in Section 5.2. The structure is subjected to a sinusoidal loading, see Figure F.2. The load is acting on the upper right part of the structure (**node 4**).

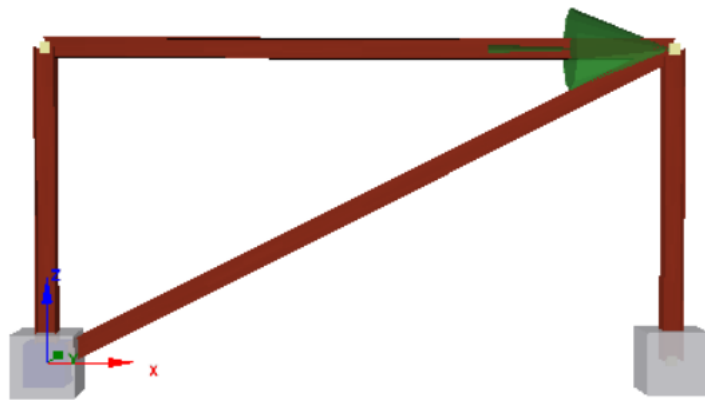


Figure F.1: Steel frame with tension only bracing bar

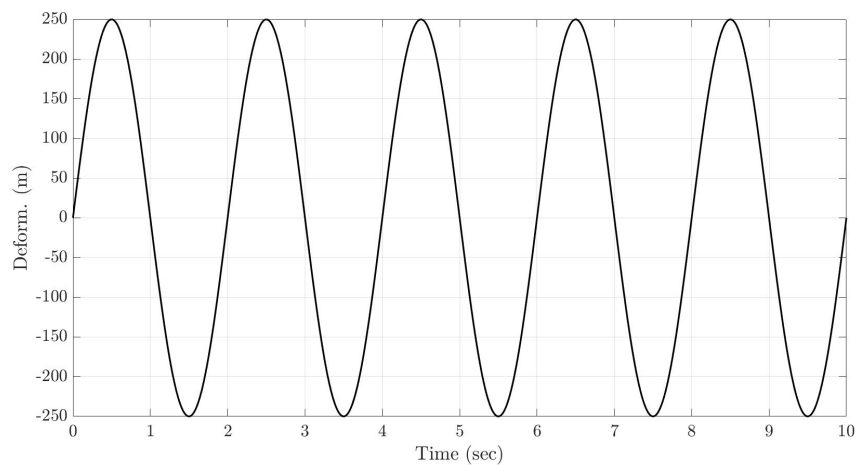


Figure F.2: Applied sinusoidal load history

The structural response, displacements of **node 4**, can be seen in Figure F.3. As it can be seen the structure is mainly displaced to the left side due to the fact that in this direction the bracing bar is

under compression. As a result of link element effect the brace bar can not resist the compressive loading. Therefore the structure is considered as unbraced in this direction. Moreover, even when the load changes sign the bracing bar remains inactive until the initial, "undeformed", shape is recovered. After this point, the load tends to deform the structure in the positive X-direction. The bracing bar is under tensile force, therefore it resists the horizontal action and the structural stiffness is significantly increased. This is the reason why the positive displacements are vary small compared to the negative ones.

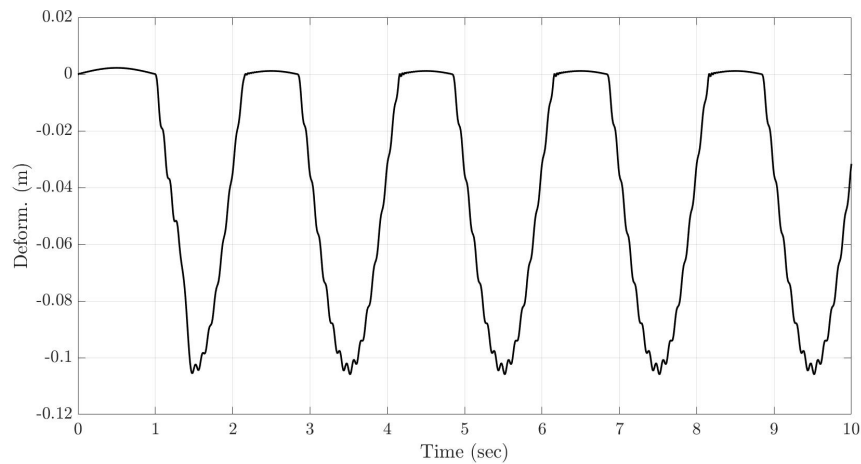


Figure F.3: Structural response (node 4)

In Figure F.4, the response of the bracing bar can be seen. It is obvious that the bar is subjected only in positive (tensile) deformations and axial forces due to link element's restrictions.

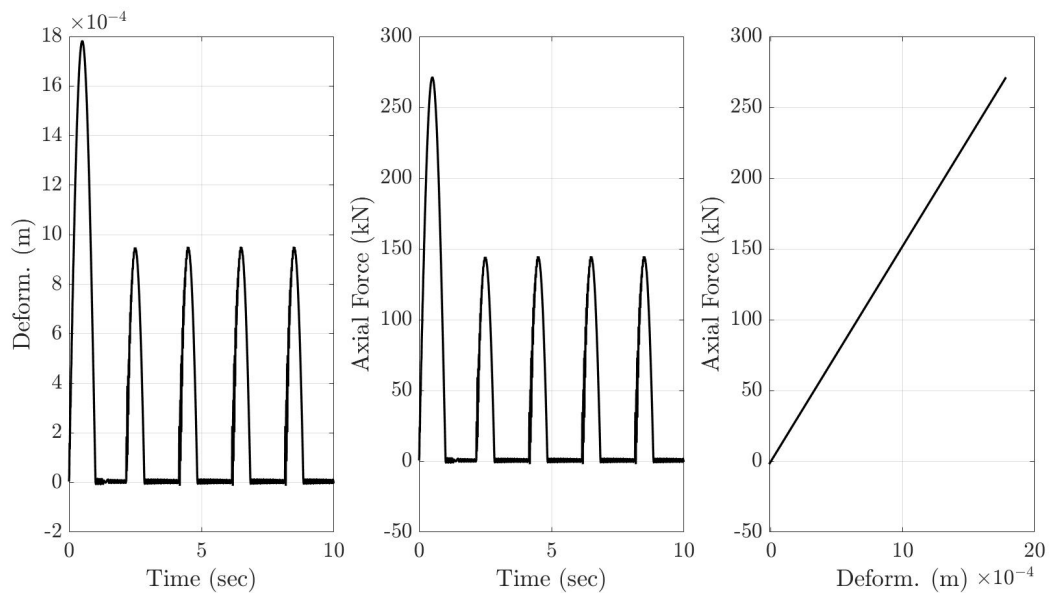


Figure F.4: Response of bracing bar: (a) time-Axial deformations, (b) time-Axial force, (c) Axial deformations- Axial force

The deformed shape of the structure at time step $0.50sec$ when the maximum load ($250kN$) is applied and at time step $1.50sec$ when the minimum load ($-250kN$) is applied, can be seen in Figures F.5 and F.6, respectively.

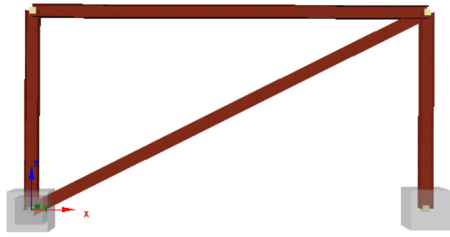


Figure F.5: Deformed shape under maximum loading, time step = 0.50sec

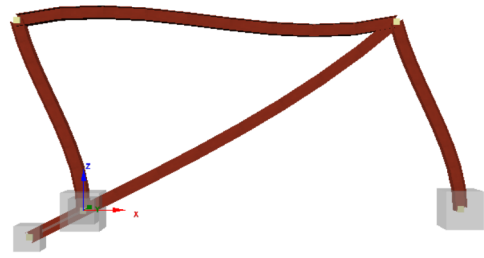


Figure F.6: Deformed shape under minimum loading, time step = 1.50sec

Pushover analysis results:

Model 2



In this case the bracing bars are simulated so that they can handle both tension and compression. However the axial stiffness is reduced by a reduction factor equal to 0.5. In this way, the behaviour of tension only bracing system is approximated.

G.1 X direction

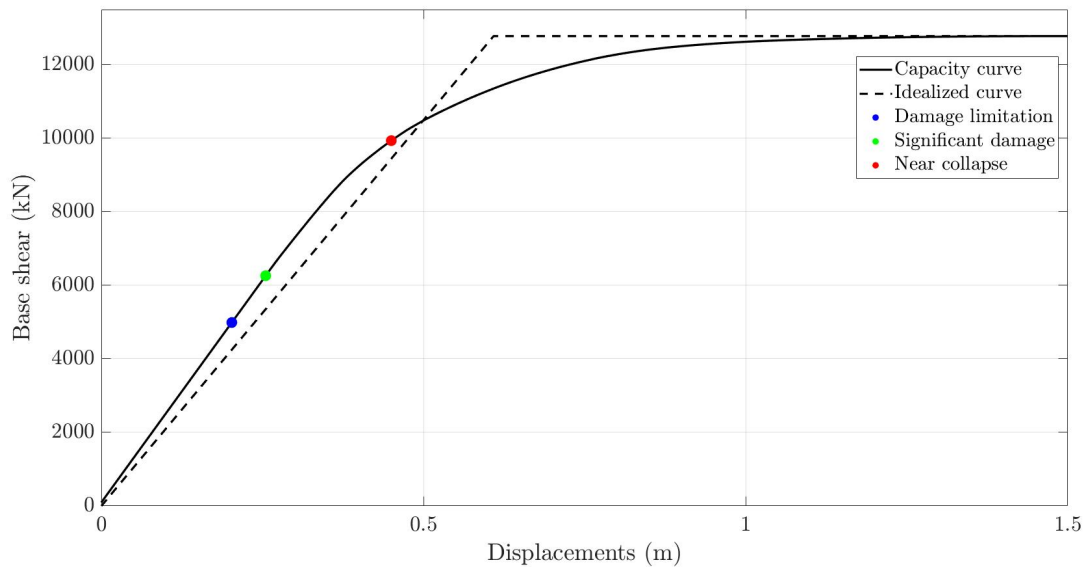


Figure G.1: Capacity curve in X-direction

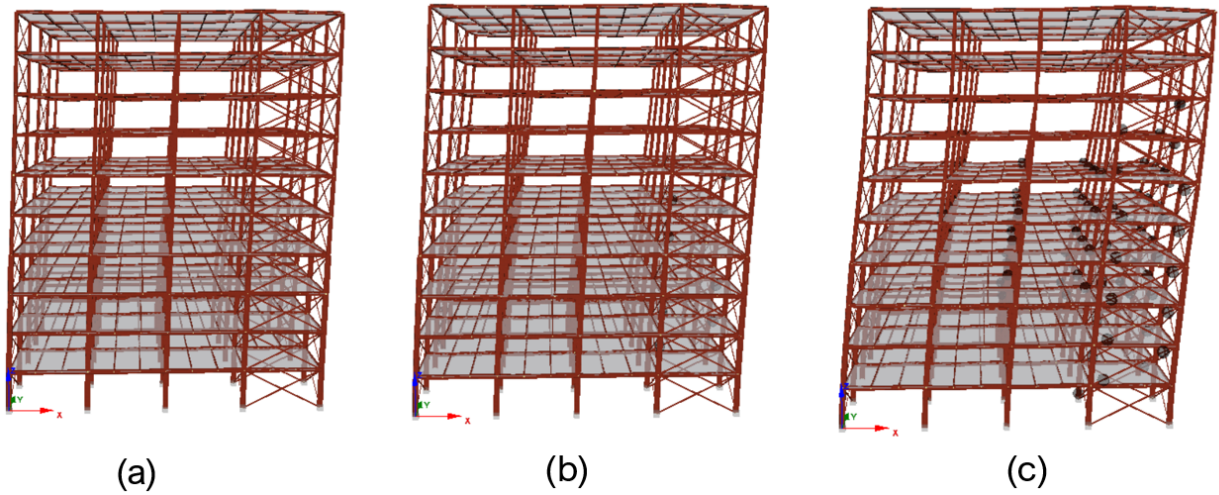


Figure G.2: Deform shape in limit states:(a) Damage limitation, (b) Significant damage, (c) Near Collapse

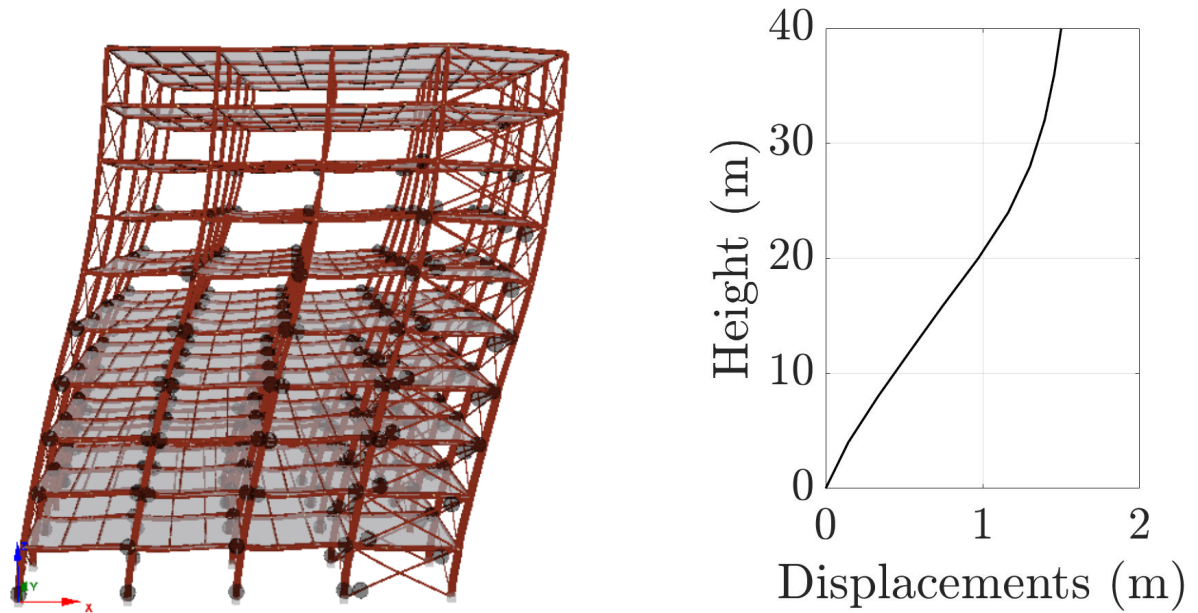


Figure G.3: Deformed shape of the structure at failure state

Figure G.4: Displacements at the center of mass in every level

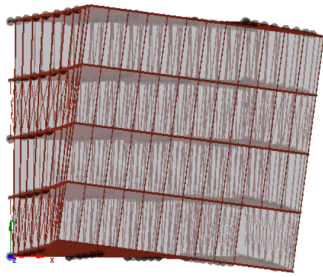


Figure G.5: Deformed shape of the structure at failure state (plan perspective)

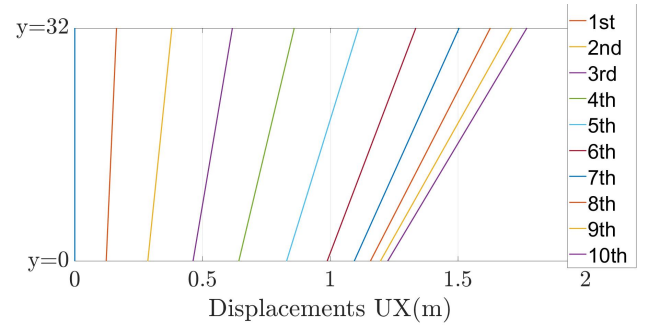


Figure G.6: Corner columns' displacements of every storey level

G.2 Y direction

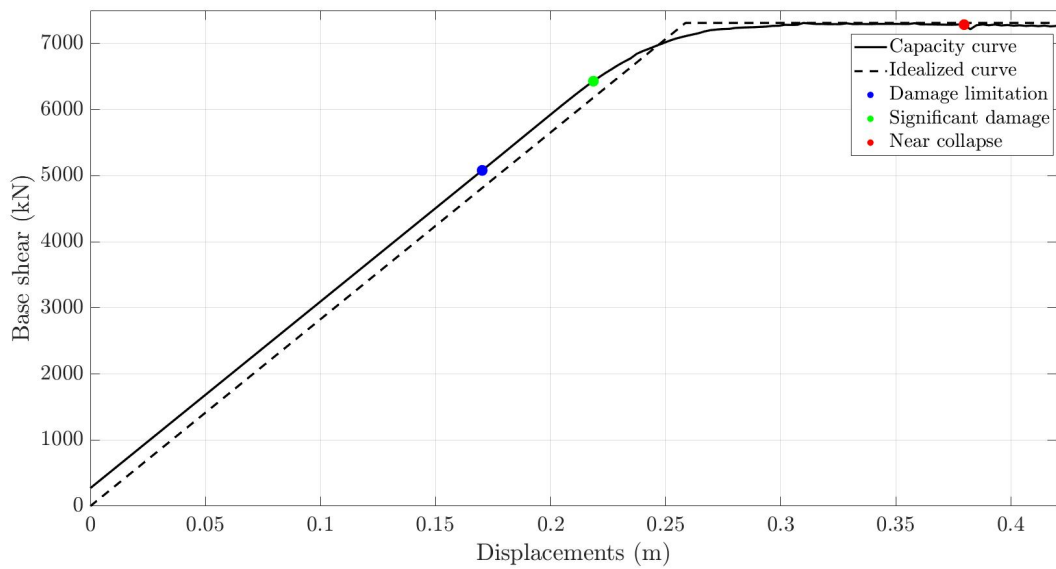


Figure G.7: Capacity curve in X-direction

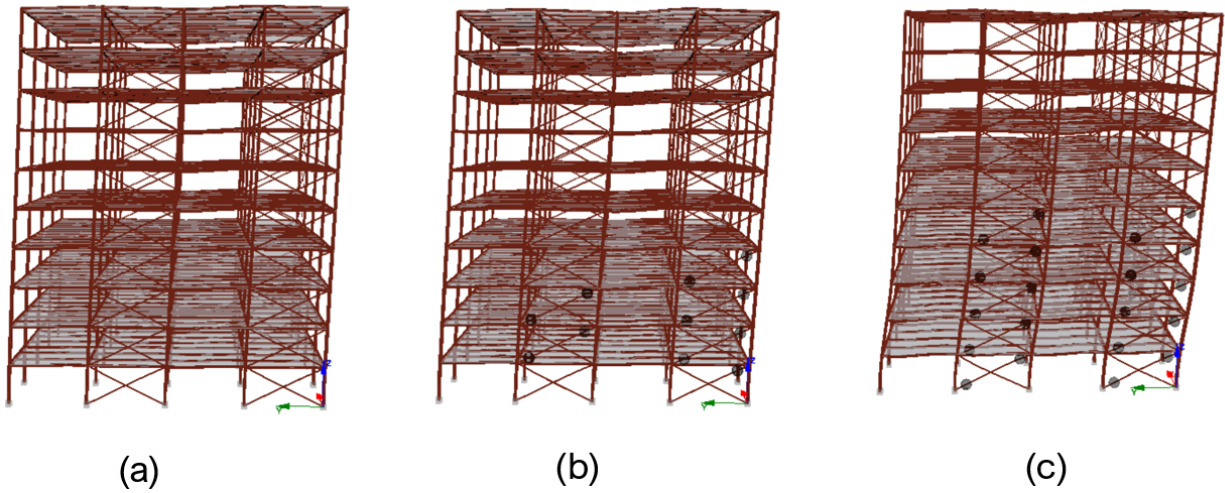


Figure G.8: Deform shape in limit states:(a) Damage limitation, (b) Significant damage, (c) Near Collapse

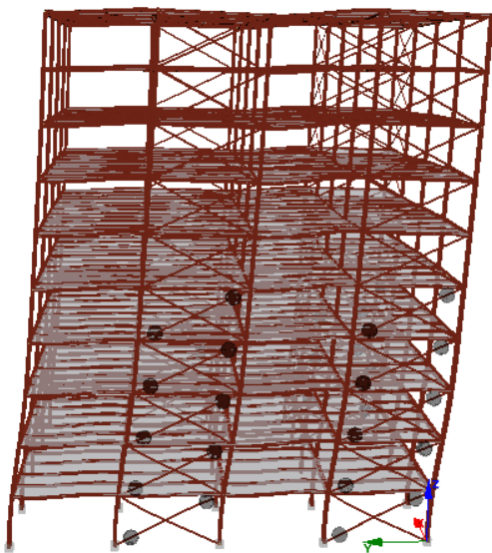


Figure G.9: Deformed shape of the structure at failure state

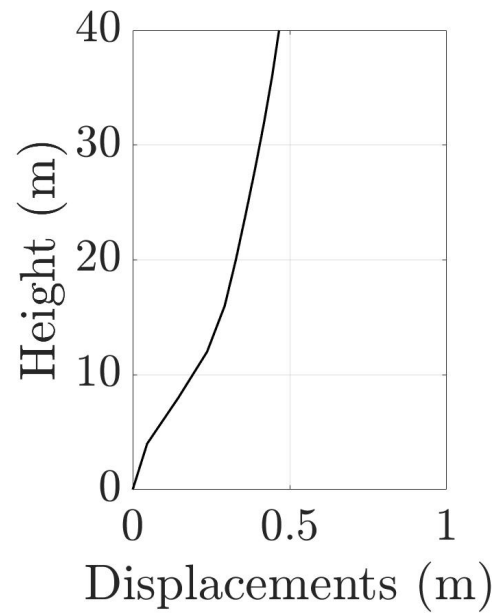


Figure G.10: Displacements at the center of mass in every level

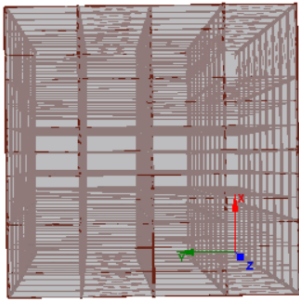


Figure G.11: Deformed shape of the structure at failure state (plan perspective)

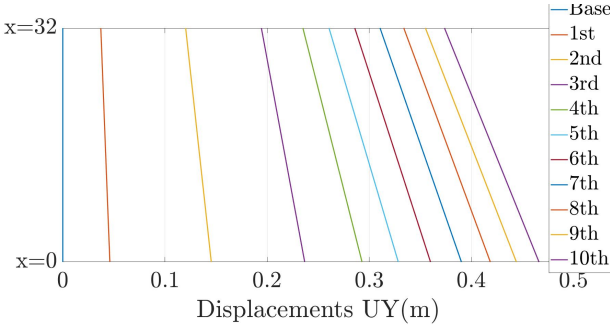


Figure G.12: Corner columns' displacements of every storey level

Nonlinear time history results

H

H.1 Northridge's original accelerogram, X direction

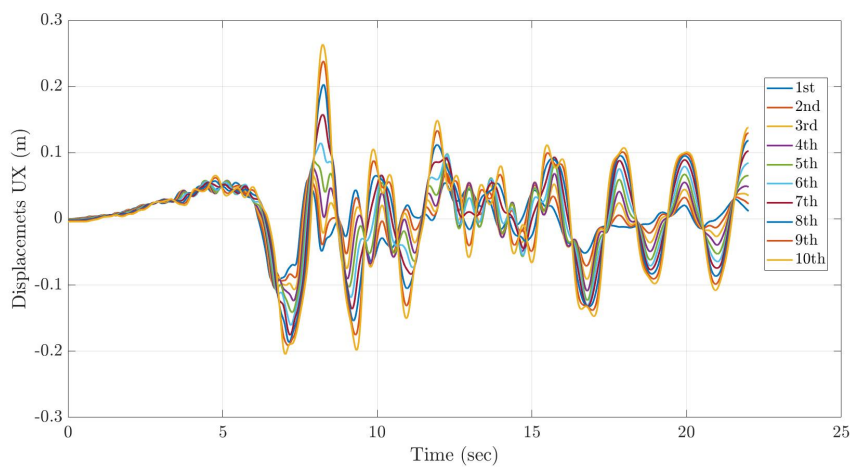


Figure H.1: Displacements of the center of mass at every storey level

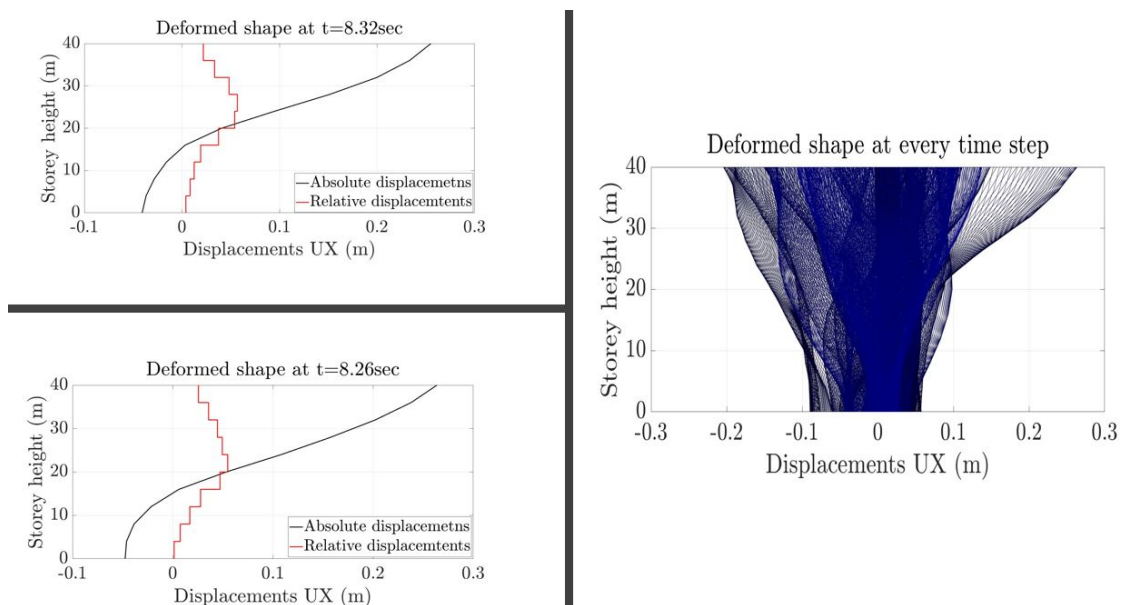


Figure H.2: (Right) Deformed shape of structure at every time step, (Upper-left) Deformed shape when maximum relative displacement occurs, (Lower-left) Deformed shape when absolute maximum displacement occurs

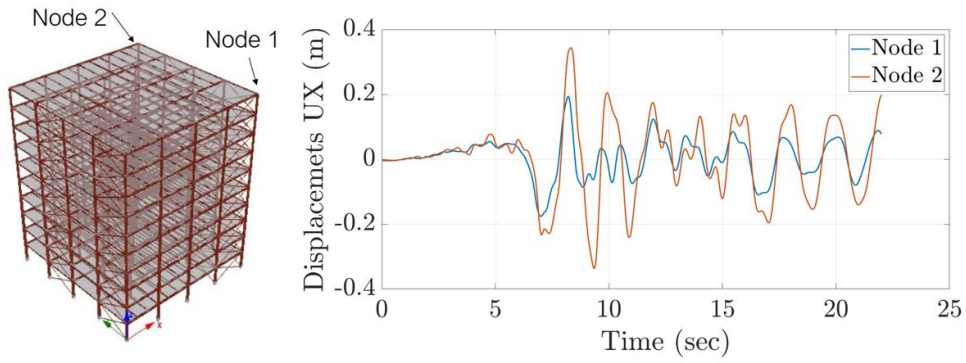


Figure H.3: Displacements on top of the two corner columns

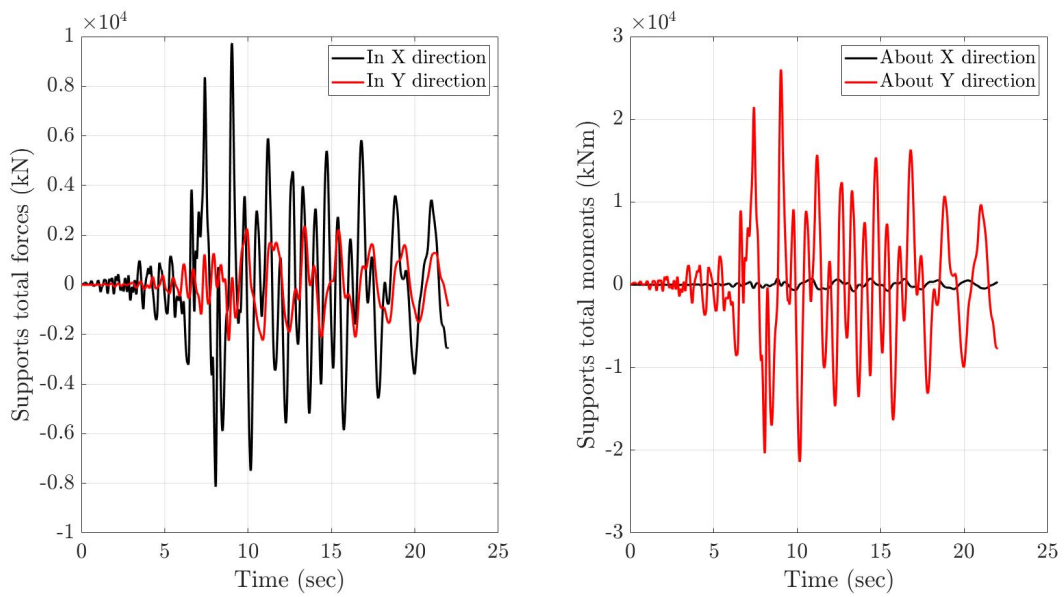


Figure H.4: Hysteretic curves of column, beam and bracing bar

H.2 Northridge's original accelerogram, Y direction

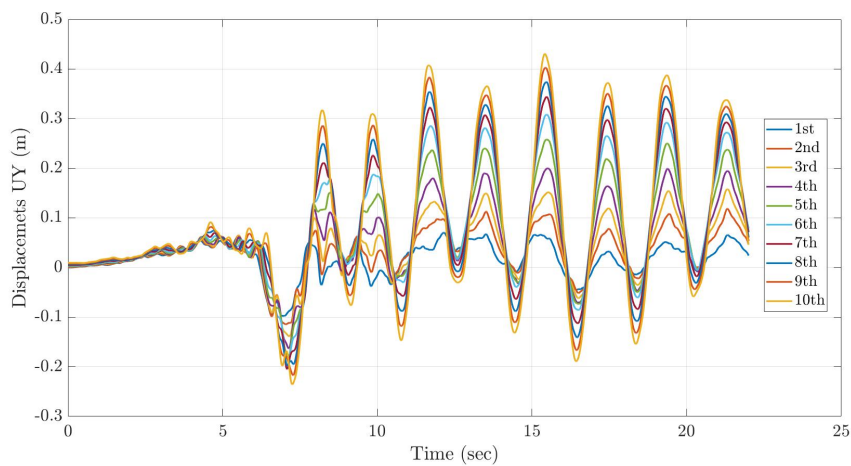


Figure H.5: Displacements of the center of mass at every storey level

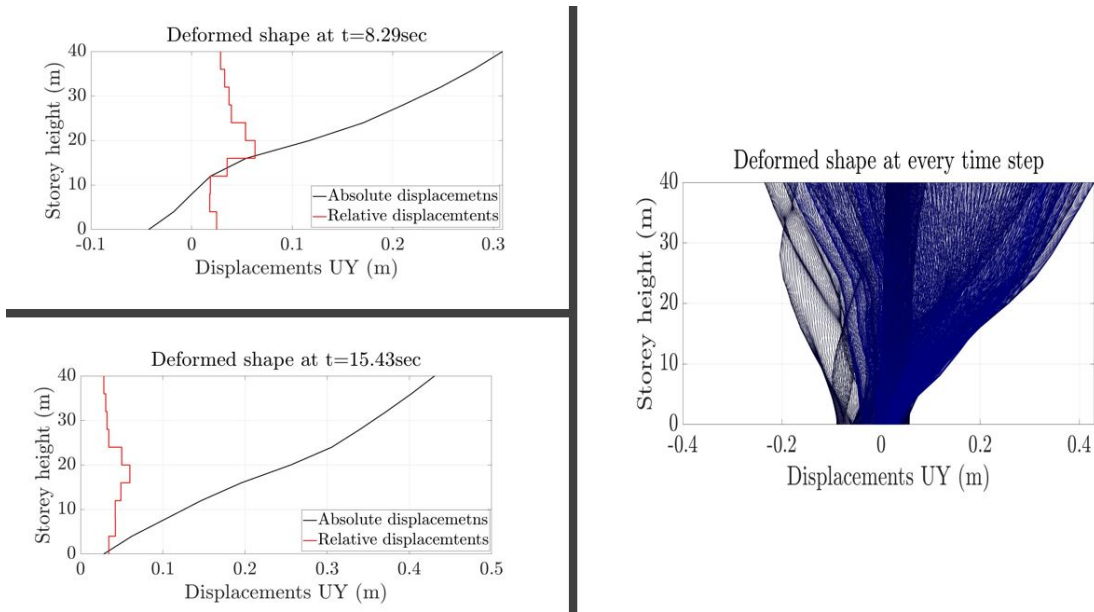


Figure H.6: (Right) Deformed shape of structure at every time step, (Upper-left) Deformed shape when maximum relative displacement occurs, (Lower-left) Deformed shape when absolute maximum displacement occurs

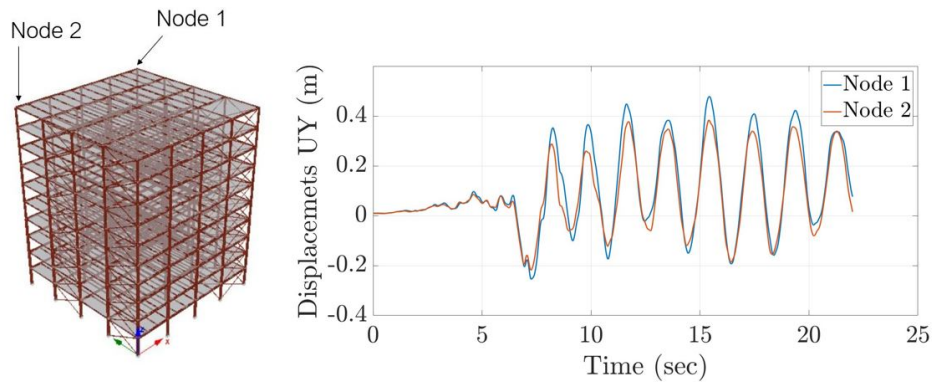


Figure H.7: Displacements on top of the two corner columns

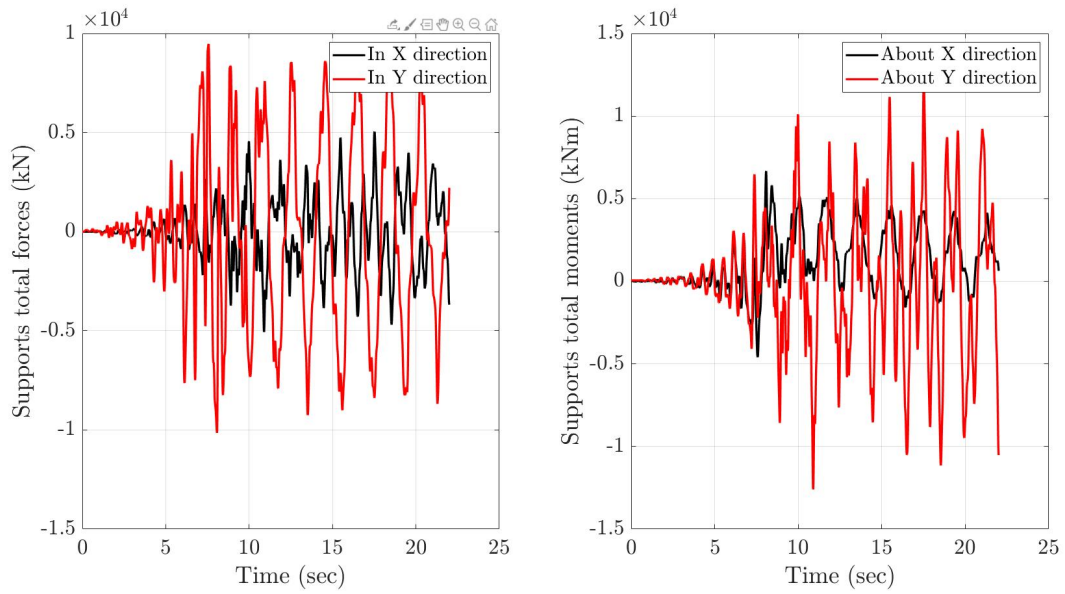


Figure H.8: Total support forces and bending moments

H.3 Artificially generated accelerogram, X direction

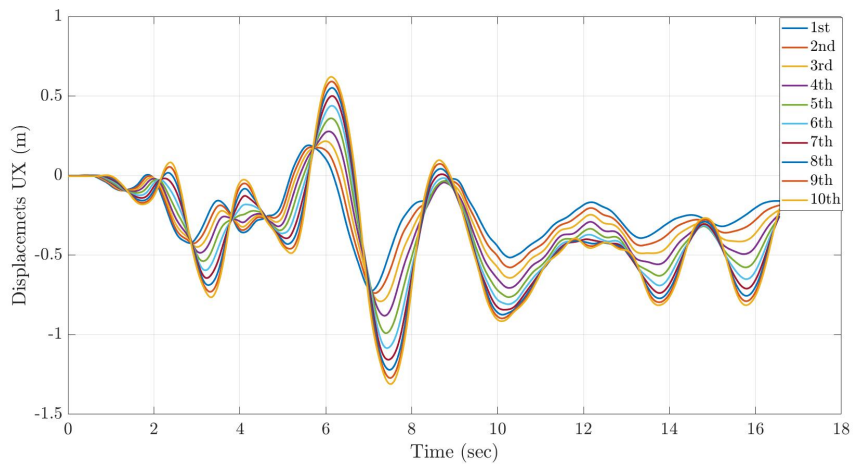


Figure H.9: Displacements of the center of mass at every storey level

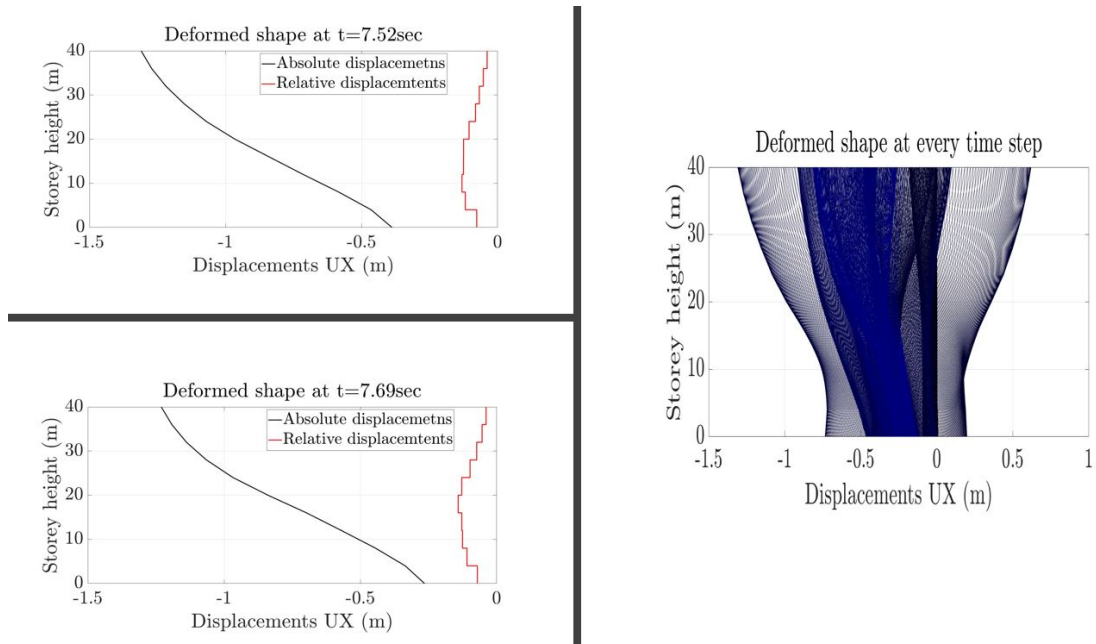


Figure H.10: (Right) Deformed shape of structure at every time step, (Upper-left) Deformed shape when maximum relative displacement occurs, (Lower-left) Deformed shape when absolute maximum displacement occurs

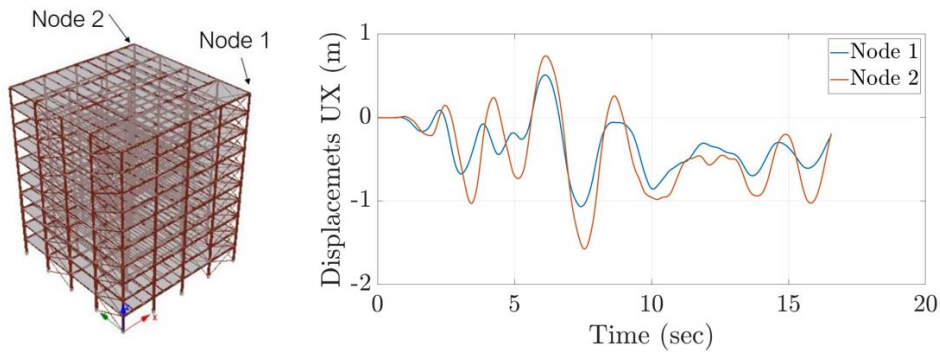


Figure H.11: Displacements on top of the two corner columns

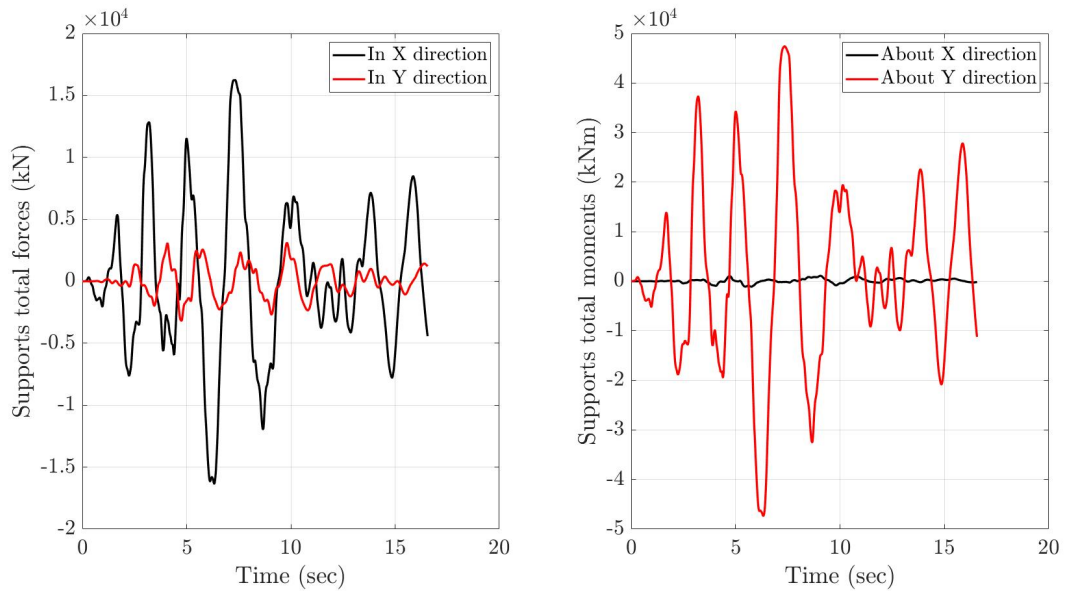


Figure H.12: Total support forces and bending moments

H.4 Artificially generated accelerogram, Y direction

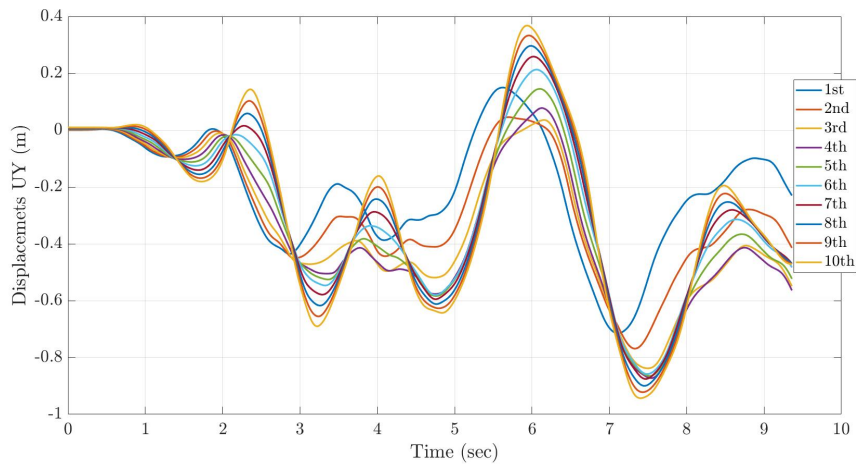


Figure H.13: Displacements of the center of mass at every storey level

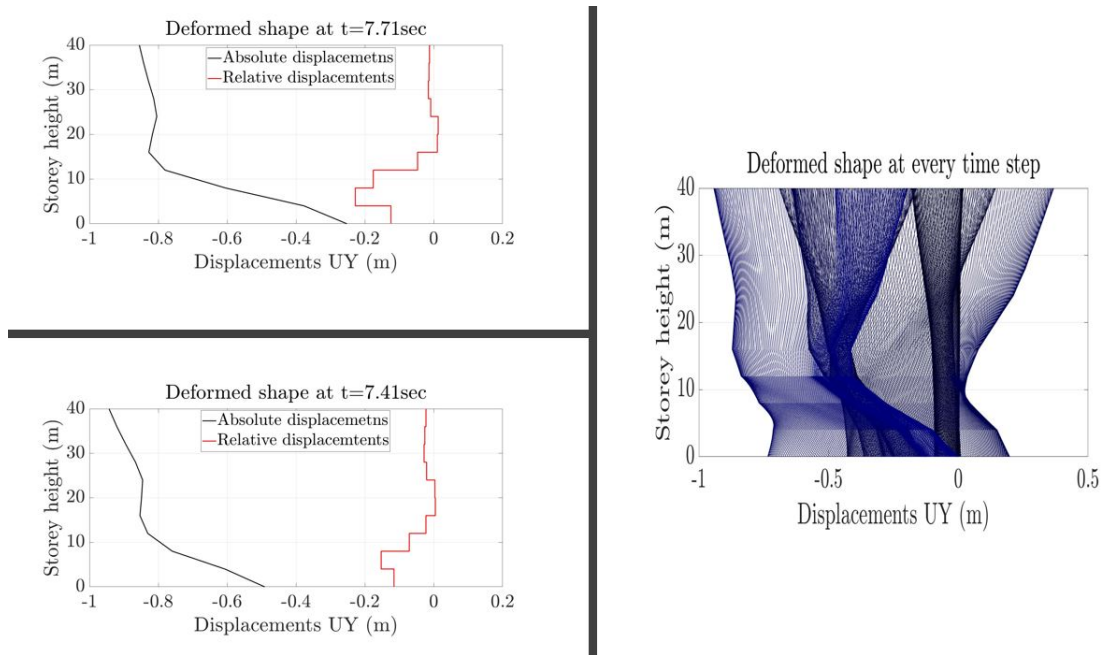


Figure H.14: (Right) Deformed shape of structure at every time step, (Upper-left) Deformed shape when maximum relative displacement occurs, (Lower-left) Deformed shape when absolute maximum displacement occurs

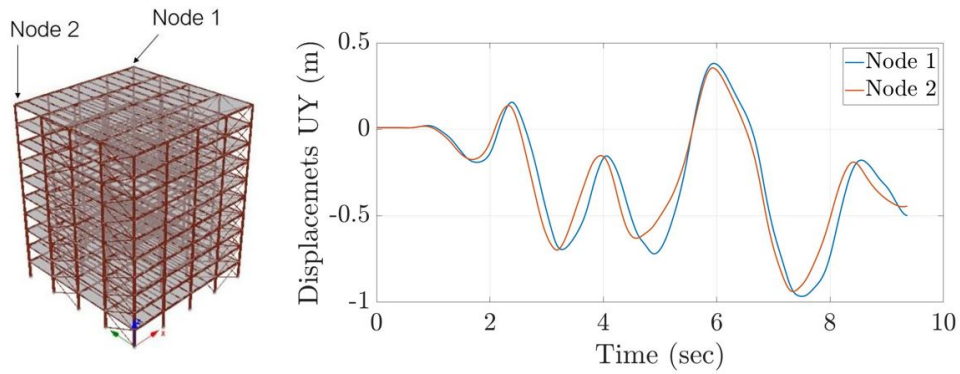


Figure H.15: Displacements on top of the two corner columns

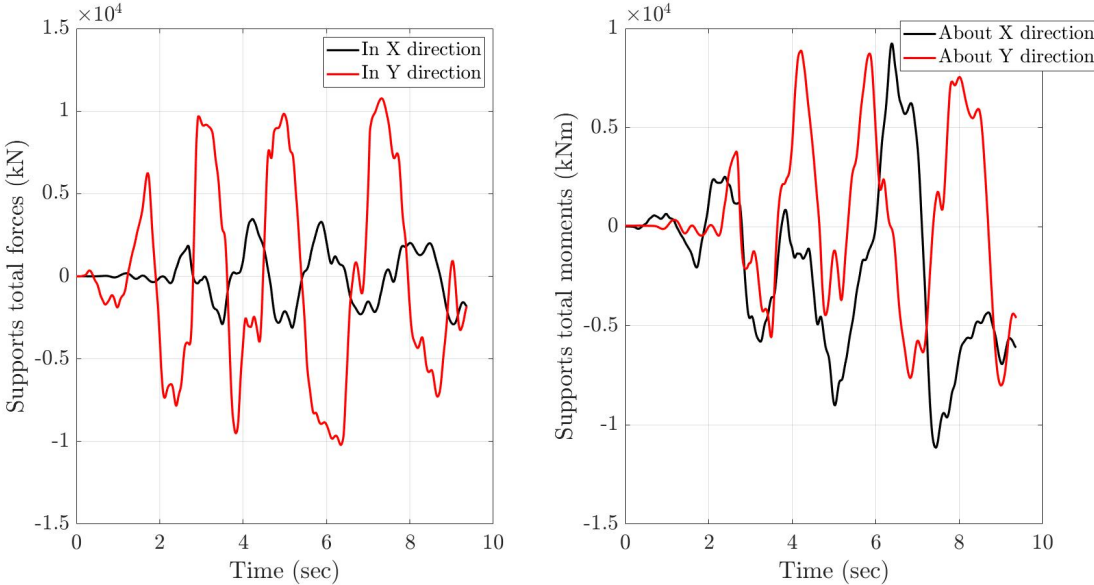


Figure H.16: Total support forces and bending moments